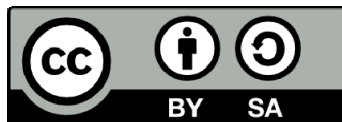# UNIVERSITAT DE BARCELONA

Estudi de sistemes de baixa dimensionalitat i correlació electrònica forta pel mètode de la matriu de transferència

M. Roser Valentí i Vall

ESTUDI DE SISTEMES DE BAIXA DIMENSIONALITAT
I CORRELACIó ELECTRòNICA FORTA
PEL MèTODE DE LA MATRIU DE TRANSFERèNCIA.

Tesi Doctoral.

M. Roser Valentí i Vall

Universitat de Barcelona.

ESTUDI DE SISTEMES DE BAIXA DIMENSIONALITAT
I CORRELACIó ELECTRòNICA FORTA
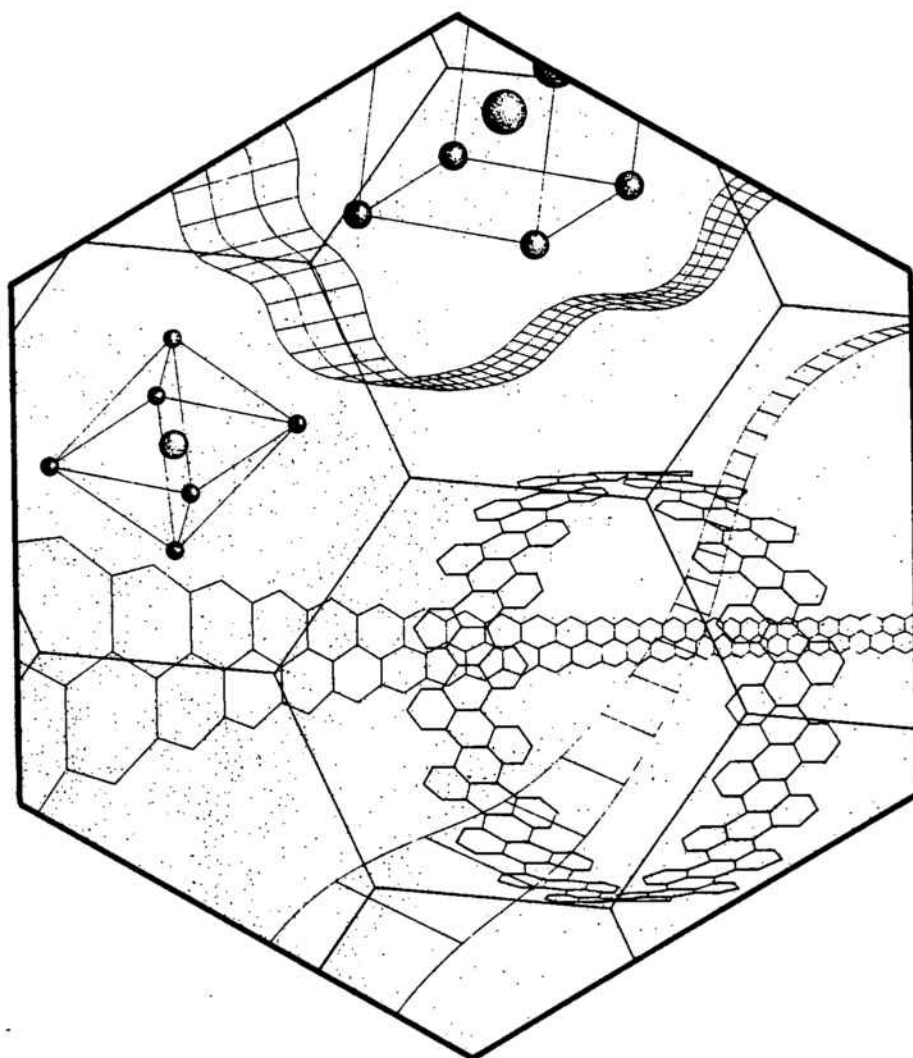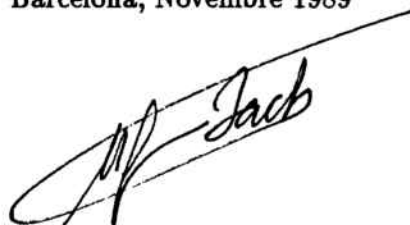PEL MèTODE DE LA MATRIU DE TRANSFERèNCIA.

M. Roser Valentí i Vall
Universitat de Barcelona

Certifico que la present Tesi doctoral
ha sigut realitzada
sota la meva direcció.
Barcelona, Novembre 1989

M. Angels García Bach
Professora Titular
de la Universitat de
Barcelona

Agraïments

Aquest treball de Tesi ha estat possible gràcies a l'ajut i col.laboració desinteressada de molts companys.

Voldria agrair especialment a la meva directora de Tesi, la Dra. M.Angels García Bach, l'enorme paciència i dedicació que ha tingut en la direcció d'aquest treball, així com, per les interessants discussions mantingudes amb ella.

I'm very grateful to Prof. D.J. Klein for the useful conversations and valuable advices he gave me during my stay in Texas A&M University at Galveston (Tx) in Spring 1989.

A l'Enrique sobretot, que sempre m'ha animat a continuar endavant i amb qui la Física ha sigut més divertida.

Al meu germà Eduard que ha tingut de passar molt de temps fent els dibuixets d'aquest treball i qui sempre m'ha donat bons consells.

Al Salvador, pel disseny de la portada i a qui estic molt agraida.

A tots els companys dels departaments de Física Fonamental i ECM amb qui he tingut la sort de compartir les tasques diaries.

To all friends that I have met in Trieste (Italy), Santa Barbara (Ca) and Galveston (Tx) for the interesting and fruitful conversations that we had.

Als departaments d'ECM, Física Fonamental i Química Orgànica de la Universitat de Barcelona, pels recursos informatics dels que he pogut disposar per a dur a terme l'edició d'aquesta Tesi.

A la CIRIT i CICYT MAT88-0163-C03-02 per l'ajut rebut durant la meva estada a Texas A&M University at Galveston.

Finalment, als meus pares.

STUDY OF LOW-DIMENSIONAL
STRONGLY CORRELATED ELECTRON SYSTEMS
BY A TRANSFER MATRIX TECHNIQUE

Contents

INTRODUCCIÓ

Els sistemes de baixa dimensionalitat han sigut i són atractius als físics per diverses raons:

- A nivell estrictament teòric són els sistemes més senzills d'estudiar, i, de fet, molts models no trivials en tres dimensions que sols poden tractar-se fent aproximacions intel.ligents, s'han resolt exactament en una dimensió. Aquesta característica els fa adients per a analitzar l'eficàcia dels mètodes aproximats que després s'aplicaran a sistemes més complicats.

Però, simultàneament, la baixa dimensionalitat els confereix d'unes propietats específiques no presents en sistemes de més dimensions.

- Experimentalment s'han trobat sistemes reals que presenten un comportament de tipus uni i bidimensional. En particular, existeixen dues famílies de gran interès tant des del punt de vista teòric com del tecnològic. Aquests són els **polímers conjugats** (poliacetilè, poliacè, poliacenacè, polifenantrè, etc.), sistemes que poden classificar-se com a *quasi-1 dimensionals*. I els **materials superconductors d'alta Temperatura de transició** (òxids de coure principalment) que són sistemes fonamentalment *bidimensionals*.

En aquest treball ens centrarem en aquestes dues famílies de sistemes esmentats.

Els **polímers conjugats** [Hayes 85] són sistemes formats bàsicament per carboni i hidrogen. Fent un anàlisi senzill de l'estructura electrònica, el seu estudi pot reduir-se a un model d'una xarxa plana amb diferents geometries, segons el polímer a tractar, amb un electró π per centre. Per exemple, el poliacè consisteix en una cadena d'hexagons on a cada vèrtex hi ha associat un electró.

Una part important en l'estudi d'aquests materials és determinar quines són les interaccions importants que hi intervenen.

La majoria de treballs sobre aquests sistemes tals com el de Yamabe *et al.* [Yamabe 82], Kertesz *et al.* [Kertesz 83], o Bozović [Bozovic 85] entre d'altres, fan un tractament per *teoria de Bandes* on es negligeix la repulsió de Coulomb.

Existeixen, però, una sèrie de resultats experimentals [Tavan 79], [Hudson 82], [Kuroda 87] que no concorden amb les prediccions de la teoria de Bandes i que

porten a concloure que cal tenir en compte la **correlació electrònica** per a una descripció correcta del comportament d'aquests sistemes.

Una altra interacció important a tenir en compte és la dels electrons amb les vibracions de la xarxa -o interacció **electró-fonó**-. En el context de l'aproximació d'electrons lliures aquesta interacció és considerada la responsable de la *inestabilitat de Peierls* [Peierls 55], o, dit d'una altra manera, és considerada responsable de que alguns d'aquests sistemes presentin trencament d'alguna simetria que fa que tinguin un comportament de semiconductor o aïllant enlloc de metal.lic. Propietats potencials d'aquests materials com la de ser conductors o superconductors depenen en gran mesura d'aquesta inestabilitat.

Els **materials superconductors d'alta Tc** ($La_{2-x}Ba_xCuO_4$, entre d'altres) són sistemes tals que a $x = 0$ són aïllants antiferromagnètics tridimensionals, i quan hi ha una petita fracció de substituyents que aporten menys electrons al sistems, $x \neq 0$, $x \ll 1$, presenten un comportament bàsicament bidimensional i passen a ser superconductors amb temperatures de transició altes -de l'ordre de $60K$.en el $La_{2-x}Ba_xCuO_4$, o $90K$ en d'altres compostos com és el $YBa_2CuO_{7-\delta}$ -. El que és interessant és que els resultats experimentals [Bednorz 88], entre d'altres peculiaritats, evidencien que es tracta de materials amb **forta correlació electrònica**.

La complexitat d'aquests sistemes pot reduir-se en una primera, però raonable aproximació a un model d'una xarxa quadrada amb un electró per nus on l'efecte de treure un petit nombre d'aquests electrons els converteix en superconductors. En la selecció de les interaccions que regeixen el comportament d'aquests materials, una de les importants és la repulsió Coulombiana entre electrons.

Així doncs, s'observa que els polímers conjugats i els superconductors d'alta Tc constitueixen dues famílies de sistemes de **baixa dimensió** on la **correlació electrònica** juga un paper destacat. La repulsió de Coulomb és difícil de tractar per ser una interacció a dos cossos en un problema de molts cossos, i això força a utilitzar models aproximats per a descriure aquests sistemes. Hi ha a la literatura essencialment dos mètodes per a estudiar els problemes de molts electrons: La teoria de **Bandes** i la teoria d'**Enllaç de València (VB)**.

En el primer mètode, potser el més estès en quan a utilització, es redueix el problema de molts cossos a equacions d'un sol electró. Els valors de les energies per aquest electró independent són les bandes d'energia i les interaccions donen lloc a

transicions entre els estats d'un electró. Dins d'aquest esquema hi ha diferents nivells d'aproximació. La separació en equacions d'un sol electró pot fer-se tot i negligint la repulsió de Coulomb entre els electrons o be incorporant-ne un valor promig de forma autocoherent, com en l'aproximació de Hartree-Fock. La correlació electrònica ha d'introduir-se posteriorment, per exemple, de forma pertorbativa, encara que això porta a càlculs complexes.

En la teoria VB, es considera els electrons fortament correlacionats. És un punt de vista d'electrons *localitzats*. Els electrons es distribueixen en els orbitals atòmics, i cada distribució possible defineix un estat de la base d'estats del sistema.

Aquest segon esquema ha estat durant molt de temps una descripció no gaire utilitzada. Per una banda, perquè el nombre d'estats possibles augmenta de forma considerable al augmentar el tamany dels sistemes. I, per altra banda, la teoria de Bandes o electrons independents semblava, en principi, donar prediccions satis-factòries per a la majoria de sistemes.

Però, com ja s'ha esmentat i es conclourà explícitament d'aquest estudi, el bon funcionament de la teoria de Bandes deixa de ser cert en sistemes on no pot negligir-se la repulsió Coulomb, entre ells els dos grups que presentem: els polímers conjugats i materials superconductors d'alta Tc. La inclusió de la correlació electrònica "a posteriori", com una pertorbació, comporta sempre una gran complexitat. Per altra banda, els resultats que s'obtenen depenen fortament del mètode utilitzat i són sovint contradictoris [Dixit 84]. En canvi, quan es parteix del límit d'electrons fortament correlacionats es troba un bon acord amb els resultats experimentals fins i tot en aproximacions senzilles. Es per això que una descripció del segon tipus, d'electrons localitzats, és la que ha estat adoptada en aquest treball.

Així doncs, els objectius que ens hem plantejat en la realització d'aquesta Tesi han sigut:

(1) Descriure els nostres sistemes tot i utilitzant l'esquema d'electrons **fortament correlacionats** amb la teoria VB. Teoria on, per pròpia definició, queda assegurada la inclusió de la repulsió de Coulomb entre electrons.

(2) Introduir la utilització de noves tècniques per a dur a terme els càlculs. Presentarem un mètode basat en una *Matriu de Transferència* que permetrà obtenir el valor de magnituds importants com és l'energia i funcions de correlació, en termes d'expressions analítiques senzilles. El problema en la teoria VB de tenir un gran

4

nombre d'estats possibles per als sistemes que es descriuen es simplifica notablement utilitzant aquesta tècnica junt amb consideracions justificades respecte als sistemes i abast de les interaccions.

(3) Dins del marc de la teoria VB, els pocs treballs realitzats fins ara, estan dedicats a l'estudi de l'estat fonamental dels sistemes i gairebé no existeixen estudis d'excitacions utilitzant aquest punt de vista d'electrons localitzats. En general s'adopten teories de camp mig o Hartree-Fock . Una part d'aquesta Tesi està dedicada a desenvolupar en l'esquema de la teoria VB, un tipus d'excitacions sobre l'estat fonamental que es caracteritzen per:

- incloure *correlació electrònica*. I, a la vegada,

- proporcionen un esquema de *bandes* que permet una interpretació en termes de *quasipartícules*.

(4) També ha estat del nostre interés contrastar les prediccions obtingudes de les dues aproximacions oposades, és a dir, des del model d'electrons independents (teoria de Bandes) i des del model d'electrons fortament correlacionats.

En el Primer Capítol es presenta un estudi de la natura de l'estat fonamental d'una família de polímers conjugats amb un electró π per centre dels quals es tracta explícitament una propietat característica de la *baixa dimensionalitat*, l'anomenada *inestabilitat de Peierls*. Els sistemes que s'han escollit són el poliacenacè, el poli(benz[m,n])antracè (PBA), el poliperilè i el polifenantrè.

El poliacenacè és interessant pel fet de que ha sigut un sistema força estudiat, principalment per teoria de Bandes a diferents nivells d'aproximació i els resultats que s'obtenen respecte el seu comportament són contradictoris. Experimentalment no s'ha aconseguit encara sintetitzar.

El PBA és un sistems amb característiques estructurals semblants al poliacenacè però no hi ha gaires treballs teòrics sobre el seu comportament, encanvi, experimentalment hi ha indicis de que es podrà sintetitzar, fet que el fa molt atractiu.

El poliperilè, ha sigut sintetitzat i estructuralment és diferent als dos sistemes anteriors.

I, per últim, el polifenantrè, el cual, dins l'esquema de teoria de bandes més elemental (*model Hückel*) té un comportament diferent als anteriors sistemes. El poliacenacè, PBA i poliperilè són sistemes sense gap energètic mentre que el polifenantrè presenta gap. És un sistema que ha sigut sintetitzat.

La *inestabilitat de Peierls* és analitzada en aquests sistemes des del punt de vista de teoria de Bandes (amb el *model Hückel*) i des del punt de vista d'electrons fortament correlacionats, és a dir, teoria VB, amb el *model de Heisenberg* que es justifica convenientment en el límit de correlació electrònica important.

L'energia de l'estat fonamental en l'esquema VB es calcula amb l'ajut del *Principi Variacional* tot i escollint assaigs adients per a la funció d'ona de l'estat fonamental. Els assaigs són expansions en subsistemes, els estats dels quals, s'associen a paràmetres variacionals a optimitzar.

Aquest Primer Capítol està dividit en tres parts. En la primera s'introdueixen els sistemes a tractar, les seves propietats, i els models que s'utilitzen per a descriure el seu comportament, així com els problemes generals que comporta el seu estudi. En la segona part es presentem els models que s'adoptaran en aquest estudi i es descriuen les tècniques utilitzades per a resoldre'ls, que inclou, el mètode de la Matriu de Transferència. Es donarà com a exemple el càlcul explícit per a un dels sistemes. En la tercera part, els resultats obtinguts són discutits.

En el Segon Capítol es presenta una petita contribució a l'estudi dels nous materials superconductors d'alta Tc, que constitueixen un exemple recent i molt interessant de sistemes on els electrons estan fortament correlacionats. Es justifica que un model adient per a tractar aquests sistemes és l'*hamiltonià de Hubbard* que en el límit de forta correlació electrònica i exactament un electró per centre pot reduir-se a un *hamiltonià de Heisenberg*. S'ha centrat l'estudi a obtenir informació sobre la natura de l'estat fonamental d'aquests sistemes, aprofitant les tècniques i els coneixements prèviament desenvolupats en el Primer Capítol per als polímers conjugats.

Finalment en el Tercer Capítol s'introdueix un tipus d'estats excitats sobre l'estat fonamental per a sistemes quasi-1-dimensionals, particularitzant al cas de polímers conjugats amb un electró π per centre des de l'optica de la teoria d'Enllaç de València. Aquestes excitacions tenen caràcter de *singulets neutres*. Cal destacar, per una banda, que mentre que l'efecte de la correlació electrònica és tingut en compte, de forma aparentment paradoxal s'obté un esquema de *bandes*, fet que seria característic d'un tractament d'electrons independents.

Els càlculs són possibles, com en els capítols anteriors, gràcies a la tècnica de la Matriu de Transferència. Aquest estudi s'aplica, explícitament, a una cadena de polifenantrè que permetrà una comparació dels resultats obtinguts i els experimentals.

INTRODUCTION

The low-dimensional systems are very attractive to physicists for various reasons:

- Theoretically, they are the simplest systems to study and, in fact, many non-trivial models in three dimensions that can only be treated approximately, have been solved exactly in one dimension. This feature makes them suitable for testing the effectiveness of the approximate methods that are to be used for more complicated systems.

But, simultaneously, the low dimensionality is the cause of some interesting properties not present in higher-dimensional systems.

- Experimentally, some real systems show a one- and two- dimensional behaviour. Particularly, there are two families of great interest not only theoretical but technological as well. These are the **conjugated planar polymers** or π-network systems (polyacetylene, polyacene, polyacenacene, polyphenanthrene, etc.), systems that can be classified as being *quasi-1-dimensional*. And the **new High-Tc superconductors** (mainly copper oxides) which are fundamentally two-dimensional systems.

In this work we are going to focus our attention specially on these two families of systems.

The **conjugated planar polymers** [Hayes 85] are systems formed basically by carbon and hydrogen. Doing a simple analysis of the electronic structure, their study can be reduced to a planar lattice model with different geometries depending on the polymer and with a π-electron per site. For instance, polyacene consists on a chain of hexagons where in each vertex there is an electron associated.

The fundamental part in the study of these systems is the determination of the important interaccions that are to be considered.

Most of the work about these systems as that of Yamabe *et al.* [Yamabe 82], Kertesz *et al.* [Kertesz 83] or Bozović [Bozovic 85] among others, do a treatment using *Band theory* where Coulomb repulsion is neglected.

Nevertheless, there are some experimental results [Tavan 79], [Hudson 82], [Kuroda 87] that don't agree with the predictions given by independent electron the-

ory. From them, it can be concluded that **electron correlation** must be considered for a correct description of these systems.

Another important interaction to be taken into account is that of the electrons with the lattice vibrations -or **electron-phonon** interaction-. In the context of independent electron approximation this interaction is considered responsible for the *Peierls instability* [Peierls 55] or, what is equivalent, for the fact that some of these systems show a broken symmetry that causes a transition from metallic to an insulator or semiconductor behaviour. Potential properties as being conductors or superconductors depend drastically on this instability.

The **new High-Tc superconductors** ($La_{2-x}Ba_xCuO_4$, among others) are systems that, when undoped ($x = 0$), are three dimensional antiferromagnetic insulators and when a small fraction of doping is introduced, $x \neq 0$, $x \ll 1$, they become superconductors with a two-dimensional behaviour. The transition temperatures to the superconducting state are high -from the order of 60K in $La_{2-x}Ba_xCuO_4$ to about 90K in $YBa_2CuO_{7-\delta}$-. It is interesting to note that experimental results [Bednorz 88] show, among many peculiarities, that they are **strong electron-correlated systems**.

The complexity of these systems can be reduced in a first, but reasonable approximation to a square lattice model with an electron per site that become superconductors when a small number of electrons is taken out. When selecting the interactions that lead the behaviour of these materials, the Coulomb repulsion cannot be neglected.

Therefore, we observe that the conjugated planar polymers and the Hi-Tc superconductors are two families of **low-dimensional** systems where the **electron correlation** is important. Coulomb repulsion is a difficult interaction to handle because it is a two body interaction in a many-body problem. This fact forces the use of approximate models to describe these systems. In the literature there are two alternative approximations to the real problem: **Independent electron** model and **Valence Bond** theory (VB).

In the first method, perhaps the most used, the description of a many-body system is reduced to a one-electron problem. Energy values for these independent electrons are grouped in energy bands and the interactions are supposed to produce transitions among one electron states. Within this scheme there are different levels of

approximation. The separation in one-electron equations can be done by neglecting completely the Coulomb repulsion or introducing self-consistently an average value as in the Hartree-Fock approximation. Electron correlation has to be introduced afterwards as a perturbation, though computations become cumbersome.

In VB theory, electrons are considered to be **strongly correlated**. It is a *localized* electron point of view. The electrons are distributed among the atomic orbitals, and each possible distribution defines a basis state upon which eigenstates are built.

This second scheme has not been practically used for a long time because the number of possible states increases enormously with the size of the system. Furthermore, Band theory seemed, at the beginning, to give satisfactory predictions for the majority of systems, so that VB theory remained aside.

Nevertheless, as previously mentioned and as it will be explicitly shown in this study, Band theory arguments are not valid anymore in systems where Coulomb repulsion cannot be neglected, among them the two groups that are here presented: polymers and Hi-Tc superconductors. 'A posteriori' inclusion of electron correlation as a perturbation is always difficult and results depend strongly on the method used. On the other side, when the strong electron correlated limit is considered, agreement with experimental results is accomplished. Therefore, a description of localized electrons has been adopted in this work.

We have focus our attention on:

(1) Describing our systems from the **strong electron correlation** point of view, with VB theory. Theory where, by definition, the inclusion of Coulomb repulsion is considered.

(2) Introducing new techniques to carry out computations. A method based on a *Transfer Matrix* will be presented. With this method the value of important magnitudes like the energy and correlation functions are obtained as simple analytic expressions. The problem in VB theory of having many possible states to describe the system is simplified when using this technique together with some justified considerations on the systems and range of interactions.

(3) Within VB theory scheme, the scarce work done up to now is mainly focused on ground states and not much has been done about excited states, where usually

mean-field theories have been adopted. One of the chapters of this disertation is devoted to develop, using VB theory, a kind of excitations on the ground state that:

- Include *electron correlation*. And, at the same time,
- a *band picture* is obtained that allows a *quasiparticle* interpretation.

(4) It has been also of our interest to compare predictions obtained using both limits, i.e. band theory limit and strong-electron correlated limit.

In the First Chapter, a study on the ground state nature of a family of conjugated planar polymers with one π electron per site is presented and a property characteristic of the *low-dimensionality*, namely *Peierls instability*, is explicitly studied. The systems that have been chosen are polyacenacene, poly(benz[m,n])antracene (PBA), polyperylene and polyphenanthrene.

Polyacenacene is interesting because a lot of discussion about it already exists in the literature, basically from band theory studies at different levels of approximation and the results obtained are contradictory. Experimentally it hasn't been synthesized yet.

PBA is a system with similar structural characteristics to polyacenacene but there isn't much theoretical work on its behaviour. Experimentally there is the possibility of being synthesized, what makes it quite attractive.

Polyperylene, structurally is different to both previous systems but it has been synthesized.

And, the last one, polyphenanthrene, has already been synthesized and, when described by band theory (Hückel model) a different behaviour from the previous systems is predicted. Polyphenanthrene has a non-zero band gap while the preceding ones are zero-width band gap systems. In the Third Chapter some of its low lying excited states will be constructed.

These systems are analyzed from Band theory point of view (with *Hückel* model) and from the strong electron correlation point of view, i.e. VB theory, with *Heisenberg* model, that is adequate in this limit.

The ground state energy, within VB theory, is obtained using the *Variational Principle*, choosing adequate ansätze for the ground state wavefunction. These ansätze are variational localized-site cluster expanded wavefunctions.

This First Chapter is divided into three parts. The first part consists on an introduction to the systems, properties, models used to describe their behaviour

11

and general problems that appear in their study. In the second part, the models here adopted are presented and the techniques used to solve them are described. Particularly, a **Transfer Matrix** is presented. As an example of how to deal with this method, an explicit computation for one of the systems is given. In the third part, results are discussed.

In the Second Chapter, a small contribution to the study of the new Hi-Tc superconductors which are a novel and very interesting example of strongly correlated systems, is presented. We shall justify that a suitable model to treat these systems is the *Hubbard hamiltonian* which, in the limit of strong electron correlation and exactly one electron per site, can be reduced to the *Heisenberg hamiltonian*. The study has been focused on obtaining information about the ground state nature of these systems, taking advantage of the techniques and knowledge developed for polymer systems in the First Chapter.

Finally, in the Third Chapter, a kind of excited states built upon the ground state are obtained for quasi-1-dimensional systems, particularizing to the conjugated planar polymers with one π electron per site. These excitations characterize for being *neutral singlets* which include the electron correlation effects. It is worthwhile to note that a *band picture* is recovered while electron correlation is included.

Computations are possible here, as well as in previous chapters, by the Transfer Matrix technique.

This study is applied explicitly to a polyphenanthrene strip that enables us to compare our results with experimental ones.

Ground State and related properties of a family of quasi-1D planar polymers.
Introduction

Contents

1 INTRODUCTION

Quasi-1-dimensional materials, such as *extended conjugated polymers* (see Fig. 1 (*b*) to (*f*)) have been suggested for a long time to be systems with potentially novel properties: metallic conductivity, stability in air, high-temperature superconductivity, ferromagnetic ordering, etc. [Pohl 67] , [Rembaum 70] , [Graovac 77] , [Ovchinnokov 77] , [Duke 82] , [Burdette 84].

1.1 Polyacetylene

Polyacetylene (see Fig. 1 (*a*)) is the most simple system in this family of conjugated polymers. It can be though as a system with one electron per site. The electronic structure of such planar chain can be described as follows. Each site is occupied by a carbon atom. A carbon atom has four valence electrons, three of them are in sp^2 orbitals and form saturated σ bonds (symmetric with respect to reflections in the plane of the system) with neighboring carbon and hydrogen atoms. The fourth electron -π electron- has the symmetry of a $2p_z$ orbital, with OZ axis perpendicular to the system plane.

The σ electrons form a filled band and the π electrons, at a rate of one per site, form an outer half-filled band. Consequently, this system should be a *metal* from band theory point of view. Nevertheless, experimental results show that polyacetylene is a *semiconductor*.

The reason of this disagreement has been attributed to the existence of a **Peierls transition** [Peierls 55]. The vibration of the atoms in the polymer chains favours an alternated structure with *two* atoms per unit cell, as a result, a band-gap opens at the Fermi level and the system is not a metal anymore. (See Fig. 3 where the band structure of a (*a*) regular and (*b*) distorted chain has been drawn.)

Experimentally, this bond alternancy is observed in *polyenes* (i.e. finite planar chains) [Yannoni 83], so that this seems to justify the use of these one-particle models where electrons move independently.
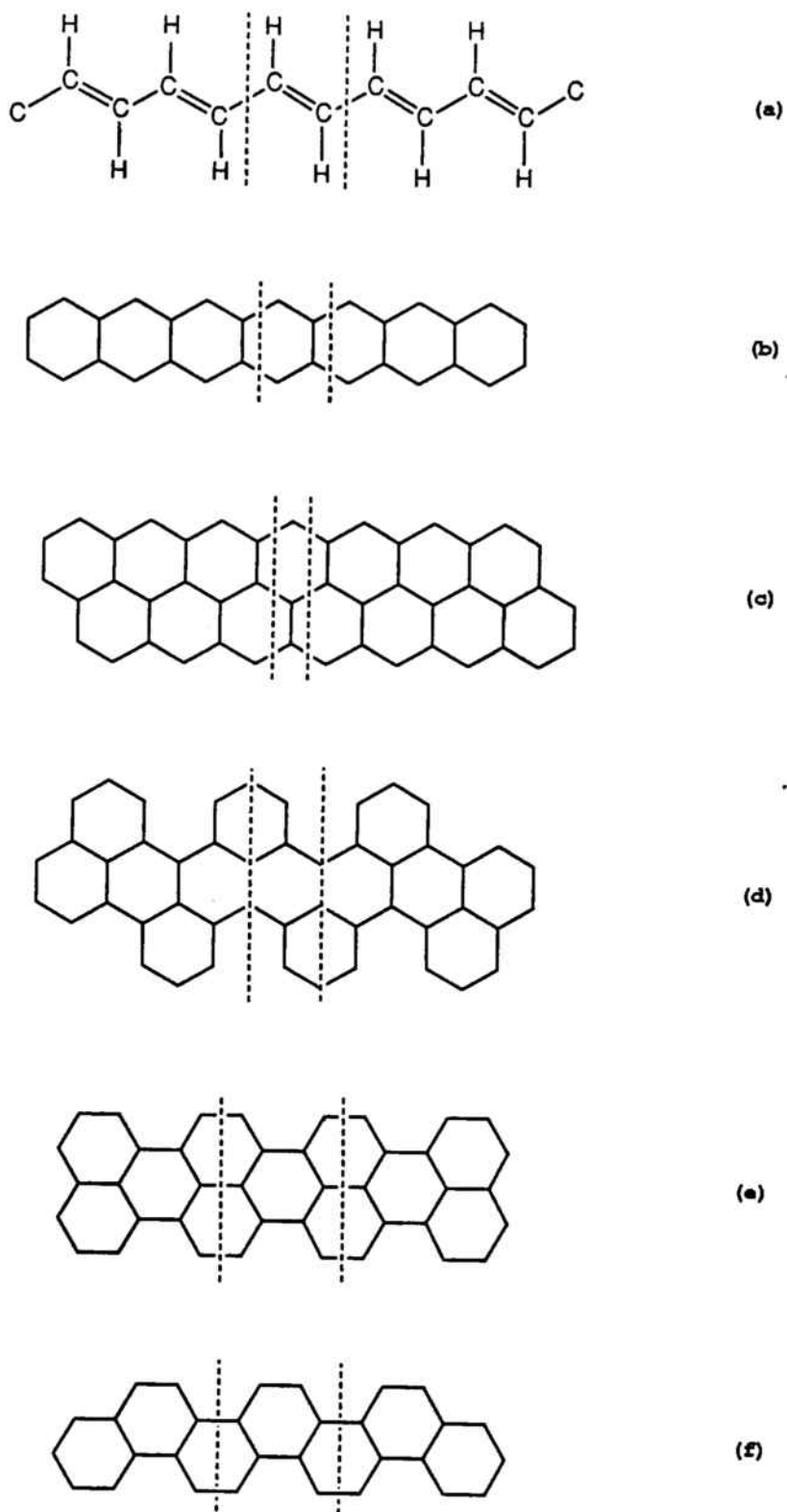
Figure 1: Polymer systems. Fragments of: (a) Polyacetylene. (b) Polyacene. (c) Polyacenacene. (d) PBA^* (see Fig. 2) (e) Polyperylene. (f) Polyphenanthrene. The zone between vertical dashed lines defines the "unit cell" of these systems. For Polyacenacene and PBA the "reduced unit cell" has been drawn instead.
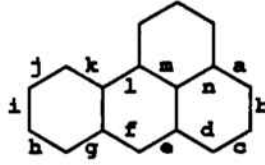
18

Figure 2: The name of this polymer is poly(benz[m,n]anthracene). As an abbreviation it will be called PBA
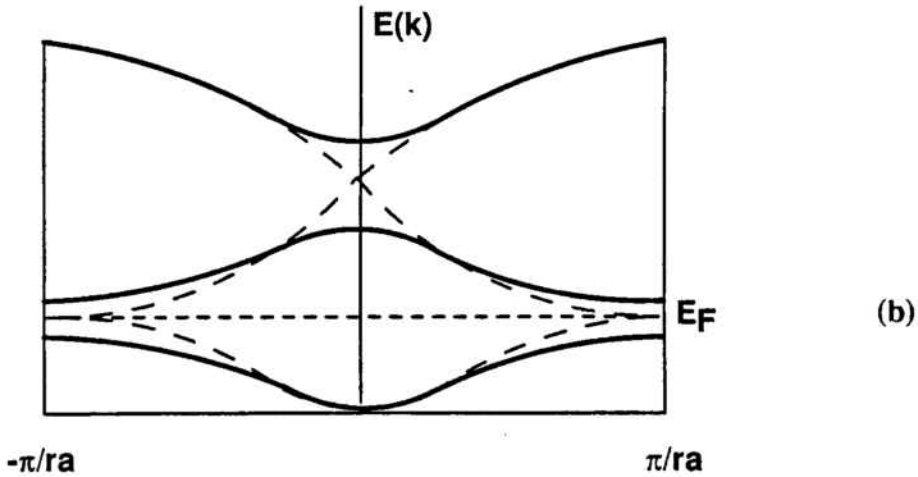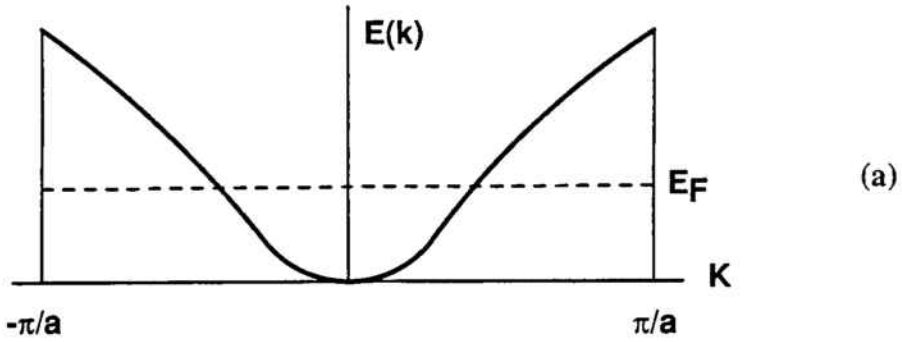
Figure 3: (a) Energy curve $\epsilon(k)$ for an electron in the potential of a regular chain with a intersite distance. The system has one electron per unit cell, therefore is half-filled (The Fermi level, ϵ_F, is in the middle of the band) and it is a metal. (b) When the chain distorts by atom displacement, repeating this displacement every r^{th} atom, the unit cell increases by r and the Brillouin zone reduces by a factor of r, the band splits and a band gap is opened at the Fermi level.

In fact, the theoretical work has mainly been focused on *single-particle* models. They are based on three assumptions:

1) Electron repulsion is *negligible*, consequently, electrons move freely and the low-energy excited states involve promoting single electrons from the closed-shell ground state.

2) σ and π electron motion is separated. Electrons move only among $2p\pi$ orbitals.

3) No change in geometry is considered when studying the ground and excited states.

One of the most used is the SSH (Su-Schrieffer-Heeger) model hamiltonian [Su 80] that, within the band theory picture, incorporates explicitly only the e-lectron-phonon interaction responsible for the Peierls distortion. These one-particle models have been very attractive because most relevant quantities (like the Peierls distortion just mentioned) could be easily calculated. This provided, for some time, a good reason for not including many-body effects, the more since those are diffi-cult to handle. However, it is becoming clear that effective single-particle models can, at most, give a qualitative description of conjugated polymers since they miss important experimentally observed features as:

- Ordering of excited states in finite polyenes [Tavan 79] , [Hudson 82].
- Negative spin densities on alternate carbon atoms [Thomann 83] , [Kuroda 87].
- The strong shift of neutral soliton absorption from the "mid - gap"
[Weinberger 84].

In particular, the first reason mentioned has been very determinative in eviden-cing band-theory failure for describing these systems. It will be discussed below in detail.

Single-particle models and, more specifically approximate molecular orbital theo-ries, predict for finite polyenes that, being the ground state a 1^1A_g state, the first *singlet* excited state is a 1^1B_u state (A, B, g, u are symmetry labels. A (B) denotes that the state is symmetric (antisymmetric) with respect to a 180^0 rotation around the symmetry axis and g (u) that is symmetric (antisymmetric) with respect to inversion at the symmetry center). These theories account quite reasonably for the properties of the $1^1A_g \longrightarrow 1^1B_u$ transition seen in *absorption* spectra.

In *emission* spectra, octatetraene and longer polyenes *fluoresce* and the origin of this fluorescence is significantly *shifted* from the $1^1A_g \longrightarrow 1^1B_u$ *absorption* origin. This *emission* was originally thought to originate from the 1^1B_u excited state, but this left with the problem of accounting for the lack of overlap between *absorption* and *emission*.

It is now well stablished [Hudson 82] that for long polyenes the *emission* derives from a different excited state that the one responsible for the strong *absorption*. It is a $2^1A_g \longrightarrow 1^1A_g$ transition, so defined through a comparison of the one-photon forbidden two-photon allowed character of the transition (g to g).

The evidence for this 2^1A_g state, not predicted by single-particle models, below the 1^1B_u state in long polyenes, implies that these models have to be revisited.

Although the three restrictions used in single-particle models contribute to the failure in explaining the existence of the 2^1A_g state, **neglecting the electron correlation** seems the most significant one.

1.2 MO theory versus VB theory

The motion of π electrons is constrained by two opposing interactions: the so-called *Hückel resonance interaction* (or kinetic energy) that tends to *delocalize* the π electrons. And the *Coulomb repulsion* that induces *localization* of π electrons at different atomic sites. When this last interaction is taken into account the system is called a *correlated* system because the motion of an electron depends on the position of the others.

Two limiting cases can be studied depending on which of those interactions is considered dominant. On one side, **Molecular Orbital** (MO) theory (or band theory) reduces the many-electron problem to one-electron equations by neglecting electron Coulomb repulsion. Molecular orbitals are defined as linear combinations of atomic orbitals. It is a one-particle theory and it yields good results for the *absorption* transitions in linear polyenes, mentioned previously, but fails in predicting the 2^1A_g excited state, apart from other phenomena.

On the other side, **Valence Bond** (VB) theory which corresponds to the opposite view where electrons are taken to be strongly correlated, it is a *localized* view. Electrons are distributed over the possible atomic orbitals, assigning each electron to a particular site. Each of the possible distributions defines a trial state. This theory has been thought for years not to be very useful because, among other reasons, the

21

number of basis states increases considerably with systems size and computations become cumbersome. But, with the experimental confirmation that in some systems electron repulsion is important (i.e. polymers, the new high-Tc superconductors...), VB theory has obtained more and more recognition in being very suitable for studying them. And, in particular, it accounts for the 2^1A_g state, which can be thought as a VB excitation [Hudson 82], [Valenti 87].

Although MO theory and VB theory correspond to two complementary limiting descriptions of a system, what the finding of a 2^1A_g excited state shows is that **electron Coulomb repulsion cannot be neglected in these systems.**

1.3 Extended Polymer Systems

The important conclusions reached in polyacetylene have awoken interest in extending the study to π-network polymers other than polyacetylene. These systems can be represented as strips very long in one direction and narrower in the transverse direction where each site is occupied by a π-electron. They are assumed translationally invariant and the strip can be divided into "unit cells". (See Fig. 1 (b) to (f)).

Much semiempirical work based on *band theory* models has been done about these systems, [Heeger 81], [Bredas 82], [Yamabe 82], [Kivelson 83], [Kertesz 83], [Tanaka 84], [Boudreaux 85], [Bozovic 85]. Most of it concerns calculations on different individual polymers.

As well as in polyacetylene, the importance of *electron correlation* in these systems is a subject of debate.

Klein *et al.* [Klein2 86] overviewed some qualitative features of these materials like occurrence of long-range ordering, lattice distorsions and solitonic excitations focusing on the two simplest complementary points of view, namely, that of the *Hückel MO model* (independent-electron picture) and that of simple *Resonance theory* which is a localized VB scheme and consists on Kekulé-structures (or nearest-neighbor valence bond states) counting. This study was an interesting attempt to

(i) describe these systems from a localized view where electron correlation can be accounted for and,

(ii) contrast predictions and find correspondences from two opposite simple pictures.

22

Following this philosophy, we have studied a family of π-network polymers with simple models and going beyond simple models in order to obtain conclusive results. Although few of these systems have been synthetized, from what is known about them and polyacetylene, it is of general belief (recent comment papers [Campbell 87]) that a proper treatment should incorporate **electron correlation** for the correct description of both, ground and excited states.

Including electron correlation is difficult when starting from the independent-particle limit. The alternative *localized* VB description has been adopted in this work in order to approach the physical reality of these systems with a constant comparison to band-theory predictions. Such phenomena as the *Peierls instability*, which is a controversial property in extended polymer systems, will be studied.

In the next section the model Hamiltonian used is introduced and the corresponding limiting cases discussed. In section 3 the Peierls instability phenomenon is presented and examined. Finally, the symmetries and possible distortions for the studied systems are discussed in section 4.

2 EFFECTIVE HAMILTONIAN

The effective hamiltonian most often employed within the context of conjugated π-electron systems that takes into account the interaction terms governing the π electrons motion, is the PPP (Parisier - Parr - Pople) hamiltonian [Salem 66], [Suzuki 67].

In terms of creation / annihilation operators, i.e., $c_{i\sigma}^{+}$ ($c_{i\sigma}$) operator which creates (annihilates) a π-electron with spin σ in an atomic orbital Ψ_i (Ψ_i are assumed to be mutually orthogonal), and with anticonmmuting relations:

$$\{c_{i\rho}^{+}, c_{j\sigma}^{+}\} = 0,$$
$$\{c_{i\rho}, c_{j\sigma}\} = 0,$$
$$\{c_{i\rho}^{+}, c_{j\sigma}\} = \delta_{ij}, \tag{2.1}$$

the PPP hamiltonian can be written as a sum of three terms,

$$H_{PPP} = H_0 + H_1 + H_2 \tag{2.2}$$

23

that depend on a set of energy parameters R_{ij} , I_i , t_{ij} which are related, approximately, to energy expectation values of Ψ_i. R_{ij} stands for the effective Coulomb interaction between electrons and cores at sites i and j. I_i is the effective ionization potential of a π electron at site i and t_{ij} is the hopping integral (or Hückel resonance integral) of an electron between centres i and j, $t_{ij} < 0$.

- H_0 accounts for the repulsion between atom cores:

$$H_0 = \sum_{i<j} R_{ij} \tag{2.3}$$

- H_1 contains the electron-core attraction term and the Hückel resonance interaction (or kinetic term) that acts on one electron at a time:

$$H_1 = \sum_{i,\sigma}(-I_i - \sum_{j\neq i} R_{ij})c_{i\sigma}^+ c_{i\sigma}$$
$$+ \sum_{<i,j>\sigma} t_{ij}(c_{i\sigma}^+ c_{j\sigma} + c_{j\sigma}^+ c_{i\sigma}) \tag{2.4}$$

where $< i,j >$ denotes that j is nearest neighbor to i.

- H_2 denotes the Coulomb repulsion between electrons

$$H_2 = \frac{1}{2} \sum_{ij,\sigma\rho} R_{ij} c_{j\rho}^+ c_{j\rho} c_{i\sigma}^+ c_{i\sigma} \tag{2.5}$$

the summation excludes all terms $(j,\rho) = (i,\sigma)$.

The resolution of this hamiltonian is almost impossible due to the large number of degrees of freedom that contains. Even in the case of restricting the calculation to a minimum set of atomic orbitals and neglecting nuclear motion, a system of $2N$ π electrons (N being the number of sites) has $\frac{(4N)!(2N)!}{(4N-2N)!}$ different states . If only states corresponding to a given total spin are considered, the number of states is further reduced, but still is very large.

A simplification of the PPP model is the *Hubbard* hamiltonian:

$$H_{Hub} = t \sum_{<i,j>\sigma} (c_{i\sigma}^+ c_{j\sigma} + c_{j\sigma}^+ c_{i\sigma}) + U \sum_i c_{i\uparrow}^+ c_{i\uparrow} c_{i\downarrow}^+ c_{i\downarrow} \tag{2.6}$$

where $t = t_{ij}$ and $U = R_{ii} - R_{ij}$ for all values of i and j nearest neighbors. This approximation neglects the Coulomb repulsion between non-onsite electrons. It is

the simplest model that retains the flexibility to range from *metallic* to *atomic* regimes. Nevertheless it continues to be a difficult model to solve.

A further simplification is obtained if either H_1 or H_2 is assumed to dominate the π electron motion. The resulting two limiting cases that are obtained from the PPP hamiltonian are: **the independent-particle description (MO)**, when H_1 is the dominant term; and the **Dirac-Heisenberg description** induced by H_2. Those are the two descriptions we mentioned before and that are here recovered as limiting cases of the PPP hamiltonian.

2.1 Hückel Model

The Hückel model derives from the PPP model when domination of H_1 is considered with neglect of the electron-core attraction term. Then,

$$H_{Huck} = \sum_{<i,j>,\sigma} \beta_{ij}(c_{i\sigma}^+ c_{j\sigma} + c_{j\sigma}^+ c_{i\sigma}) \tag{2.7}$$

where i and j are neighboring sites, $\beta_{ij} \equiv t_{ij}$ is the "resonance integral" between sites i and j, for simplicity $\beta_{ij} = \beta$. $c_{i\sigma}^+$ ($c_{i\sigma}$) creates (destroys) an electron of spin σ in the orbital on site i. In the LCAO approximation, Molecular Orbitals are defined as linear combinations of atomic orbitals.

2.2 Heisenberg Model

The antiferromagnetic Heisenberg spin hamiltonian derives from the PPP model when H_2 is the dominant term; that is, in the strong electron correlation limit.

In this limit, after disregarding the hopping term, the lowest energy states of π systems are given by determinants,

$$\Phi = |\Psi_1\sigma_1\Psi_2\sigma_2...\Psi_n\sigma_n| \tag{2.8}$$

where each atomic orbital, Ψ_i, is occupied once. All 2^{2N} different spin configurations have the same energy. *Ionic* VB structures with one, two, ... doubly occupied atomic orbitals are higher in energy (because of H_2 being dominant). This spin degeneracy is lifted when the hopping term, t_{ij}, that allows electrons to move, is considered. The way this degeneracy is lifted is by splitting the singlet covalent states from the triplet covalent states.

A simple example to study this effect is that of two neighbor electron system. Their possible single determinant wavefunctions are:

$$\Phi_1 = |\Psi_1\alpha\Psi_2\alpha| \quad \Phi_2 = |\Psi_1\beta\Psi_2\beta|$$
$$\phi_3 = |\Psi_1\alpha\Psi_2\beta| \quad \phi_4 = |\Psi_1\beta\Psi_2\alpha|$$
$$\Phi_5 = |\Psi_1\alpha\Psi_1\beta| \quad \Phi_6 = |\Psi_2\alpha\Psi_2\beta| \tag{2.9}$$

where α and β stand for "up" and "down" spins respectively.

The two first determinants correspond to covalent triplet states, the two following can be coupled to a triplet and a singlet state respectively,

$$\Phi_3 = (\frac{1}{\sqrt{2}})(\phi_3 + \phi_4)$$
$$\Phi_4 = (\frac{1}{\sqrt{2}})(\phi_3 - \phi_4) \tag{2.10}$$

and Φ_5, Φ_6 are singlet ionic states. The corresponding hamiltonian matrix elements are:

$$\begin{pmatrix} R_{12} & 0 & 0 & 0 & 0 & 0 \\ 0 & R_{12} & 0 & 0 & 0 & 0 \\ 0 & 0 & R_{12} & 0 & 0 & 0 \\ 0 & 0 & 0 & R_{12} & 2t_{12} & 2t_{12} \\ 0 & 0 & 0 & 2t_{12} & R_{11} & 0 \\ 0 & 0 & 0 & 2t_{12} & 0 & R_{22} \end{pmatrix}$$

After diagonalizing, the covalent triplet states Φ_1, Φ_2, Φ_3 are not coupled. And the covalent singlet state Φ_4 is coupled to the ionic states Φ_5, Φ_6 lowering its energy. This singlet state experiences a splitting from the triplet covalent states. A perturbative computation in terms of the parameter $\frac{t_{12}}{R_{11}-R_{12}}$ (assuming $R_{22} = R_{11}$) yields, up to second order, to a value of the energy splitting,

$$2J = 2[\frac{t_{12}^2}{R_{11} - R_{12}}] \tag{2.11}$$

with $J > 0$ also called "exchange parameter". And the hamiltonian reduces to the *Heisenberg* model,

$$H_{Heis} = \sum_{<i,j>} J(\bar{S}_i\bar{S}_j - 1/4) \tag{2.12}$$

where $\bar{S}_i$ denotes the spin operator for one electron on site i.

The set of *covalent* structures doesn't allow a complete description of the π electron motion. But for **strong electron repulsion** $(R_{11} - R_{12}) \gg t_{12}$, the bands of *covalent* and *ionic* structures are clearly separated in energy by the amount of energy needed to move an electron to a neighboring occupied site. Then, in the *VB limit* one expects that ionic structures are not important for low-energy excited states and the *Heisenberg* hamiltonian is good enough to account for the important physics in this regime.

Effects of higher-lying states can still be included in effective "exchange parameter" values [Malrieu 82].

We have mentioned here the derivation of this hamiltonian via degenerate perturbation theory. It will be explicitly developed in the Second Chapter of this thesis, in the *Hi-Tc Superconductors* framework. There are alternative derivations, via cluster expansion techniques [Poshusta 89], that are appropiate even in many cases where perturbation theory appears inadequate.

This model hamiltonian will be used in the description of polymer systems **within VB scheme,** beyond *Resonance theory.*

3 PEIERLS / SPIN-PEIERLS INSTABILITY

Our interest in the extended polymer systems relies in that they have mainly been described with single-electron models (at different levels of approximation) being predicted to have interesting properties such as the so-called *Peierls instability.*

3.1 Generalities

Within a crude model that ignores electron-electron interactions, fluctuations, interchain interactions, etc., the *Peierls* theorem states that for every simple metallic **one-dimensional** (1D) polymer, i.e., a periodic chain of identical atoms with the conduction band partially occupied, the regular chain structure will never be stable since there always exists a static distortion Q (of amplitude Q and wavelength $\lambda = 2\pi/q$, q wavevector that belongs to the Brillouin zone) such that the following conditions apply:

(1) q is equivalent to $2k_F$ (k_F is the wavevector on the Fermi surface).

(2) Q breaks the symmetry of the chain.

(3) Q opens a gap Δ at the Fermi level E_F.

(4) Δ is proportional to Q, for small Q.

(5) The total electronic energy varies as $Q^2 ln Q$.

This distortion can be thought of originating from the *electron - phonon* interaction.

When dealing with **quasi-1D** systems, like the polymer strips in Fig. 1 (b) to (f), for which a structure in unit cells has been defined, there has been a lot of discussion whether the Peierls argument is still applicable. Many calculations have been done using band theory at different levels of approximation and different results are obtained:

- Tight-binding SCF-MO (Self Consistent Field - Molecular Orbital) method at the level of CNDO (Complete Neglect of Differential Overlap) [Yamabe 82].

- Pseudopotential techniques parametrized to reproduce one-electron energy levels (VEH) [Bredas 82]

- Hückel model and extended Hückel model (where the effect of σ electrons is considered) [Kertesz 83].

- SSH model [Kivelson 83].

- Tight-binding with line-group theoretical arguments [Bozovic 85].

In fact, Bozović [Bozovic 85] and Klein [Klein2 86] have managed to generalize Peierls theorem to extended π-systems within simple band-theoretic models.

Namely, when electron-electron interaction is neglected, the total energy is the sum of the occupied band-orbital energies. Then, a band is filled up to an orbital energy ϵ_F (Fermi energy) at which there is no band gap. There are different ways to realize this situation (see Fig. 4) (The first one is the corresponding to the original Peierls theorem, wavevector $k_F = \pm\pi/2$).

If there is a lattice distortion which mixes pairs of very nearly degenerate orbitals, their band-orbital energies should respond very nearly linearly to this off-diagonal perturbation. And, if one of the members of this pair of near-degenerate orbitals is just above the Fermi level and the other just below, this distortion should lower the ground state energy, so that it is **favored** to occur.
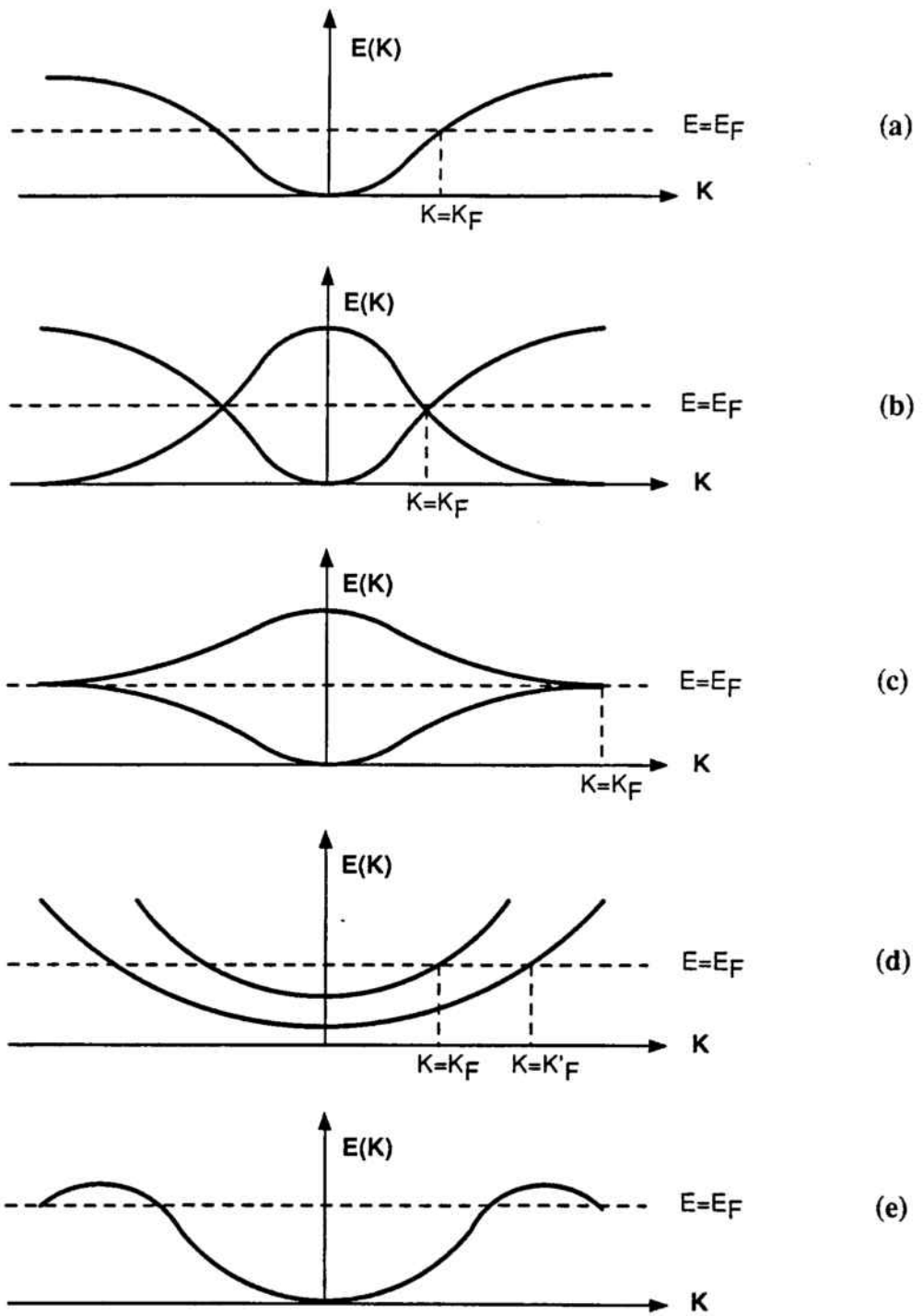
28

Figure 4: Five hypothetical types of band structures with zero-width band gap at the Fermi level ϵ_F.

This mixing can happen, among other possibilities, for

(a) Orbitals at wavevectors $k = k_F + \Delta k$ and $k' = \pm k_F \pm \Delta k$ originally in the same band. (See Fig. 4 (a))

(b) Orbitals at the same $|k| = |k'|$ in two bands intersecting at $k = k_F$. (See Fig. 4 (b) and 4 (c))

(c) Orbitals near k_F and $\pm k'_F$. (See Fig. 4 (d) and 4 (e))

A distortion increasing the unit cell size by n (and correspondingly dividing the Brillouin zone by n) allows this mixing if k and k' reduce to the same wavevector in the new smaller zone. When n is large, i.e. the distortion is comparatively global, the mixing and subsequent band-splitting will be small. The most interesting case is $n = 2$, the distortion corresponds to *dimerization*.

Depending on the shape of the band, a *distortion* opening a band gap can give rise to qualitative different *energy responses*.

In the simplest band theory model, i.e. Hückel model:

$$H_{Huck} = \beta \sum_{<i,j>,\sigma} (c^+_{i\sigma}c_{j\sigma} + c^+_{j\sigma}c_{i\sigma}) \tag{3.1}$$

a small perturbation can be expressed in terms of a parameter δ $(-1 < \delta < 1)$, introduced in the Hückel resonance integrals with *linear* dependence.

Since this perturbation is off-diagonal, the band-energy corrections will be of the order of δ^2, except when orbitals of nearly the same energy are mixed. If all nearly degenerate orbitals near a given energy ϵ are occupied, their perturbation doesn't affect the total energy because the off-diagonality of the perturbation guaranties opposed orbital energy corrections which cancel when summed. Only nearly degenerate orbitals near the Fermi surface are important.

A fast computation of the energy response to such perturbation is the following:

Supposing that the degeneracy is exact at the Fermi surface at wavevector $k = k_F$ and that near ϵ_F the zero order orbital energies (above and below ϵ_F) have a dependence $\sim |k - k_F|^n$, $n \epsilon Q$. We have that for a small perturbation $\sim \delta$, corrections for each orbital energy are $\sim \delta$. The average over these orbital corrections gives the total contribution to the ground state energy,

$$\sim \int_{q^n \leq \delta} \delta dq \sim \delta^{1+1/n} \tag{3.2}$$

where $q \equiv |k - k_F|$. Going up to second-order perturbation theory, the energy correction for each orbital is $\sim \delta^2/|k - k_F|^n$, then the total correction is,

$$\sim \int_{q^n \geq \delta} (\frac{\delta^2}{q^n})dq \sim \begin{matrix} \delta^2 ln\delta & n = 1 \\ \\ \delta^{1+1/n} & n > 1 \end{matrix} \tag{3.3}$$

The overall correction to the energy is, finally,

$$\Delta E \sim \begin{matrix} \delta^2 ln\delta & n = 1 \\ \\ \delta^{1+1/n} & n > 1 \end{matrix} \tag{3.4}$$

Then,

$\Delta E \sim \delta^2 ln\delta$ corresponds to Fig. 4 (a)

$\Delta E \sim \delta^{3/2}$ corresponds to Fig. 4 (c)

$\Delta E \sim \delta$ corresponds to a partially filled band of nonbonding orbitals.

These are band theory predictions whenever the system is submitted to an unstabilizing linear perturbation.

The Peierls argument has its analogous when the opposite limit, a localized model, is considered. Namely, an antiferromagnetic Heisenberg chain is unstable to displacements of sites along the chain. In this case the instability is called a **spin-Peierls** transition (**spin** because of Heisenberg Hamiltonian) and the reason for this transition can be attributed to the *spin-phonon* coupling.

Few computations exist within this picture for π-network extended polymer systems, where the original spin-Peierls phenomenon can be generalized. Attention has been focused in this direction, and comparisons to band-theory predictions will be made.

3.2 Spin-Peierls Model

A Spin-Peierls system can be described as a set of quasi-1D antiferromagnetic strips of spins $s = 1/2$ parallel distributed that only at very low temperatures

show a three-dimensional character. The antiferromagnetic interaction is considered only between neighbors of the same strip, neglecting the magnetic coupling between strips. The energy due to the phonons, which are 3D collective modes, can be expressed in terms of creation / annihilation boson operators:

$$\sum_{\bar{q},\alpha} w_0(\bar{q},\alpha) b_{q\alpha}^+ b_{q\alpha} \tag{3.5}$$

where $b_{q\alpha}^+$ ($b_{q\alpha}$) is the creation (annihilation) operator of a 3D phonon with wavevector $\bar{q}$ on branch α. And $w_0(\bar{q},\alpha)$ is the non-renormalized phonon energy.

The total hamiltonian is then:

$$H_T = H_H + \sum_{\bar{q},\alpha} w_0(\bar{q},\alpha) b_{q\alpha}^+ b_{q\alpha} \tag{3.6}$$

with

$$H_H = \sum_{<i,j>} J_{ij} \bar{S}_i \bar{S}_j \tag{3.7}$$

the Heisenberg hamiltonian ($< i,j >$ denotes that i and j are n.n.). The "effective" exchange energy J_{ij} is taken as a function of the three dimensional separation of sites i and j and of the *spin-phonon* coupling.

A simple description of the distortion effect between neighboring sites i and j can be given in terms of a parameter δ_{ij} so that

$$J_{ij} = J(1 + \delta_{ij}) \tag{3.8}$$

δ_{ij} measures the strength of the distortion, $-1 < \delta_{ij} < 1$, $J > 0$.

When the contribution of the Heisenberg term to the total energy (3.6) has a dependence in δ_{ij} faster than δ_{ij}^2 (for small δ_{ij}), a corresponding distortion is predicted at low temperatures. This is because that term will dominate the term due to the soft mode which has a δ_{ij}^2 dependence.

3.3 How does electron-electron interaction affect the Peierls Transition?

The inclusion of the electron-electron interaction in the study of the Peierls transition has awoken controversial opinions.

In the 1D case, the original explanation of the Peierls instability [Peierls 55] was done with band theory where the phonons, with wavevector $2k_F$ (k_F wavevector on the Fermi surface) couple to the electrons of the band and a band-gap is opened on the Fermi surface; the energy of the occupied band lowers and that of the empty band rises. So that *dimerization* is explained without considering electron correlation effects.

When the electron-electron interaction is included in these models as a *perturbation*, a lowering of the dimerization is predicted and this doesn't agree with experimental results.

But, on the other side, if the hamiltonian used describes the electron correlation from the beginning, like PPP or Hubbard with $U \gg t$ or Heisenberg model, dimerization of chains is obtained. [Ohmine 78], [Paldus 79], [Klein2 79], [Durcasse 82], [Soos 83], [Dixit 84], [Valenti 87].

Therefore, from chains dimerization, it cannot be concluded that electron repulsion is negligible. And, in fact, a study from the *strong-electron correlation* point of view predicts correctly the observed instability.

The same argument should hold for *quasi-1D systems*.

4 SYMMETRIES AND DISTORTIONS OF THE STUDIED SYSTEMS

The systems studied are polymeric strips of finite width and infinite length ($L \longrightarrow \infty$) with periodic boundary conditions along L (see Fig. 1 (c), (d), (e), (f)). All π-sites are assumed to be equal, with no hetero-atoms and with an average of one π-electron per π-site. These systems are presumed to be *translationally symmetric*; so that the strips may be divided into *unit cells* or *reduced unit cells*, which are defined as minimal collections of sites equivalent under the action of an extended translation group, including screw rotations (operation that consists on a two-fold rotation around an axis centered on a symmetry point, followed by a translation of half a unit cell). The additional symmetry operations that are important in these systems, if they exist, are reflections in planes normal to the molecular plane and / or two-fold rotations with axes normal to the molecular plane.

Particularly, the polymer strips studied are the following:

- Polyacenacene.

- Polyperylene.

- Poly(benz[m,n]anthracene) ≡ PBA

-Polyphenanthrene.

In order to choose the interesting distortions to be studied on the polymer strips, attention has been paid to the behaviour predicted for these systems by the two *simplest* complementary models; *Hückel model* and *Resonance theory*.

The **Hückel model** is the simplest one-particle model already presented in a previous subsection.

Resonance theory (or Kekulé-structure counting) is defined within the VB method. The *Kekulé* structures are VB states that have their origin in Pauling [Pauling 58] ideas about localized chemical bonds in molecules, particularly benzene, and have found many applications in polymer systems [Wheland 56], [Coulson 52], [Pullman 62]. A Kekulé structure is a total spin-zero state that consists on a product of nearest-neighbor singlet-paired spins. It has a graphical representation (see Fig. 5) by drawing straight lines between pairs of sites whose electron spins are coupled to singlet.
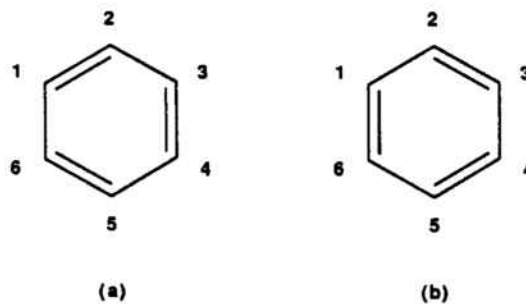

Figure 5: Possible Kekulé structures for benzene molecule. (a) $| K_a >= (\alpha_1\beta_2 - \alpha_2\beta_1)(\alpha_3\beta_4 - \alpha_4\beta_3)(\alpha_5\beta_6 - \alpha_6\beta_5)$. And (b) $| K_b >= (\beta_2\alpha_3 - \alpha_2\beta_3)(\beta_4\alpha_5 - \alpha_4\beta_5)(\beta_6\alpha_1 - \beta_1\alpha_6)$. Where α and β stand for "up" and "down" spin respectively.

Resonance theory consists on counting the number of these structures for a molecular system. In fact, interesting information can be obtained from this simple counting. For instance, a molecule is considered to be more stable, the more Kekulé structures it has.

Klein *et al.* ([Klein2 86] and [Klein4 89]) have proven a relation between the two

opposite point of view models that is relevant in the study of π-network systems, i.e.
*Hückel model predicts a zero-width band gap for a π-network polymer, if and only if,
there are two cardinality-degenerate maximal Kekulé phases* . For different *Kekulé
phases* it is meant sets of Kekulé structures that don't mix. And for *cardinality-
degenerate* that those phases contain the same number of Kekulé structures.

When defining possible distorsions on the polymer strips, we have been interested
in finding those that:

- Open the band gap
- Lift the degeneracy of Kekulé phases

always preserving translational invariance.

Once the distortions have been stablished, they will be studied:

- within band theory and

-within VB scheme beyond Resonance theory in terms of the Spin-Peierls Heisen-
berg model.

4.1 Polyacenacene

This polymer is formed by benzene rings attached one another as shown in Fig.
1 (c). A reduced unit cell can be defined (zone between dashed lines in Fig. 1 (c)).

The spatial symmetry of this polymer consists on the following operations:

- an inversion center i

- a horizontal plane, σ_h, that contains the molecule.

- a two-fold rotation axis, C_{2a}, perpendicular to the σ_h plane centered at the inversion
point.

- a two-fold rotation axis, C_{2b}, parallel to the molecular plane.

- a vertical plane, σ_v, perpendicular to the molecular plane that contains the C_{2b}
axis.

- a screw axis C_s that passes through the inversion center of the molecule.

- the translation operation along the strip.
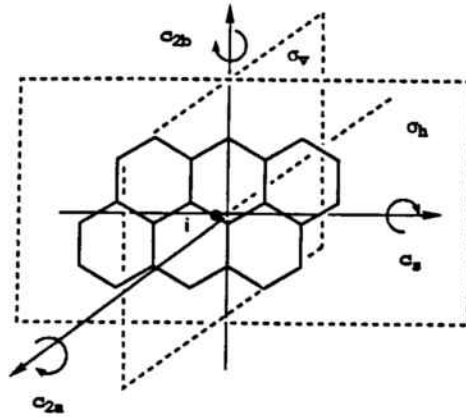
All these elements are drawn in Fig. 6.

Figure 6: Symmetry elements of Polyacenacene

Polyacenacene has three sites per reduced unit cell. In the band picture, there is a half filled band and, consequently, a *zero-width band gap* is predicted, regardless of distortions which preserve the screw axis symmetry.

In the simplest VB picture (i.e. Resonance theory), there are *two cardinality-degenerate maximal Kekulé phases*, as Klein theorem predicts. Defining P as the number of "double bonds" crossed by an obliqued line (as shown in Fig. 7), there are two Kekulé phases $P = even$ and $P = odd$, and they don't mix because of the cyclic symmetry of the strip. They are degenerate because they both contain one Kekulé structure.
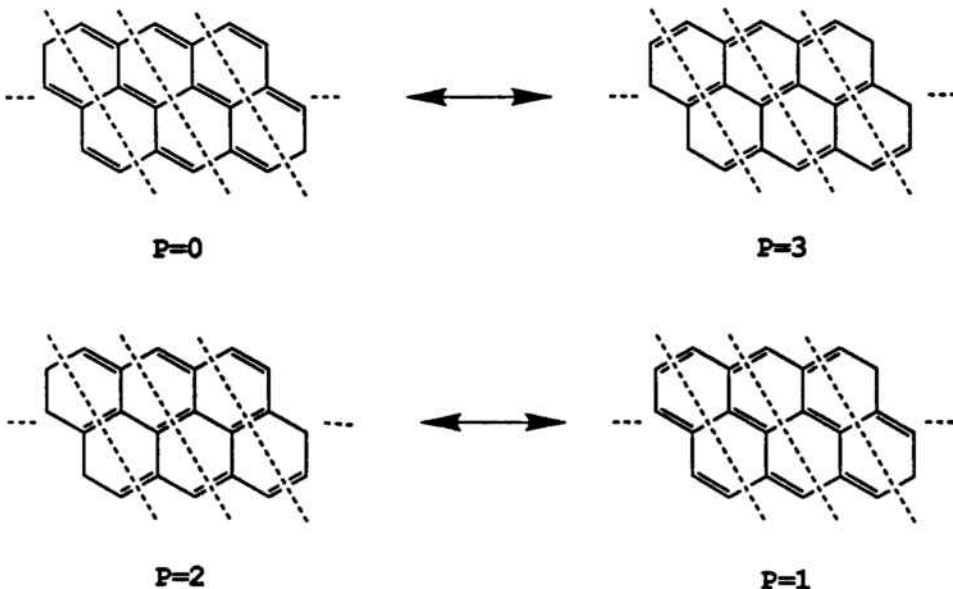

P=0   P=3

P=2   P=1

Figure 7: Representation of the different non-mixing phases of Polyacenacene. Each phase contains one Kekulé structure.

36

A distortion that may open the band gap and lift the degeneracy of Kekulé phases requires the **destruction** of the primitive screw axis symmetry, leaving a basic unit cell twice the size of the reduced unit cell of the system (see Fig. 8 (a)).

There are four bonds per reduced unit cell and eight per unit cell, so that eight bond-stretching distortions can be found per unit cell.

However, interest is focused, for the reasons above mentioned, in breaking the primitive screw axis symmetry preserving translational invariance. The distortions to be considered are then those which are *antisymmetric* with respect to interchange of the two reduced unit cells in a new unit cell.

The bonds of the new unit cell are numbered, taking advantage of the system symmetries, as shown in Fig. 8 (b) where $l = 0, 1, 2, 1'$ correspond to one reduced unit cell and $l = \bar{0}, \bar{1}, \bar{2}, \bar{1}'$ label the next reduced unit cell. Each bond has a distortion parameter δ_l associated.

Two symmetry elements are chosen to label the interesting distortions,

- the screw axis C_s

- a vertical plane, σ_v, perpendicular to the molecular plane.

(They have been drawn in Fig. 8 (c))

In Table 1 the different distortions are presented. They are classified depending on whether they are symmetric $(+1)$ or antisymmetric (-1) with respect to C_s and σ_v. These symmetry requirements impose constraints on the δ_l parameters. They are given in the Table.

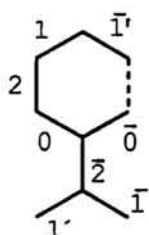| Distortion	C_s	σ_v	Restrictions on the δ_l
A	+1	-1	$\delta_0 = \delta_{\bar{0}} = \delta_2 = \delta_{\bar{2}} = 0$
			$\delta_1 = \delta_{\bar{1}} = -\delta_{1'} = -\delta_{\bar{1}'}$
B	-1	+1	$\delta_0 = \delta_{\bar{0}} = 0$
			$\delta_1 = \delta_{\bar{1}'} = -\delta_{\bar{1}} = -\delta_{1'}$
			$\delta_2 = -\delta_{\bar{2}}$
C	-1	-1	$\delta_1 = \delta_{1'} = -\delta_{\bar{1}} = -\delta_{\bar{1}'}$
			$\delta_2 = \delta_{\bar{2}} = 0$
			$\delta_0 = -\delta_{\bar{0}}$

Table 1: Distortions considered for the Polyacenacene strip.

In all these possible distortions, δ_0, δ_1, δ_2 are assumed to be mutually independent. In Fig. 9 some examples of those hypothetical distortions have been represented.
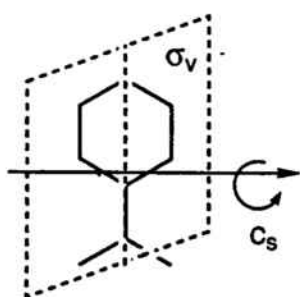
37
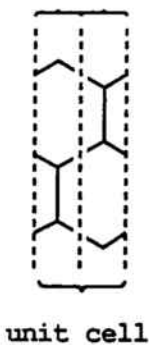
Figure 8: Polyacenacene analysis. (a) "Reduced unit cell" and "unit cell". (b) Labels associated to bonds. (c) Symmetry elements chosen to label distortions: the screw axis C_s and the vertical plane σ_v.
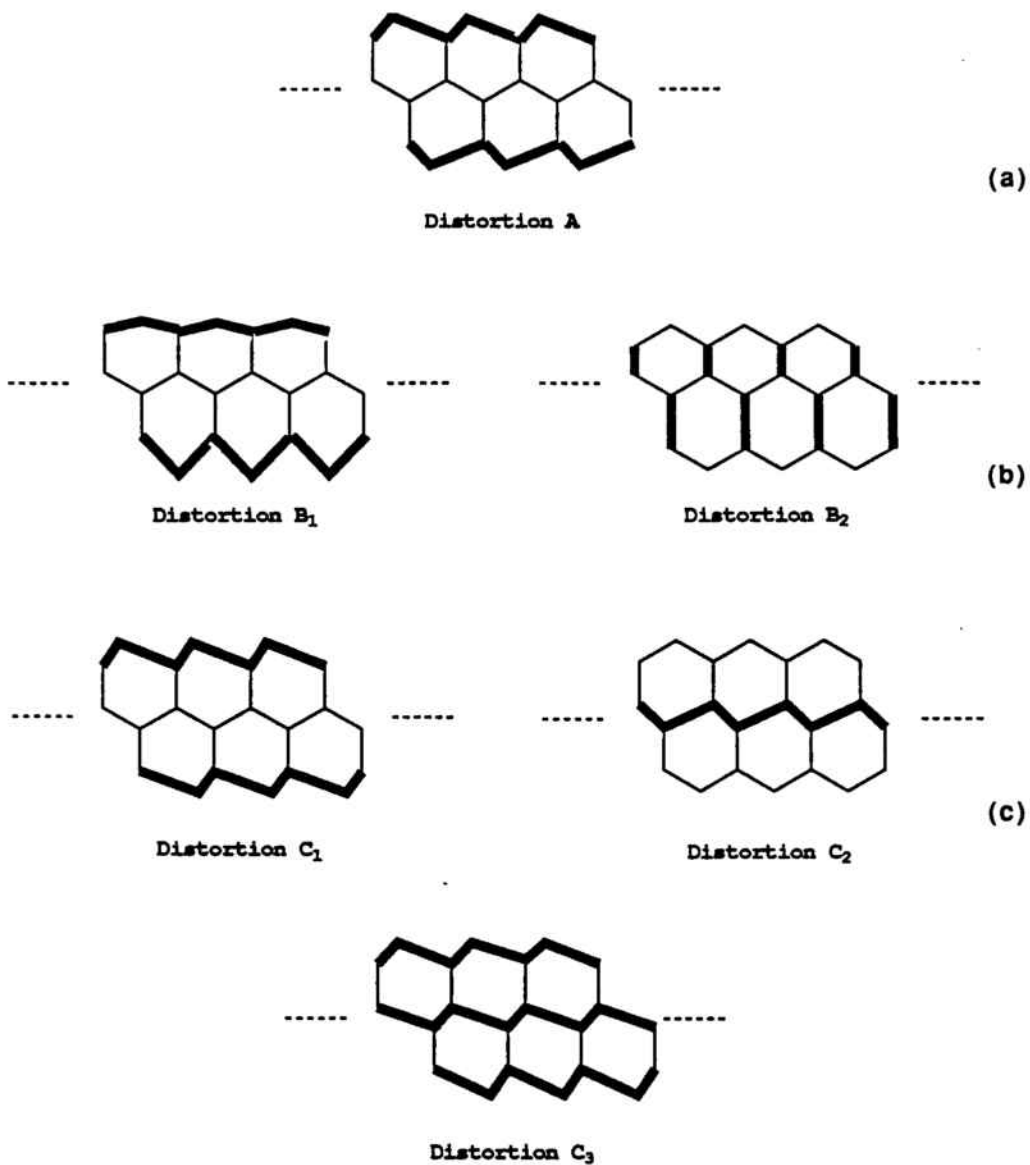
Figure 9: Some hypothetical distorsions for Polyacenacene. (a) Distortion A with $\delta_1 > 0$. (b) Distortion B_1 with $\delta_1 > 0$ and $\delta_2 = 0$ and Distortion B_2 with $\delta_2 > 0$ and $\delta_1 = 0$. They can be combined. (c) Distortion C_1 with $\delta_1 > 0$ and $\delta_0 = 0$, Distortion C_2 with $\delta_1 = 0$ and $\delta_0 > 0$, Distortion C_3 with $\delta_1 > 0$ and $\delta_0 < 0$.

4.2   Poly(benz[m,n]anthracene) (PBA)

Polymer formed by a polyacene strip where added benzenes have been alternatively attached (see Fig. 1 (d)). A reduced unit cell can be defined for this system as shown in Fig. 1 (d) between the dashed lines.

The spatial symmetry of this system contains:

- an inversion center i

- a horizontal plane, σ_h, that contains the molecule.

- a two-fold rotation axis, C_2, contained in the σ_h plane.

- two screw-axis C_{sa} and C_{sb} perpendicular one another centered at the inversion center.

- the translation operation along the strip.

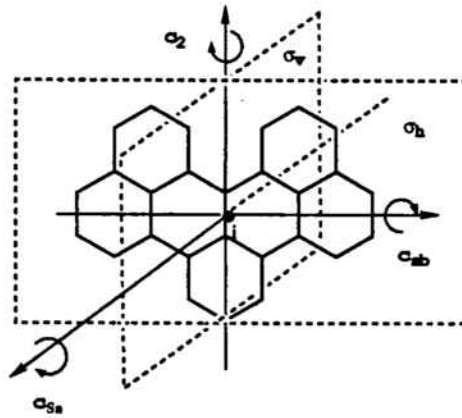These operations are represented in Fig. 10.

Figure 10: Symmetry elements of PBA

PBA has seven sites per reduced unit cell, therefore it is a half-filled band system and, like polyacenacene, a zero-width band gap is predicted in the band picture.

Resonance theory, following Klein's theorem, should predict two cardinality degenerate maximal Kekulé phases.

Being P the number of "double bonds" crossed by obliqued lines as drawn in Fig. 11 and 12, there are two different possibilities; $P = 0$, $P = 1$.

For $P = 0$ the number of Kekulé structures is $\sim 4^L$ (L strip-length). The counting is done analyzing the possible Kekulé fragments in one unit cell compatible with the condition that in the previous and the following units there is no bond

40

crossed ($P = 0$ *going to* $P = 0$) (see Fig. 11). Then, for the whole strip of length L, it will be this number to the power of L.

For $P = 1$, the "double bond" crossed can have two positions (see Fig. 12). As the counting is done analyzing what happens in the evolution from one unit cell to the next, a matrix has to be defined whose elements refer to the different positions of the "double bond" ($(1,1)$ $(1,2)$ $(2,1)$ $(2,2)$) for one step evolution, ($P = 1$ *going to* $P = 1$). The value of each matrix element corresponds to the number of Kekulé fragments in one unit cell, compatible with the condition that in the previous and following unit cells there is one bond located as indicated in Fig. 12. These positions are in correspondence with the matrix element labels. The matrix values are:

$$\begin{pmatrix} 2 & 1 \\ 4 & 2 \end{pmatrix}$$

The maximum eigenvalue is $\Lambda = 4$; the number of possible Kekulé structures is then $\sim 4^L$.

In this system, P identifies the different phases. Kekulé structures belonging to a P phase don't mix with those from a different P phase because of the cyclic symmetry of the system.

It has been shown, then, that there are two cardinality- degenerate maximal Kekulé phases, i.e. $P = 0$ and $P = 1$.
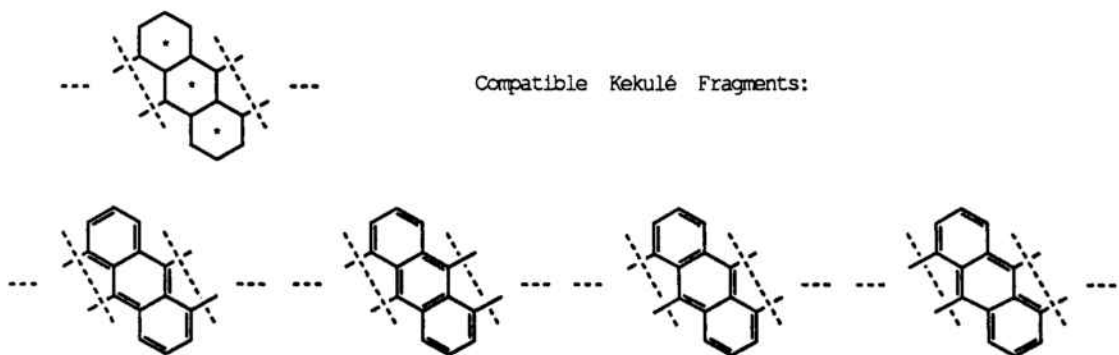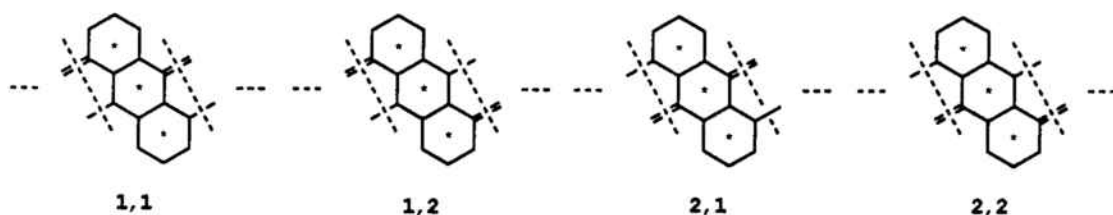
P=0 going to P=0

Figure 11: The Kekulé phases for PBA are defined by the parameter P. P is the number of "double bonds" crossed by the drawn dashed lines. (*) stands for any compatible configuration. For the $P = 0$ *going to* $P = 0$ case there are four possible Kekulé fragments.

P=1 going to P=1

1,1   1,2   2,1   2,2

Compatible Kekulé Fragments:
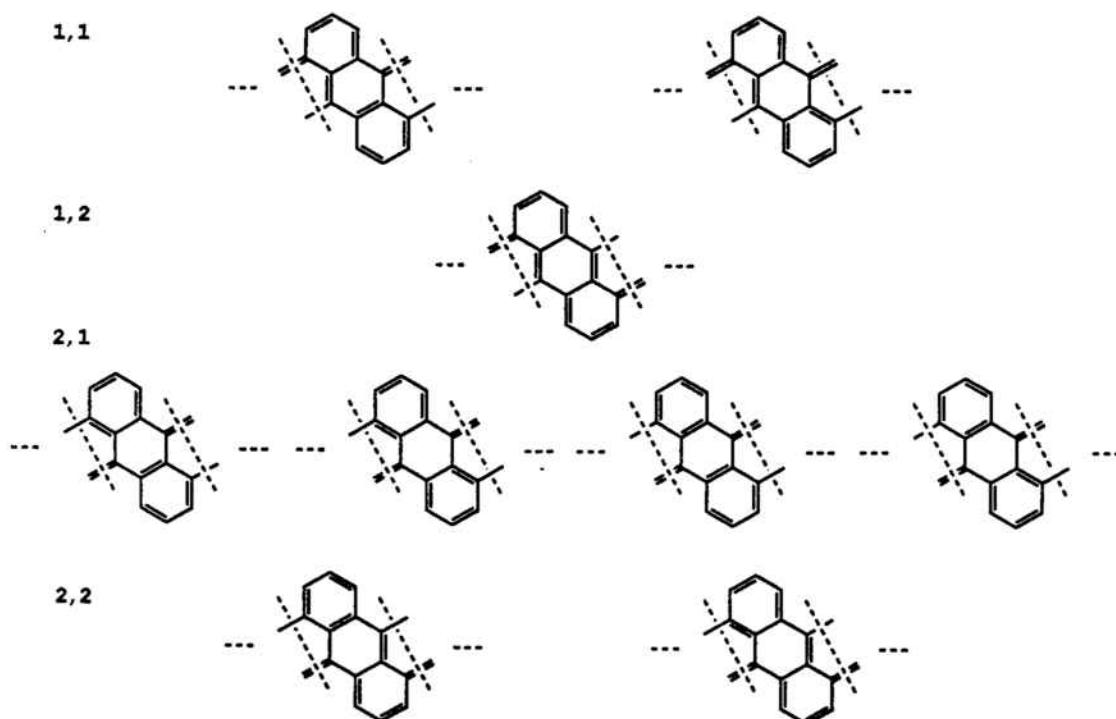
1,1

1,2

2,1

2,2

Figure 12: $P = 1$ *going to* $P = 1$ case for PBA. (*) stands for any compatible configuration. As the "double bond" crossed can have two positions, a matrix has to be defined for the 11, 12, 21, 22 positions that contain all compatible Kekulé fragments corresponding to this case. Those have been drawn below.

42

Like in the polyacenacene polymer, the interesting distortions that may open the band gap and lift the degeneracy are those that are *antisymmetric* under interchange of two reduced unit cells.

The symmetry operations chosen to label them are:
- the screw axis, C_s, and
- a vertical plane σ_v

both drawn in Fig. 13 (c).

Bonds are enumerated, using the symmetries of the system, as follows (see Fig. 13 (b)). $l = 1, 2, 3, 4, 1', 2', 3', 4'$ label one reduced unit cell and $l = \bar{1}, \bar{2}, \bar{3}, \bar{4}, \bar{1}', \bar{2}', \bar{3}', \bar{4}'$ the next reduced unit cell. A distorsion parameter, δ_l, is associated to each bond.

The different distortions are given in Table 2. They are classified according to their symmetry properties under the C_s and σ_v operations (symmetric, $(+1)$, or antisymmetric, (-1)). These properties translate on to constraints for the δ_l parameters, they are presented in the Table.

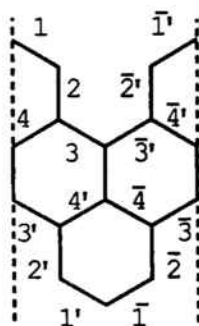| Distortion	C_s	σ_v	Restrictions on the δ_l
A	+1	-1	$\delta_i = \delta_{\bar{i}} = -\delta_{i'} = -\delta_{\bar{i}'}$
B	-1	+1	$\delta_i = \delta_{\bar{i}'} = -\delta_{i'} = -\delta_{\bar{i}}$
C	-1	-1	$\delta_i = \delta_{i'} = -\delta_{\bar{i}} = -\delta_{\bar{i}'}$

Table 2: Distortions considered for the PBA strip. $i = 1, 2, 3, 4$.

In all these possible distortions δ_1, δ_2, δ_3, δ_4 are assumed to be mutually independent. Some examples of possible distorsions are represented in Fig. 14.
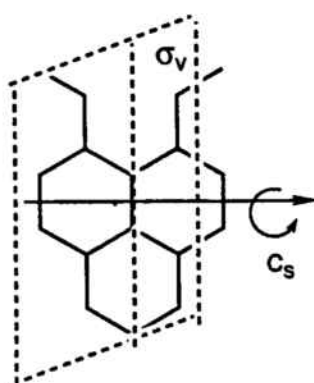
2 reduced unit cells

(a)
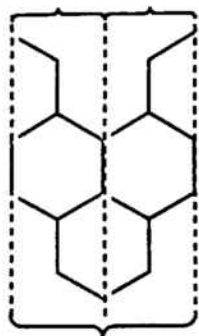
unit cell

(b)

(c)

Figure 13: PBA analysis. (a) "Reduced unit cell" and "unit cell". (b) Bond labels. (c) Symmetry elements chosen to label distortions: a screw axis C_s and a vertical plane σ_v.
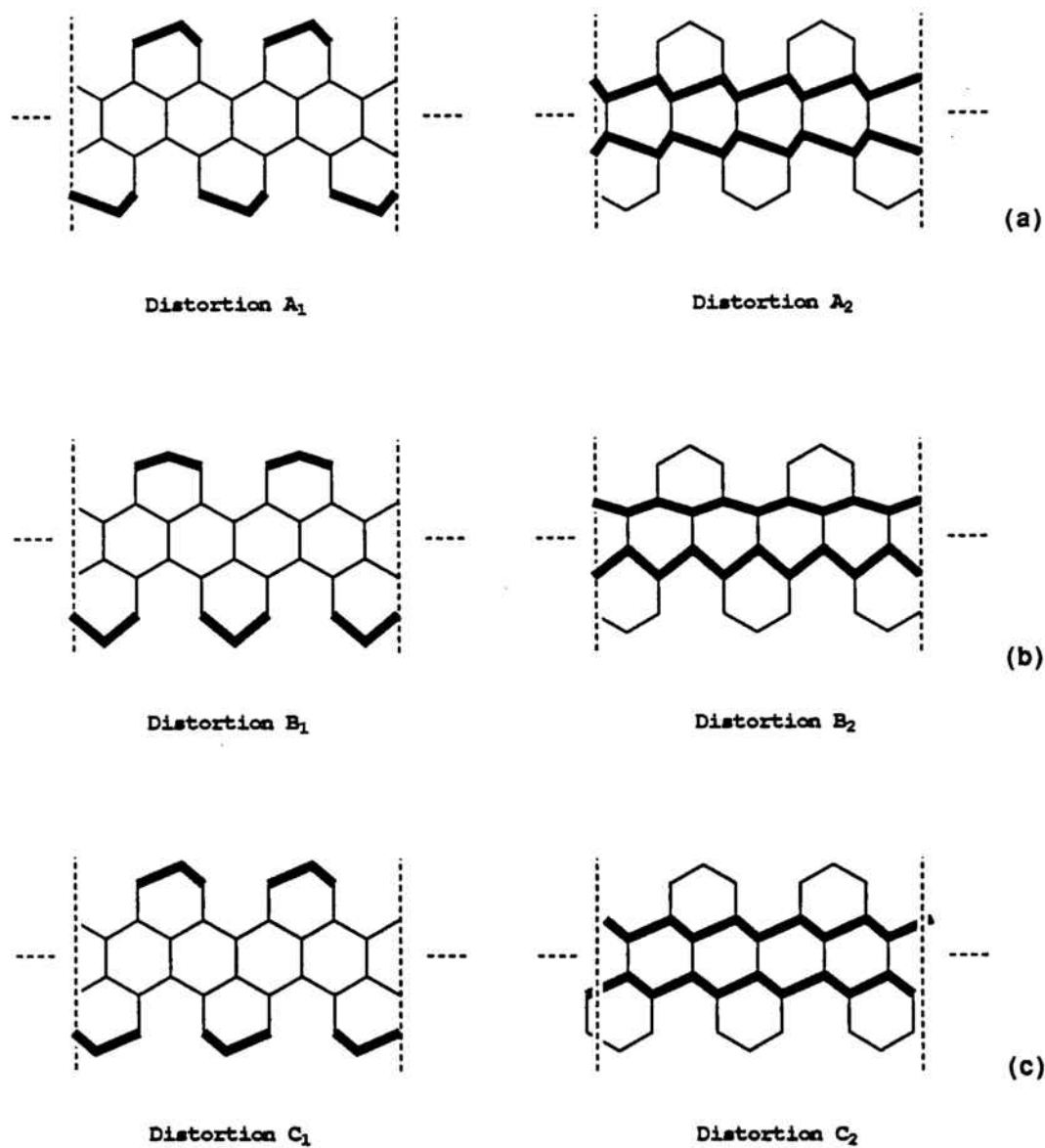
Distortion A₁

Distortion A₂

(a)

Distortion B₁

Distortion B₂

(b)

Distortion C₁

Distortion C₂

(c)

Figure 14: Some hypothetical distortions for PBA. (a) Distortion A_1 with $\delta_1 > 0$ and $\delta_2 = \delta_3 = \delta_4 = 0$, Distortion A_2 with $\delta_3 > 0$, $\delta_4 < 0$ and the rest set to zero. Those two distortions can be combined. (b) Distortion B_1 with $\delta_1 > 0$ and the rest set to zero, and Distortion B_2 with $\delta_3 > 0$, $\delta_4 > 0$ and the rest equal to zero. They can be combined. (c) Distortion C_1 with $\delta_1 > 0$ and the rest equal to zero, and Distortion C_2 where $\delta_3 > 0$, $\delta_4 < 0$ and the rest are equal to zero. Combination of these two distortions is possible.

45

4.3 Polyperylene

This polymer is formed by attached benzene rings as drawn in Fig. 1 (e). The unit cell is defined between the dashed lines in the graph.

The spatial symmetry of this system consists on the point group D_{2h} and the translation operation along the strip.

The symmetry elements of the D_{2h} group are:

- an inversion center i

- a horizontal plane, σ_h, that contains the molecule.

- a two-fold rotation axis, C_{2a}, perpendicular to the σ_h plane and centered at the inversion point.

- two two-fold rotation axis, C_{2b} and C_{2c} parallel to the molecular plane.

- two vertical planes σ_{v1} and σ_{v2} perpendicular to the molecular plane.
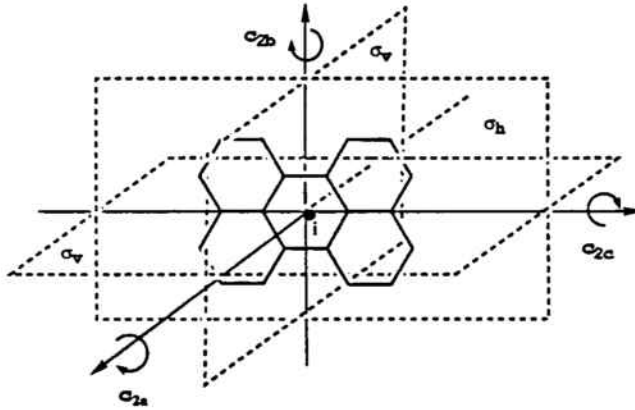
All these elements are represented in Fig. 15

Figure 15: Symmetry elements of Polyperylene

This system has a different behaviour from the two previous cases.

To start with, no reduced unit cell can be defined. It has ten sites per unit cell, therefore it doesn't correspond to a half-filled band system. Nevertheless, Hückel model predicts a zero-width band gap (computations are shown in the next Part of this Chapter) and, correspondingly, Resonance theory should predict two cardinality degenerate maximal Kekulé phases.

Being P the number of "double bonds" crossed by a vertical line, see Fig. 16 and 17, P can have the values $P = 0$, $P = 1$, $P = 2$.

46
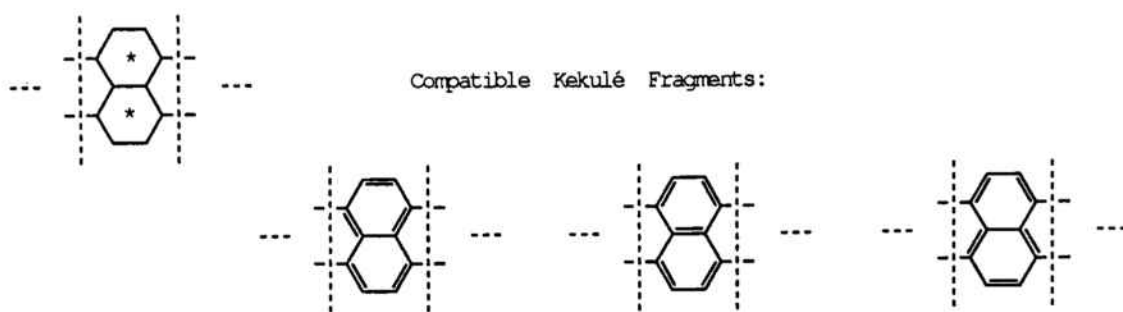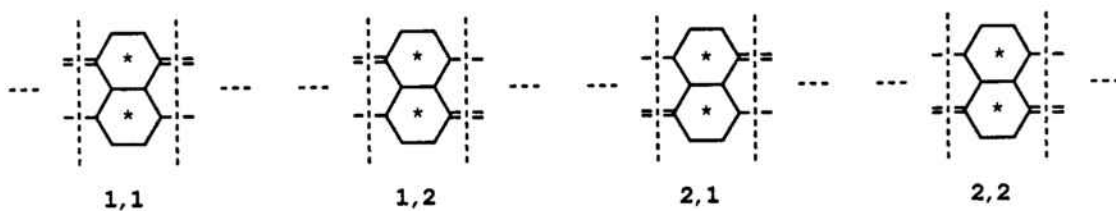
Figure 16: Kekulé phases for Polyperylene defined by P. (*) stands for any compatible configuration. $P = 0$ and $P = 1$ cases are drawn. (a) $P = 0$ *going to* $P = 0$. Three Kekulé fragments can be found. (b) $P = 1$ *going to* $P = 1$. There are four possible positions for the "double bonds", they are represented by 11, 12, 21, 22. The Kekulé fragments compatible with these situations have been drawn below.
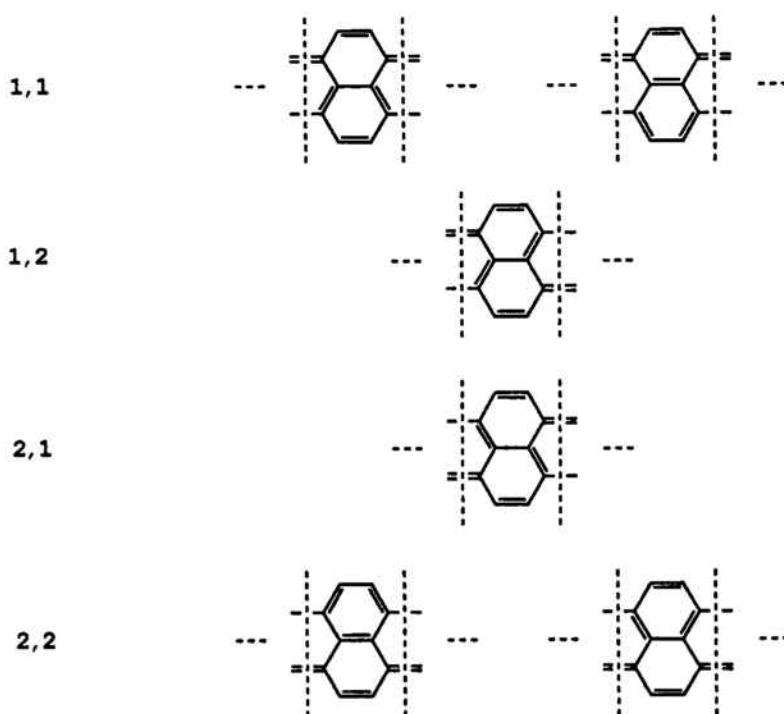
47

P=2 going to P=2   **(c)**
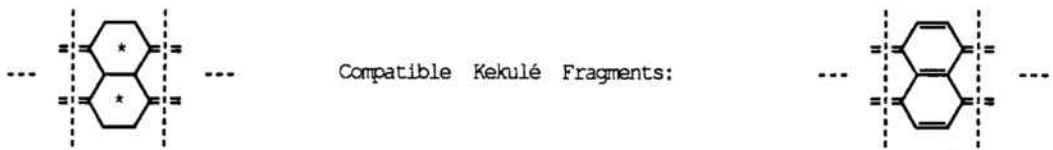

Compatible Kekulé Fragments:

Figure 17: Kekulé phases for Polyperylene corresponding to the $P = 2$ *going to* $P = 2$ case. (∗) stands for any compatible configuration. Only one Kekulé fragment is possible.

For $P = 0$ the number of Kekulé structures is $\sim 3^L$. They are represented in Fig. 16 (a).

For $P = 1$, a matrix can be defined whose matrix elements label the different $P = 1$ *going to* $P = 1$ possibilities as shown in Fig. 16 (b) . The corresponding values are,

$$\begin{pmatrix} 2 & 1 \\ 1 & 2 \end{pmatrix}$$

After diagonalizing, the maximum eigenvalue is $\Lambda = 3$, the number of possible Kekulé structures is then $\sim 3^L$.

For $P = 2$ the number of Kekulé structures is $\sim 1^L$, drawn in Fig. 17.

P denotes the different Kekulé phases. $P = 0$ and $P = 1$ correspond to the two maximal cardinality degenerate phases.

There is no screw axis symmetry in this system. In order to define the distortions that may break the zero-width band gap and the degeneracy, the symmetry elements chosen to label them are:

- a vertical plane, σ_v perpendicular to the molecular plane,

- a horizontal C_2 axis contained in σ_v as shown in Fig. 18 (c).

The labels given to bonds are represented in Fig. 18 (b) and, like in the previous polymers, a distortion parameter δ_l is associated to each of those l bonds. A *totally symmetric* distortion will also be considered for this system.

48
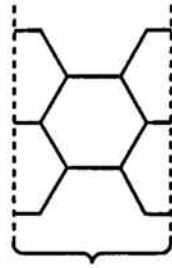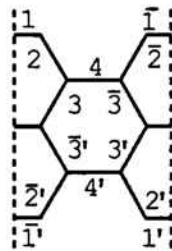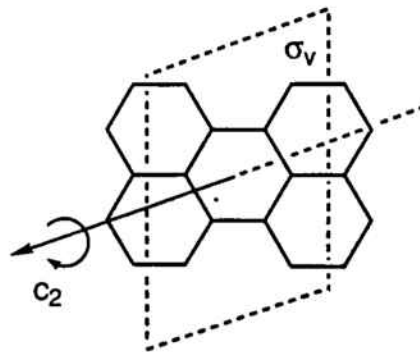
Figure 18 Polyperylene analysis. (*a*) "Unit cell". (*b*) Bond labels. (*c*) Symmetry elements chosen to label distortions: a two-fold rotation axis C_2 perpendicular to the molecular plane, and a vertical plane σ_v.

The different distortions considered for Polyperylene are given in Table 3, They are distinguished according to their symmetry properties with respect to σ_v and C_2 (symmetric, $(+1)$ or antisymmetric (-1)). These considerations impose restrictions on the distortion parameters δ_l. They are presented in the Table.

Distortion	C_2	σ_v	Restrictions on the δ_l
A	-1	+1	$\delta_j = \delta_{\bar{j}} = -\delta_{j'} = -\delta_{\bar{j}'}$ $\delta_4 = \delta_{4'} = 0$
B	+1	-1	$\delta_j = \delta_{\bar{j}'} = -\delta_{j'} = \delta_{\bar{j}}$ $\delta_4 = \delta_{4'} = 0$
C	-1	-1	$\delta_i = \delta_{i'} = -\delta_{\bar{i}} = -\delta_{\bar{i}'}$
D	+1	+1	$\delta_i = \delta_{\bar{i}} = \delta_{i'} = \delta_{\bar{i}'}$

Table 3: Distortions considered for the Polyperylene strip. $j = 1, 2, 3$ and $i = 1, 2, 3, 4$.

Some hypothetical distortions for this system have been drawn in Fig. 19.

Distortion C₁   Distortion C₂   (a)

Distortion B₁   Distortion B₂   (b)

Distortion D₁   (c)

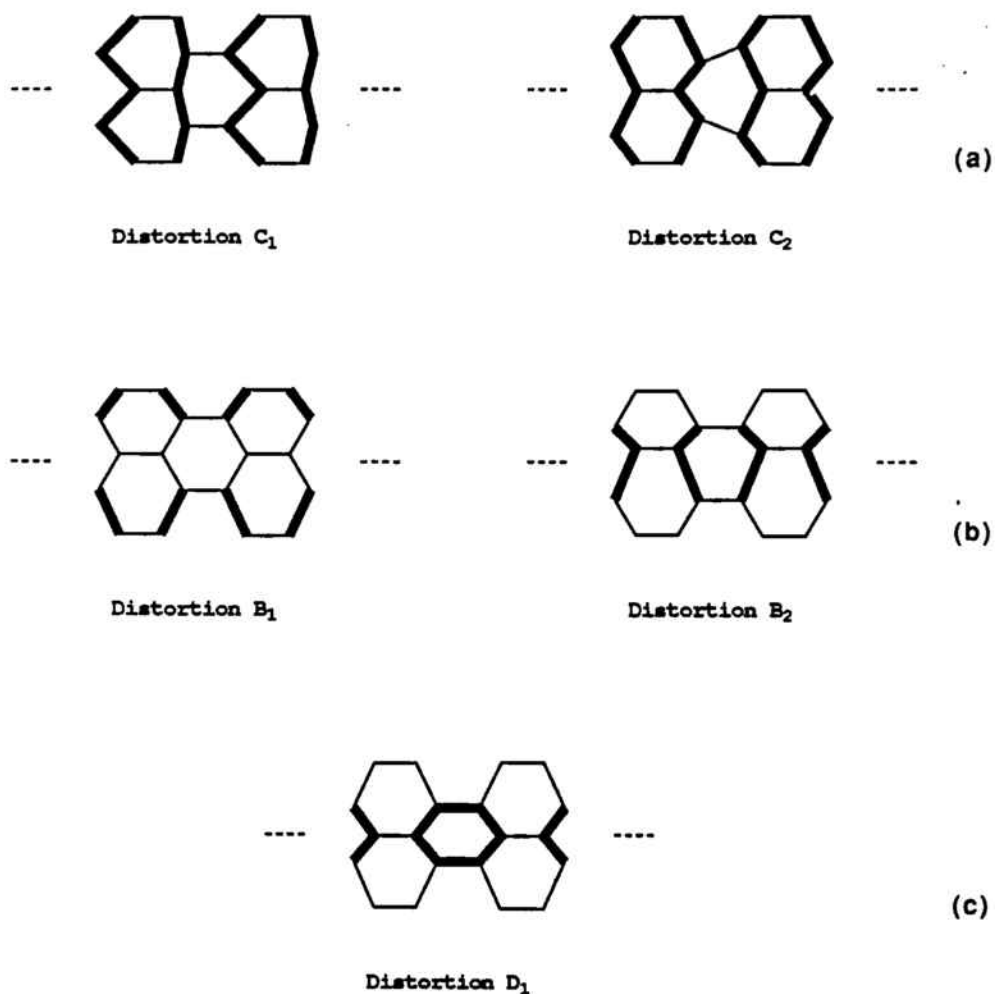**Figure 19:** Possible distortions for Polyperylene. (a) Distortion C_1 with $\delta_2 > 0$, $\delta_3 > 0$ and the rest set to zero. And Distortion C_2 with $\delta_2 < 0$, $\delta_3 > 0$ and the rest equal to zero. (b) Distortion B_1 with $\delta_2 > 0$ and the rest set to zero. And Distortion B_2 where $\delta_3 > 0$ and the rest are zero. (c) Distortion D_1 with $\delta_3 > 0$, $\delta_4 > 0$ and the rest equal to zero.

4.4 Polyphenanthrene

This π-network system is formed by benzene rings disposed as drawn in Fig. 1 (f). The unit cell is the zone defined between the dashed lines.

The symmetry elements of this strip are,

- a horizontal plane, σ_h, that contains the molecule.
- a vertical plane, σ_v, perpendicular to the molecular plane.
- a C_2 axis contained in the σ_v plane.
- the translation operation along the strip.

They have been drawn in Fig. 20.
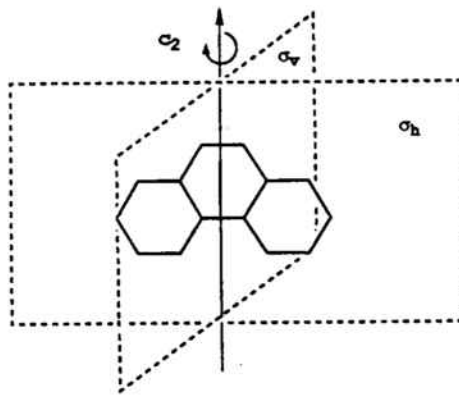
Figure 20: Symmetry elements of Polyphenanthrene

Polyphenanthrene has eigth sites per unit cell, it doesn't correspond to a half-filled band system and Hückel model predicts a non-zero width band gap, consequently, there shouldn't exist two cardinality-degenerate maximal Kekulé phases.

Defining P as the number of "double bonds" crossed by vertical lines as drawn in Fig. 21 and 22, there are three different phases; $P = 0$, $P = 1$, $P = 2$ that don't mix among them.

For $P = 0$ the number of Kekulé structures is $\sim 1^L$.

For $P = 1$, as in previous cases, a 2×2 matrix is defined to account for the different possibilities drawn in Fig. 19 (b). The corresponding values are,

$$\begin{pmatrix} 1 & 1 \\ 1 & 2 \end{pmatrix}$$

with maximum eigenvalue $(3 + \sqrt{5})/2$. The number of Kekulé structures is then

$\sim ((3+\sqrt{5})/2)^L$. And for $P=2$ phase, there are $\sim 1^L$ Kekulé states.

There are two cardinality-degenerate phases but they aren't *maximal*.

P=0 going to P=0 (a)

Compatible Kekulé Fragments:

P=1 going to P=1 (b)

1,1   1,2   2,1   2,2

Compatible Kekulé Fragments:

1,1

1,2

2,1

2,2
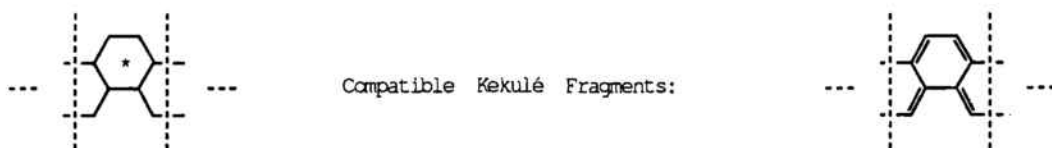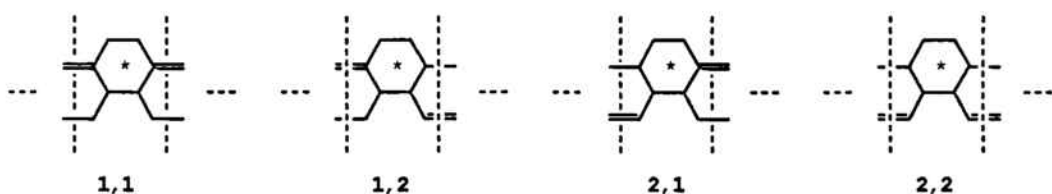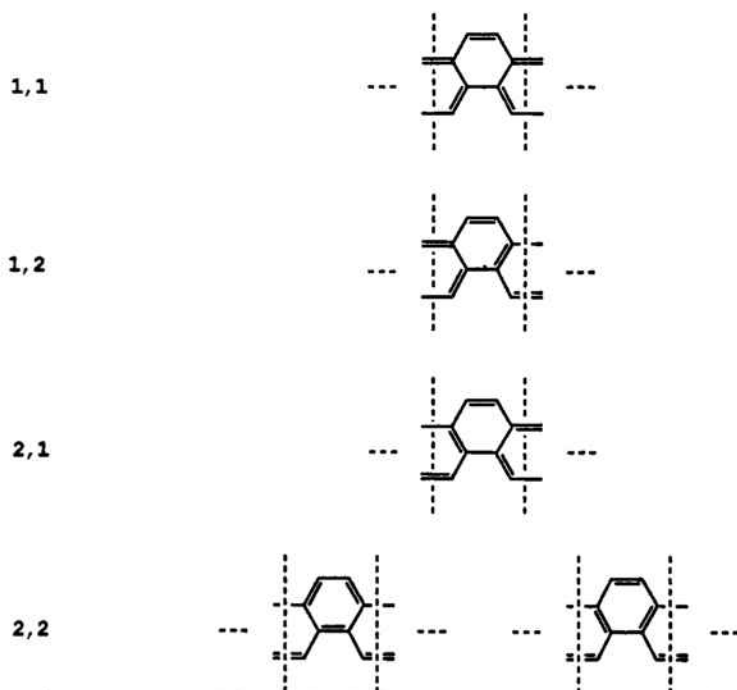
Figure 21: P defines the different non- mixing Kekulé phases for Polyphenanthrene. The $P=0$ and $P=1$ cases have been drawn. (*) stands for any compatible configuration. (a) $P=0$ *going to* $P=0$. Only one Kekulé fragment is compatible. (b) $P=1$ *going to* $P=1$. Four possible one-"double bond" positions are possible (11, 12, 21, 22). The compatible Kekulé fragments are shown below.

53

P=2 going to P=2 (c)

Compatible Kekulé Fragments:
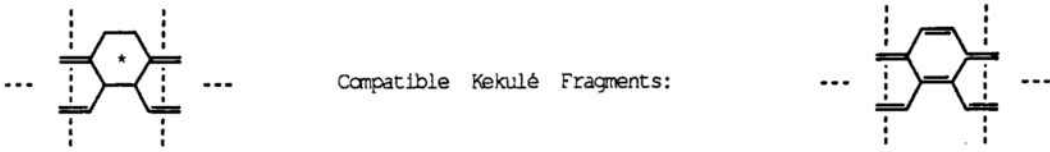
Figure 22: Kekulé fragments for Polyphenanthrene for the $P = 2$ *going to* $P = 2$ case. (*) stands for any compatible configuration. Only one Kekulé fragment is possible.

For this system, the study of distortions is not relevant because there is no zero band-gap to open, or, what it is the same, there is no degeneracy to break, so that the *apparent instability* present in the other systems doesn't exist here. Nevertheless, the ground state of this system has been investigated because,

(i) it has been synthesized

(ii) in the Third Chapter some interesting excitations are predicted for it.

Ground State and related properties of a family of quasi-1D planar polymers.
<u>Computations</u>

Contents

1 TRANSLATIONALLY ADAPTED HÜCKEL MODEL

Band-theory computations have been carried out with the Hückel model. This is a very simple model within the independent electron scheme approximation and a quick reference to band theory predictions.

This model can be expressed in terms of a hamiltonian presented in previous sections:

$$H_{Huck} = \sum_{<i,j>,\sigma} \beta_{ij}(c_{i\sigma}^+ c_{j\sigma} + c_{j\sigma}^+ c_{i\sigma}) \tag{1.1}$$

with i and j nearest neighbors, $\beta_{ij} < 0$ the "Hückel resonance integral" (or hopping term) between sites i and j, and $c_{i\sigma}^+$ ($c_{i\sigma}$) is the creation (annihilation) operator of an electron of spin σ in the orbital centered on site i, $|i>$.

For a cyclic translationally invariant strip of length L where the division in *unit cells* is implicit, the Hückel model can be rewritten in a more suitable way: any orbital shall be labelled by two indexes $|a,i>$, a stands for any unit cell in the system $a = 1, 2, ..., L$ and i for a particular site of the unit cell a where the orbital is centered.

The hamiltonian can be expressed as:

$$H = \sum_{a,\mu} H(a,\mu) \tag{1.2}$$

where $a + \mu$, $\mu = 0, +1, -1$, refers to a and to the cells nearest neighbors to it, $a + 1$ or $a - 1$ respectively. And,

$$H(a,\mu) = \sum_{i,j} \beta_{ij}(\mu)\Lambda(a + \mu, j/a, i) \tag{1.3}$$

where $\beta_{ij}(\mu)$ is the "Hückel resonance integral" between *neighboring* sites (a, i) and $(a + \mu, j)$, for any value of a. The matrix elements of the Λ operator are:

$$< a',j' \mid \Lambda(a,j/b,i) \mid b',i' > = \delta_{aa'}\delta_{jj'}\delta_{bb'}\delta_{ii'}. \tag{1.4}$$

Taking advantage of the translational invariance symmetry of the system, *translational symmetry adapted* states can be defined:

$$| j; k > \equiv \frac{1}{\sqrt{L}} \sum_{a=1}^{L} e^{ika} | a, j > \qquad (1.5)$$

with wavevector

$$k = \frac{2\pi n_k}{L}, \qquad (1.6)$$

and $n_k = 0, 1, ..., L - 1$.

The matrix elements of the Hamiltonian between these new states are:

$$< j; k | H | i; k' > = \frac{1}{L} \sum_{a,b} e^{-ikb} e^{ik'a} < b, j | H | a, i >$$

$$= \frac{1}{L} \sum_a \sum_\mu e^{i(k'a - ka - k\mu)} < a + \mu, j | H | a, i >$$

$$= \sum_{m\mu} e^{-ik\mu} \beta_{ij}(\mu) \frac{1}{L} \sum_a e^{i(k'-k)a}$$

$$= \delta_{kk'} \sum_\mu e^{-ik\mu} \beta_{ij}(\mu). \qquad (1.7)$$

Diagonalizing the hamiltonian matrix, the energy bands $\epsilon(k)$ are finally obtained.

Modification of the resonance integral, β, due to the *electron-phonon* interaction (which causes the *Peierls* instability) can be considered by an "effective Hückel resonance integral" :

$$\beta_{ij} = \beta(1 + \delta_{ij}) \qquad (1.8)$$

where δ_{ij} is the distortion parameter that measures the strenght of the perturbation between centres i and j, $-1 < \delta_{ij} < 1$.

1.1 Example: Polyacenacene

Undistorted and distorted Hückel model has been applied to some π-network systems. Polyacenacene is presented here explicitly.

Polyacenacene structure can be reproduced from a "reduced unit cell" by the translation symmetry operation and screw rotations. When working with the "reduced unit cell", the *Jones* zone will be obtained in the k space.

The orbitals are numbered as shown in Fig. 1. For the undistorted case, matrix elements are evaluated according to expression (1.7). Then, relabelling

$$< j; k | H | i; k > \equiv H(j, i), \qquad (1.9)$$

we have

$$H(1,1) = 0$$

$$H(1,2) = 0$$

$$H(1,3) = \beta e^{-ik_J} + \beta e^{ik_J} = 2\beta cos k_J$$

$$H(2,1) = 0$$

$$H(2,2) = 2\beta cos k_J$$

$$H(2,3) = \beta$$

$$H(3,1) = 2\beta cos k_J$$

$$H(3,2) = \beta$$

$$H(3,3) = 0 \tag{1.10}$$

where k_J means that the k vector is defined in the Jones zone.

The diagonalization of the hamiltonian matrix, $|H - \epsilon I| = 0$, (ϵ denotes the energy bands, $\epsilon = \epsilon(k)$, and I is the identity operator) leads to the following secular equation,

$$x^3 - Cx^2 - (C^2 + 1)x + C^3 = 0 \tag{1.11}$$

where $C \equiv 2cos k_J$ and $x \equiv \epsilon/\beta$. Three energy levels are obtained in the Jones zone.
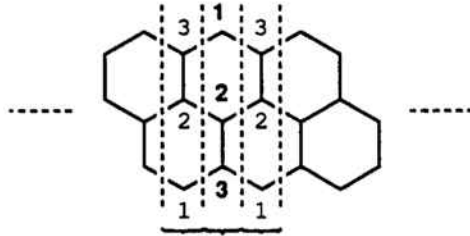
Figure 1: Numbering of orbitals in a "reduced unit cell" of polyacenacene. Neighboring reduced unit cells are also drawn within the dashed lines.

To study possible distortions in the system, the reduced unit cell description is not applicable anymore because some distortions break the screw axis symmetry and the whole unit cell has to be considered. Any bond ij has a distortion parameter associated, δ_{ij}, as was shown in section 4.1 in the Introduction, and computations

are similar to the undistorted case provided that β_{ij} is modified now according to (1.8). Results shall be given in the Results section.

2 Beyond Resonance Theory. ANTIFERROMAGNETIC SPIN - 1/2 HEISENBERG MODEL

We attempt here to go beyond Kekulé-structure counting (or Resonance theory) (see section 4 in the Introduction) within the VB picture, using the Heisenberg hamiltonian previously introduced (see section 3.2 in the Introduction).

This model hamiltonian has been exactly solved for the one dimensional undistorted chain [Hulthen 38] and exact solutions have also been obtained for small finite systems by direct diagonalization.

Apart from these particular cases, no other exact solution is known and different methods have been developed in order to obtain good approximated results as Monte Carlo numerical calculations ([Hirsch 85], [Reger 88], [Barnes 88]), real-space renormalization group techniques ([Dasgupta 81], [Zivkovic 89]), mean-field theories ([Inui 86]), variational method ([Klein 83], [Huse 88], [Liang 88]), etc.

2.1 Variational Method

We are interested in describing the ground state of the polymer systems. Many of the above mentioned techniques, like Monte Carlo calculations and real-space renormalization group techniques, give accurate results for the ground state *energy* but further information is difficult to obtain.

The variational method has been chosen here because the nature of the ground state can be studied through the knowledge of the approximate wavefunction.

This method consists on proposing a trial ground state wavefunction $|\Psi>$ as a function of some parameters to be determined by optimization of the expression:

$$E(\Psi) = \frac{<\Psi \mid H \mid \Psi>}{<\Psi \mid \Psi>} \tag{2.1}$$

where H is the model hamiltonian. The *variational principle* assures that the result will be an upper bound to the exact ground state energy, and it will be the best

upper bound in the subspace where $|\Psi>$ has been defined because it is obtained by minimization.

The efficiency of this method relies on making good guesses for the trial ground state wavefunction.

Some variational ansätze are proposed in this work as possible ground state wavefunctions of the π-network systems.

Since the Heisenberg hamiltonian conmutes with the total spin operators $\bar{S}^2$ and S^z,

$$[H_H, \bar{S}^2] = [H_H, S^z] = 0 \tag{2.2}$$

the eigenfunctions of the hamiltonian can be selected to be also spin eigenfunctions. Furthermore, the Lieb and Mattis theorem [Lieb 62] assures that the ground state will be a total spin-zero eigenfunction. These considerations reduce considerably the subspace in which the trial wavefunction will be defined.

3 VARIATIONAL ANSÄTZE

The trial ground state wavefunctions chosen are *variational localized-site cluster-expanded ansätze*, i.e. wavefunctions expressed as a sum of terms that depend on variational parameters, each of which describes the *local* features of the system.

Two alternative ansätze have been proposed with different features: a *Néel-state-based* ansatz and a *Resonating-Valence-Bond* ansatz, in particular, a Kekulé-structure based approach has been used.

Néel state
The Néel state can be expressed as

$$| \Phi_N >= \prod_i^{i \epsilon A} \alpha(i) \prod_j^{j \epsilon B} \beta(j) \tag{3.1}$$

where A and B denote the two sets of sites in which the system may be partitioned such that each member of one set is a nearest neighbor solely to sites of the other set (this is valid for alternant systems). And $\alpha(i)$ and $\beta(i)$ represent the spin-up and spin-down states for site i.

The Heisenberg energy of this state for a system of N sites with one electron per site is obtained straightforward,

$$< \Phi_N \mid H_H \mid \Phi_N >= -\frac{1}{8} z J N \qquad (3.2)$$

where z is the mean coordination number (average number of nearest neighbors per site).

Kekulé state

A (non-normalized) Kekulé state (or Nearest-Neighbor Valence-Bond, NNVB, state) is defined:

$$\mid K >= \prod_{<i,j>}^{K} [\alpha(i)\beta(j) - \beta(i)\alpha(j)] \qquad (3.3)$$

where $< i,j >$ denotes that i and j are nearest neighboring sites, i.e. $\mid K >$ is a total spin-zero state where each site is coupled to singlet with one of its nearest neighbors. It can also be expressed in terms of the spin raising and lowering ($S_i^{\pm}$) operators on site i,

$$\mid K >= \prod_{i}^{\epsilon A} \prod_{j}^{<i,j>} (I - S_i^- S_j^+) \mid \Phi_N > \qquad (3.4)$$

where I is the identity operator.

The Heisenberg energy for a system of N sites with one electron per site corresponding to this state can be easily computed using Rümer rules [Rumer 32] (see next section), and

$$\frac{< K \mid H_H \mid K >}{< K \mid K >} = -\frac{3}{8} J N. \qquad (3.5)$$

If energies (3.2) and (3.5) are plotted as a function of the coordination number, z, (see Fig. 2) it is observed that the Néel state is favored for highly coordinated systems, while for systems where any site has, on average, few nearest neighbors (low-dimensional systems), the singlet paired valence bond states are preferred for their description.

$E_N = -1/8\ Z$

$E_K = -3/8$
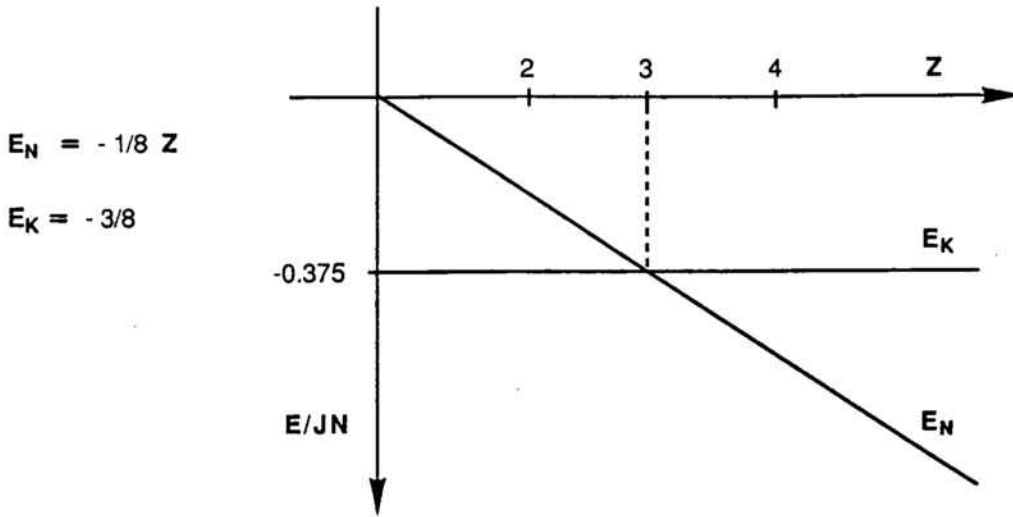
Figure 2: Heisenberg energies comparison of the Néel state and a single Kekulé state in terms of the coordination number z.

In fact, Néel-state-based approaches are usually applicable to inorganic antiferromagnets which typically involve three-dimensional structures of relatively high coordination number, z. While the type of valence bond states such as the Kekulé structures have been limited to small finite systems, basically organic molecules, till (besides some exceptions [Klein3 86]) the discovery of new high-Tc superconductors where all these valence bond ideas have been applied again to describe such strongly-correlated electron systems [Anderson1 87].

Extended polymer systems have, on average, $z = 3$ nearest neighbors per site. Competition on these two type of states to describe the ground state is stablished.

3.1 Néel-state-based Ansatz

Taking the Néel state, $\mid \Phi_N >$, as a reference state, a lowering on the Heisenberg energy will be obtained if an ansatz is defined within a space containing Φ_N and some additional states obtained after applying the XY part of the Heisenberg operator to Φ_N, i.e., the Heisenberg hamiltonian can be rewritten,

$$H_H = J \sum_{<i,j>} (S_i^z S_j^z + (S_i^+ S_j^- + S_i^- S_j^+)) \tag{3.6}$$

63

where

$$S_i^{\pm} \equiv \frac{1}{\sqrt{2}}(S_i^x \pm iS_i^y) \qquad (3.7)$$

are the spin raising and lowering operators.

The action of $S_i^{\pm}S_j^{\mp}$ on $\mid \Phi_N >$ induces corrections that can be introduced in terms of a *nearest-neighbor pair excitation* operator,

$$P = \sum_i^{\epsilon A} \sum_j^{<i,j>} x_{ij}S_i^-S_j^+ \qquad (3.8)$$

where x_{ij} are parameters to be determined by energy optimization. The Néel-state-based ansatz is chosen as an expansion in terms of this P operator acting on the Néel state,

$$\mid \Psi_0 >= e^P \mid \Phi_N > \qquad (3.9)$$

Namely, states where an arbitrary number of couples of neighboring spins have been flipped, weighted by a variational parameter per flip, are added to the Néel state. It is a localized-site cluster-expanded wavefunction. In general, it is not a spin-zero wavefunction (depending on the value of the variational parameters) but can give an approximate description of the ground state.

3.2 Resonating Valence Bond Ansätze

Two ansätze have been chosen, a "short-range Resonating Valence Bond" or, what is the same, a Kekulé-structure based approach, and a "higher-range Resonating Valence Bond" ansatz.

Any singlet valence bond state is defined as a product of pairs of spins coupled to singlet. The set of the linearly independent singlet VB states can be used as a basis of the subspace of spin zero states. This is a very large basis and approximations have to be done in order to make the problem tractable. A reasonable approach is to retain only the subset of Kekulé structures (or NNVB).

Then, an improvement upon the single Kekulé structure energy, given in (3.5) above, is obtained by considering a weighted sum over the different possible global Kekulé structures of the system, i.e.

$$\mid \Phi >= \sum_K c_K \mid K > \qquad (3.10)$$

with the variational parameters, c_K, chosen as a product of variational scalars x_{ij}, each one associated to a pair of spins coupled to singlet in the Kekulé structure.

The trial wavefunction is then,

$$| \Phi_0 >= U_0 \prod_i^{\epsilon A} \sum_j^{<i,j>} x_{ij}(I - S_i^- S_j^+) | \Phi_N > \qquad (3.11)$$

where $|K >$ is represented by eq. (3.4) and U_0 indicates that the terms to be retained are those where each site is referred only once. This ansatz is of short-range type.

A further lowering of the energy can be obtained by enlarging the basis set of valence bond singlets with states containing longer pairings.

Higher order valence bond singlets may be built by locally modifying a typical Kekulé structure. This has been done here by allowing an arbitrary number of recouplings among adjacent couples of singlets (see Fig. 3 where it has been represented on the polyacenacene backbone). Labelling by $\hat{q}_{ef}$ the operator that leads the recoupling between pairs e and f, an overall "higher range" valence bond excitation operator can be defined,

$$Q = \sum_{<e,f>} x_{ef} \hat{q}_{ef} \qquad (3.12)$$

where x_{ef} are variational parameters associated to the new created singlet pairs. Then, an improved ansatz is defined in terms of $| \Phi_0 >$ and the operator Q,

$$| \Phi_1 >= U(e^Q) | \Phi_0 > \qquad (3.13)$$

where U retains the terms that are unlinked in the series expansion of e^Q, namely, those products of $\hat{q}_{ef}$ where no index is repeated. And all parameters contained in Q and $| \Phi_0 >$ will be determined simultaneously upon optimization of (2.1).

Figure 3: Action of the $\hat{q}_{ef}$ operator on any two adjacent spin-paired neighbors. The pairings are represented by straight lines. x_{ef} is the variational parameter associated to this new singlet.

4 TRANSFER MATRIX TECHNIQUE

4.1 Ground State Energy

An upper bound to the exact ground state energy of the Heisenberg model for the extended polymer systems will be obtained by minimizing the expression:

$$E(\Psi) = \frac{< \Psi \mid H_H \mid \Psi >}{< \Psi \mid \Psi >} \tag{4.1}$$

in terms of the variational parameters that are contained in the trial ground state wavefunction $\mid \Psi >$.

In order to carry out computations, advantage has been taken of the following facts:

- Interactions in the model hamiltonian are of *short range*. (We are dealing with a nearest-neighbor interacting hamiltonian).

- The trial ground state ansätze chosen, $|\Psi_0 >$, $|\Phi_0 >$ and $|\Phi_1 >$ are variational localized-site cluster-expanded wavefunctions. That is, they are functions of parameters that depend on neighboring sites of the system.

- The extended π-network systems, which characterize for being of finite width, w, and cyclic length L, with $L \longrightarrow \infty$, can be represented as an ordered succession of *zones* or "unit cells".

All these considerations allows us to deal with the systems locally by zones or monomer units.

A *transfer matrix*, T_q, containing the local features of the particular ansatz and the system, and a *connection matrix*, $C_{p+1 \rightarrow p+c}$, containing the peculiarities of the interaction part can be defined in a way that the matrix elements in (4.1) reduce to products of these T_q and $C_{p+1 \rightarrow p+c}$ matrices. q and p are labels for monomer units and c measures the range of the interaction. The translational symmetry invariance of the systems assures that these matrices are independent of q and p, and we can drop these subscripts. To simplify, $C_{1 \rightarrow c}$ shall be denoted C.

Every ansatz proposed has a graphical representation on the backbone of the π-network system, the partition in unit cells favors the possibility of defining *local states* for that system and the ansatz chosen.

A *local state* consists on a possible configuration that can be drawn in a unit cell containing the contributions from the *bra* and *ket* part of (4.1) matrix elements. The set of all possible configurations define the different local states. By translational

66

invariance, local states are **independent** of the unit cell. They will be labelled by e_n where n ranges over the whole set.

Once they have been obtained, the transfer matrix elements,

$$T_{nm} \equiv <e_n \mid T \mid e_m> \tag{4.2}$$

define a weighted sum over the various ways a local state e_m in a unit cell may succeed a local state e_n from the previous unit cell. The weight of every term in the sum consists on the variational parameters that characterize the particular way e_n evolves to e_m, and additional factors proceeding from Rümer's superposition rules [Rumer 32].

The **overlap** $<\Psi \mid \Psi>$ is then evaluated in terms of the T matrix. It will be the trace (because of periodic boundary conditions) of the T matrix to the power of number of unit cells, i.e. L,

$$<\Psi \mid \Psi> = tr T^L. \tag{4.3}$$

For $L \longrightarrow \infty$, the largest eigenvalue Λ of T dominates (4.3) and it reduces to

$$<\Psi \mid \Psi> \simeq \Lambda^L <\Lambda, l \mid \Lambda, r> \tag{4.4}$$

where $<\Lambda, l|$ and $|\Lambda, r>$ are the left and right eigenvectors corresponding to Λ.

The **hamiltonian expectation value** over Ψ can be evaluated in a similar way as a product of transfer matrices. An extra matrix, the connection matrix C, is defined in the zone where the interaction takes place.

The matrix elements

$$C_{nm} \equiv <e_n \mid C \mid e_m> \tag{4.5}$$

are a weighted sum over the various ways a local state e_m in a unit cell a may succeed a local state e_n from the previous $a - c$ unit cell when the Heisenberg interaction is taking place in sites within those two unit cells. The weight of every term in C_{nm} contains, apart from the variational parameters in the zone coming from all possible contributions to Ψ, the extra features due to the interaction.

The hamiltonian matrix element is expressed,

$$<\Psi \mid H_H \mid \Psi> = JL <\Psi \mid \frac{1}{2} \sum_i^{unit\ cell} \sum_j^{<i,j>} \bar{S}_i \bar{S}_j \mid \Psi>$$
$$= JL\, tr\{T^{L-c}C\}. \tag{4.6}$$

67

In the long length limit, $L \longrightarrow \infty$, the largest eigenvalue Λ of T dominates (4.6) and,

$$< \Psi \mid H_H \mid \Psi > \simeq JL\Lambda^{L-c} < \Lambda, l \mid C \mid \Lambda, r > . \tag{4.7}$$

And the energy expectation value per unit cell in J units reduces to,

$$E = \frac{< \Lambda, l \mid C \mid \Lambda, r >}{\Lambda^c < \Lambda, l \mid \Lambda, r >} \tag{4.8}$$

which is a simple expression to evaluate. Optimization in terms of the variational parameters contained in the expression will give an upper bound to the exact ground state energy of the system.

All the computational complexity lays in the matrices T and C. Their simplicity depends on:

- The ground state ansatz chosen.

- The width of the π-network system.

- The range of the interaction. The shorter the range, the simpler the C matrix will be.

The energy expression can be generalized when considering possible distortions. The connection matrix in a unit cell is decomposed in a sum of matrices C^{ij} each one containing the features of the interaction between sites i in the unit cell and its neighbor j,

$$C = \frac{1}{2} \sum_i^{unit\ cell} \sum_j^{<i,j>} C^{ij} \tag{4.9}$$

Changes due to distortion considerations are to be defined in this expression:

$$C' = \frac{1}{2} \sum_i^{unit\ cell} \sum_j^{<i,j>} (1 + \delta_{ij}) C^{ij} \tag{4.10}$$

with δ_{ij} the distortion parameter between sites i and j.

5 COMPUTATIONAL EXAMPLE: Polyacenacene

Computation of the (2.1) expression has been carried out for all the π-network systems and with the different previously proposed ansätze. Specific calculations are shown here for polyacenacene. For the rest of the systems, similar considerations are applicable.

5.1 Néel-based Ansatz

Any term contributing to the Néel-based wavefunction can be represented by drawing lines between neighboring spins $< i, j >$ that have been flipped due to the action of the "excitation operator" P. This operator assigns a variational parameter x_{ij} to an ij flipping. There are eight parameters that can be defined in a polyacenacene unit cell (see Fig. 4(a)). They are independent of the unit cell by translational invariance.

The different *local states* in a unit cell corresponding to this ansatz have been drawn in Fig. 4(b) on the polyacenacene backbone where, the particular choice done for the "unit cell" is shown. The *thick lines* in the picture are the contributions coming from the *bra*, $< \Psi|$, and the *curved thin lines* correspond to the *ket* part, $|\Psi >$, contributions. From all the imaginable ways of combining flipped spins in *bra* and *ket*, only those where the same spins are flipped in both, *bra* and *ket* parts will be accounted for in the overlap. Any other case is zero by orthogonality. A total of 14 *local states* are found.

Given a *local state* in a zone, the contributions that come from every *local state* in the next zone compatible with it, are given by the transfer matrix elements. In Fig. 5, a representation of transfer matrix elements for some local states in polyacenacene is given. T is a 14×14 matrix and $< \Psi \mid \Psi >$ reduces to (4.3).

The computation of the hamiltonian matrix element, $< \Psi \mid H \mid \Psi >$, can be easily carried out if the **'transposition hamiltonian'**,

$$H_t = J \sum_{<i,j>} (i,j), \tag{5.1}$$

is used instead of the common Heisenberg one with spin operators. Since a transposition between two neighboring spin-1/2 sites i and j, can be defined as

$$(i,j) = 2\bar{S}_i\bar{S}_j + 1/2, \tag{5.2}$$

then conversion of H_t to the Heisenberg hamiltonian is straightforward:

$$H_t = 2H_H + Ln/2, \tag{5.3}$$

where n is the number of interactions between neighbors per unit cell.

69

(a)

"Unit cell" :

(b)

"Local states"

$<e_1|$ $<e_2|$ $<e_3|$ $<e_4|$

$<e_5|$ $<e_6|$ $<e_7|$ $<e_8|$

$<e_9|$ $<e_{10}|$ $<e_{11}|$ $<e_{12}|$

$<e_{13}|$ $<e_{14}|$
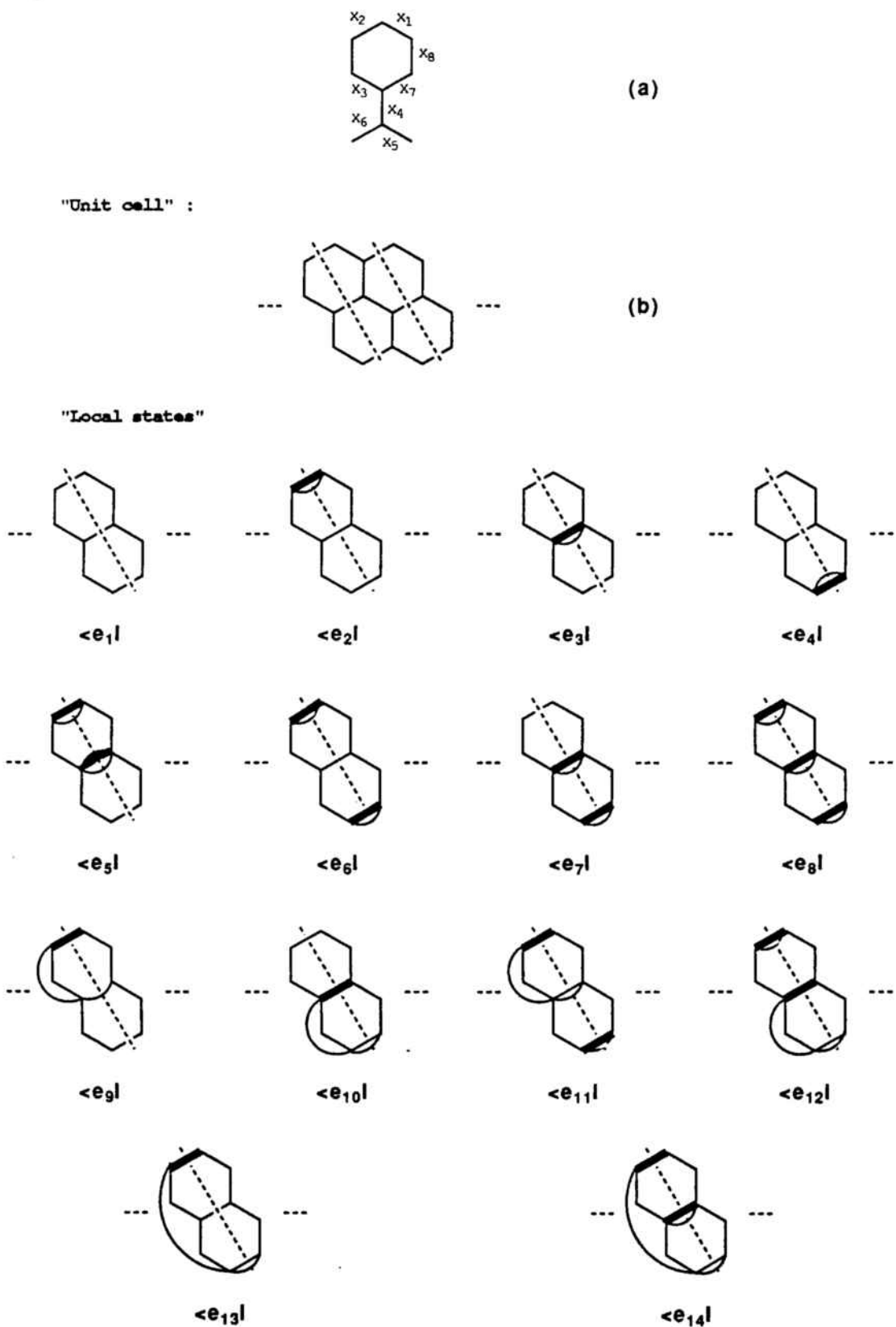
Figure 4: Computation with the Néel-based ansatz. (a) Variational parameters associated to each possible spin-flip in a unit cell. In the undistorted case $x_1 = x_2 = x_5 = x_6$, $x_3 = x_7$ and $x_4 = x_8$ by symmetry. (b) Choice of "unit cell". Representation of the 14 local states for polyacenacene strip. The *thick lines* correspond to the contributions coming from the *bra* part of the $< \Psi_0 | \Psi_0 >$ overlap and the *curved thin lines* correspond to the *ket* contributions. In $< e_9|$ to $< e_{14}|$ states, lines on the left connecting non n.n. sites mean several connected *bra* and *ket* spin-flips coming from previous unit cells.

70
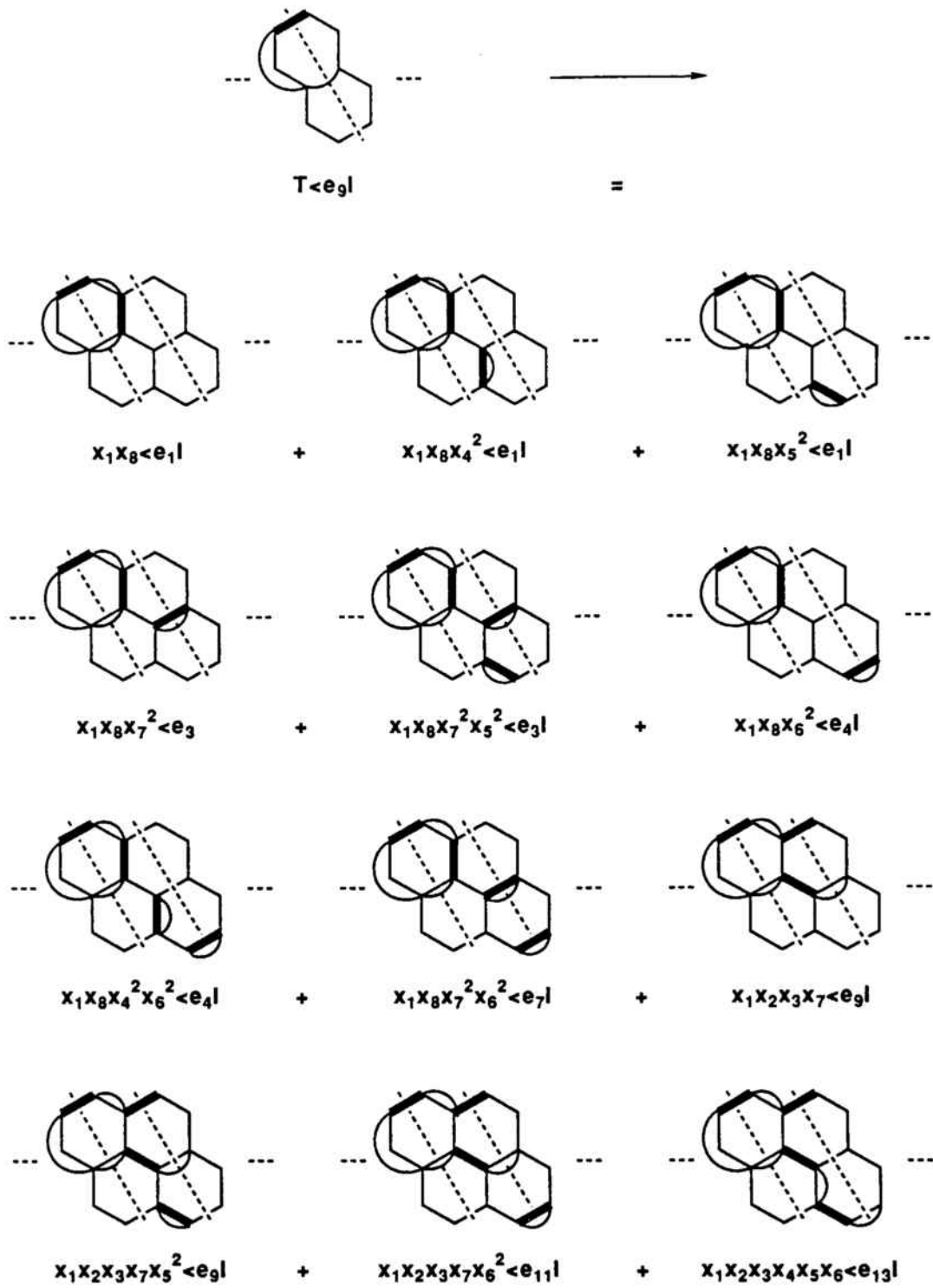
Figure 5: Evolution of $< e_9|$ state from one zone to the next. The contributions define the T_{9m}, m ranging, matrix elements of the transfer matrix.

$< \Psi \mid H_t \mid \Psi >$ will be a product of transfer matrices defined for every unit cell, similarly to $< \Psi | \Psi >$, except in the unit cell(s) where the (i,j) interactions in H_t are taking place. A connection matrix, C, is considered in this zone(s).

Given any zone or unit cell, C is defined, as mentioned in the previous section, as

$$C = \frac{1}{2} \sum_i^{unit\ cell} \sum_j^{<i,j>} C^{ij} \tag{5.4}$$

where matrices C^{ij} contain the contributions due to the interaction (i,j) between sites i in a unit cell and its neighbor j. They can be expressed as a sum of two terms.

The first one accounts for the cases where the transposition interaction (i,j) acts on sites with different spin orientation. It is equivalent to a spin-flip of sites i and j. Therefore, it plays the same role as operators in P or P^+ but without the variational parameter x_{ij} associated to it. It can be expressed in terms of a derivative of T, $\partial T / \partial x_{ij}$.

The second term has the contributions corresponding to the case where i and j have the same spin orientation, then (i,j) action is equivalent to the identity, i.e. (i,j) acts on a state obtained from $|\Phi_N >$ where i and not j or, j but not i are affected by the "pair excitation operator" P. We shall term it as the 'identity-like' contribution.

Any other possibility doesn't contribute to C^{ij}.

The polyacenacene strip has eight different pair interactions per unit cell (see Fig. 6), then,

$$C = C^{12} + C^{23} + C^{34} + C^{45} + C^{56} + C^{21'} + C^{43'} + C^{65'}. \tag{5.5}$$
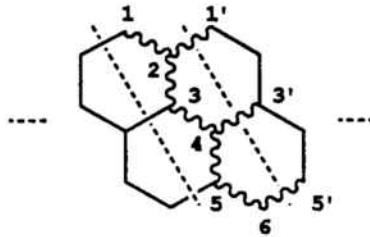

Figure 6: Possible interactions between nearest neighbors in a unit cell. They are represented by wiggling lines joining the interacting sites in the backbone of the system.

As mentioned previously, each of these matrices is a sum of a $\partial T/\partial x_{ij}$ term and an 'identity-like' term. $\partial T/\partial x_{ij}$ matrices are easy to obtain from the T expression. The 'identity-like' contributions can also be written in terms of the transfer matrix although a two unit cell analysis is needed.

Let's take the $(1,2)$ interaction in polyacenacene. Denoting by V^{12} the two-zone matrix corresponding to this 'identity- like' term, the mn matrix element is:

$$V_{mn}^{12} = \sum_k (T_{mk} - T_{mk}|_{x_2=0})(T_{kn}|_{x_1=x_2=x_8=0})$$
$$+ \sum_k (T_{mk}|_{x_2=0})(T_{kn}|_{x_1=0} - T_{kn}|_{x_1=x_2=x_8=0}) \qquad (5.6)$$

where $T_{mk}|_{x_l=0}$ denotes the mk matrix element of T with the parameter x_l set to zero. The two summations correspond to the cases drawn in Fig. 7.
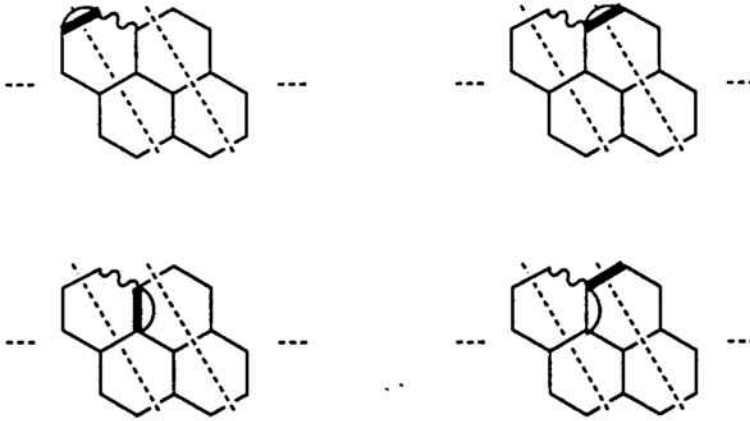
Figure 7: Contributions to the matrix elements V_{mn}^{12}. The first picture corresponds to the first summation in (5.6) and the rest of the pictures contributions are considered in the second summation.

As it is a two-zone analysis, correspondingly, C^{12} will also describe two consecutive zones, then

$$C^{12} = T\frac{\partial T}{\partial x_1} + V^{12} \qquad (5.7)$$

The rest of the C^{ij} matrices are calculated similarly, and the hamiltonian matrix element reduces to the expression (4.6) where the "interaction range" c is equal to two because, as shown, two unit cells are needed to evaluate it.

73

The distorted case is studied following definition (4.10). Results for this system and the rest of the π-polymer family are presented in the Results section.

5.2 RVB Ansätze

In the computation of $< \Psi \mid \Psi >$ and $< \Psi \mid H \mid \Psi >$ when $|\Psi >$ is $|\Phi_0 >$ or $|\Phi_1 >$, as those ansätze are linear combinations of *valence bond* structures, Rümer diagrams and rules [Rumer 32], [McWeeny 69] are used.

A *Rümer diagram* consists on representing a valence bond state by drawing directed lines (bonds) between pairs of sites that are paired to singlet.

It can be shown [McWeeny 69] that, for any two linear independent valence bond states $|s >$ and $|s' >$, the following rules apply:

$$< s \mid s' >= 2^{n(s,s')} \tag{5.8}$$

where $n(s, s')$ is the number of islands (or closed loops) counted when drawing $< s|s' >$ in terms of Rümer diagrams. And

$$< s|\bar{S}_i\bar{S}_j|s' >= -3/4 < s|s' > \tag{5.9}$$

if i and j belong to the same island, or

$$< s|\bar{S}_i\bar{S}_j|s' >= 0 \tag{5.10}$$

otherwise.

$< \Psi \mid \Psi >$ and $< \Psi \mid H_H \mid \Psi >$ are evaluated considering the previous rules and the contribution of the variational parameters that have been chosen for these ansätze to be assigned to every singlet pair.

Given a unit cell, a *local state* will be defined in terms of the possible Rümer overlaps that can take place in that zone coming from the *bra*, $< \Psi|$, and *ket*, $|\Psi >$, contributions of $< \Psi \mid \Psi >$.

For the "short-range" RVB, $|\Phi_0 >$, there is only one *local state* for polyacenacene. In this system, as was shown in the first part of the chapter, the Kekulé structures don't mix, they belong to different Kekulé phases, therefore, choosing one of this Kekulé structures as the basis set, only couplings with itself are possible (see Fig. 8. Note that the "unit cell" has been chosen in a convenient way).

74
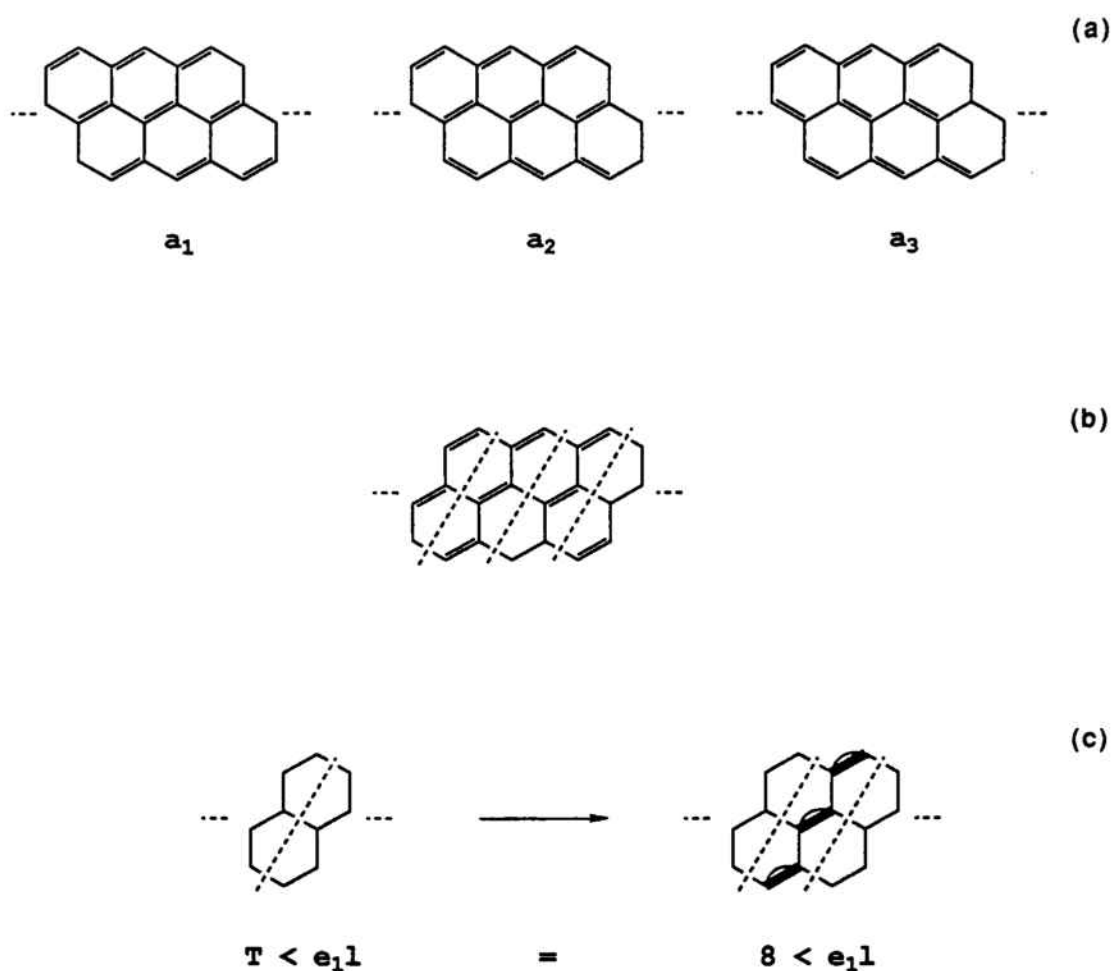
Figure 8: (a) Some possible Kekulé structures for polyacenacene. They all characterize for being mutually non mixing. (b) a_1 has been chosen as the one-element basis for $|\Phi_0>$. Dividing the strip as shown, there is only one *local state*, e_1. (c) T_{11} matrix element. The *thick lines* correspond to the singlet pair contributions from the *bra* of $<\Phi_0|\Phi_0>$ and the *curved thin lines* correspond to the *ket* contributions.

When $|\Psi>$ is $|\Phi_1>$, i.e. higher range VB states are considered, the number of possible *local states* increases up to 60. The reference Kekulé structure chosen in order to build these new states has been the corresponding to $P=3$ phase. Any other Kekulé reference gives equivalent results.

The transfer matrix elements are obtained studying the evolution of each local state from one zone to the next, where both, the variational parameter contribution

and the island-counting are taken into account.

For wavefunction $|\Phi_0>$, T is a 1×1 matrix and there is only one relevant parameter that, by normalization, can be taken equal to 1 (see Fig. 8(c)).

For wavefunction $|\Phi_1>$, T is a 60×60 matrix and five variational parameters are to be considered. They are associated to the first order allowed "higher range" singlet couplings (see Fig. 9). Complexity in computations increases enormously when going to higher order approximations.
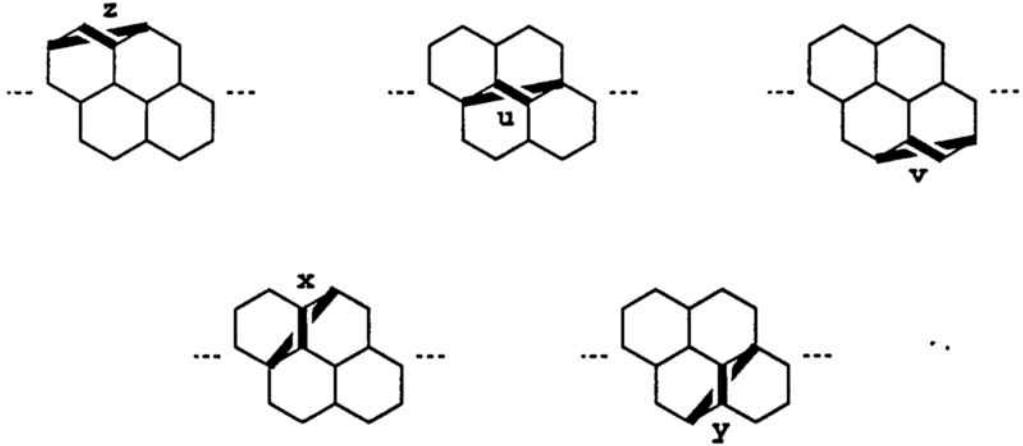
Figure 9: Variational parameters associated to the possible singlet pairs (represented by thick lines) in a unit cell for wavefunction $|\Phi_1>$.

$< \Psi \mid \Psi >$ can be written as (4.3).

The connection matrix C, defined in $< \Psi \mid H \mid \Psi >$ computation for the zone where the interaction takes place, following Rümer rules, considers whether the particular spins interacting belong to the same island or not.

For polyacenacene, C is the sum:

$$C = C^{12} + C^{23} + C^{34} + C^{45} + C^{56} + C^{21'} + C^{43'} + C^{65'} \qquad (5.11)$$

where the numbering of sites is the same as in Fig. 6. When doing computations with $|\Phi_0>$, only $C^{21'}$, $C^{43'}$ and $C^{65'}$ are different from zero; in any other case the interaction takes place between spins that don't belong to the same island. The energy per site in J units for the undistorted strip of length L and 6 sites per unit

cell reduces to

$$E/6LJ = \frac{< \Psi \mid H \mid \Psi >}{< \Psi \mid \Psi > 6LJ}$$
$$= (\frac{-3}{4 \times 6}) \frac{8^{L-1} \times 3 \times 8}{8^L} = -0.375 \qquad (5.12)$$

The distorted case takes into account (4.10) definition. It will be revisited in the Results section.

The computation of the energy with $|\Phi_1 >$ requires more work. The connection matrix C is a 60×60 matrix that contains the contributions of all interactions per unit cell (see (5.11)) and a two-zone analysis is required.

Results and discussion for undistorted and distorted polyacenacene as well as PBA, polyperylene and polyphenanthrene will be found in the Results section.

Ground State and related properties of a family of quasi-1D planar polymers.
Results and Discussion

Contents

1 RESULTS

Polyacenacene, PBA, Polyperylene and Polyphenanthrene have been examined from **band theory** point of view (Hückel model) and within the strong electron correlation limit with the **VB localized** method (Heisenberg model).

Peierls (band theory) and **spin-Peierls** (Heisenberg model) instabilities have been studied for every system. They are expressed in terms of "effective integrals" $-\beta_{ij}$ (in Hückel model) and J_{ij} (in the Heisenberg model)- which have a linear dependence on a *distortion parameter δ*.

A distortion for a system will be favored if the energy response to the perturbation due to δ has a dependence in δ faster than δ^2 (for small δ values) to compensate the vibrational or phonons energy which behave as δ^2.

In Table 1 we enumerate the computations that have been carried out for these systems. Results for every π-network system are presented separately.

SYSTEMS	HUCKEL	Ψ_0	Φ_0	Φ_1
Polyacenacene	Yes	Yes	Yes	Yes
PBA	Yes	–	Yes	–
Polyperylene	Yes	Yes	Yes	–
Polyphenanthrene	Yes	Yes	Yes	–

Table 1: Enumeration of the results presented. Ψ_0 labels the Néel-state-based ansatz. Φ_0 denotes the "short range" RVB ansatz. Φ_1 labels the "higher range" RVB ansatz.

It is worthwhile to note that the "higher range" RVB ansatz, Φ_1, was only computed for polyacenacene since:

- Φ_0, the "short-range" RVB ansatz, gives a very poor result for the ground state energy in polyacenacene, basically because there is no Kekulé-structure mixing so that Φ_0 is written in terms of one only state. An improvement on this ansatz, like Φ_1, is needed. While for the rest of the systems this isn't the case, and Φ_0 provides already good results.

- Φ_1 computation for polyacenacene is still tractable (transfer and connection matrices are 60×60 matrices). On the other hand, for PBA, polyperylene and polyphenanthrene the T and C matrix dimensions increase enormously. Furthermore, most of the interesting information in these systems is already provided by Φ_0.

Polyacenacene is the system that we have examined in more detail.

The distortions for these π-network polymers have been studied following the rule that in any distortion where different **independent** *distortion parameters* δ_{ij} are considered, they will be given the same value in order to be able to talk of a unique δ parameter.

1.1 POLYACENACENE

1.1.1 HÜCKEL MODEL

Polyacenacene has 3 sites per reduced unit cell, and, correspondingly, 6 sites per unit cell. It is a half-filled system. In Fig. 1 the energy bands in the Jones zone have been drawn and in Fig. 2 the corresponding Brillouin zone has been plotted $k_B = 2k_J$.
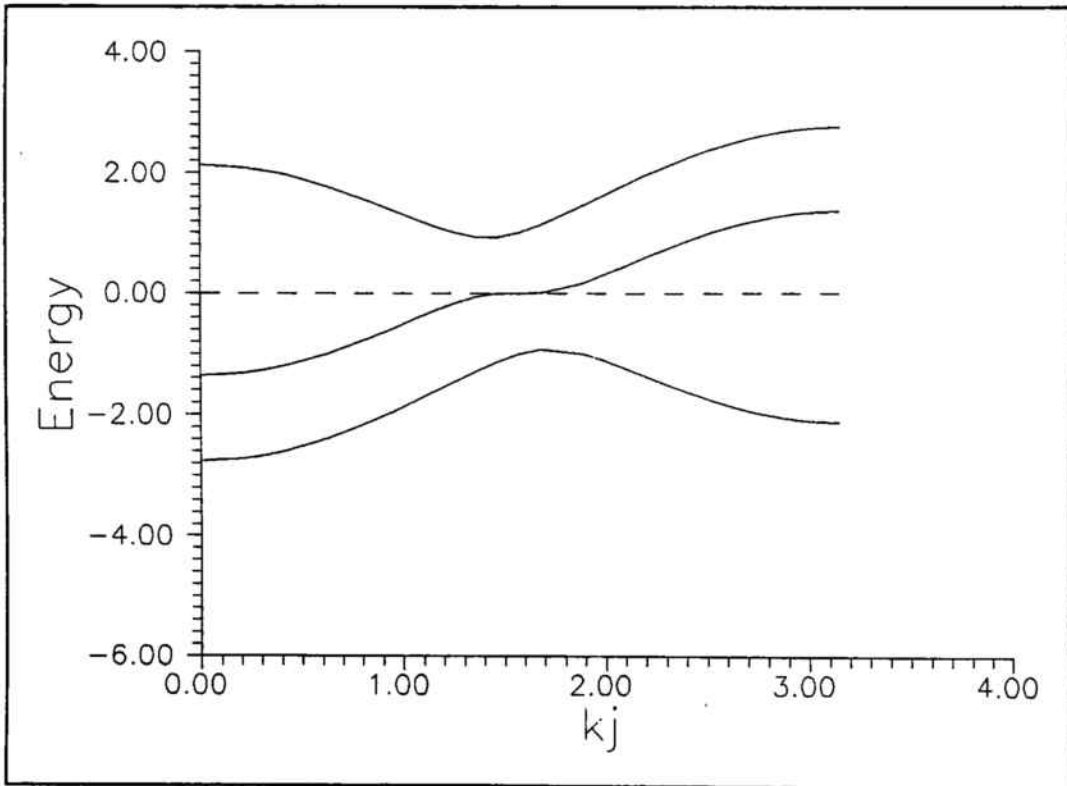
Figure 1: Energy bands for polyacenacene in the Jones zone, ($k_j \ \epsilon \ [0, \pi]$). The dashed line corresponds to the Fermi level.
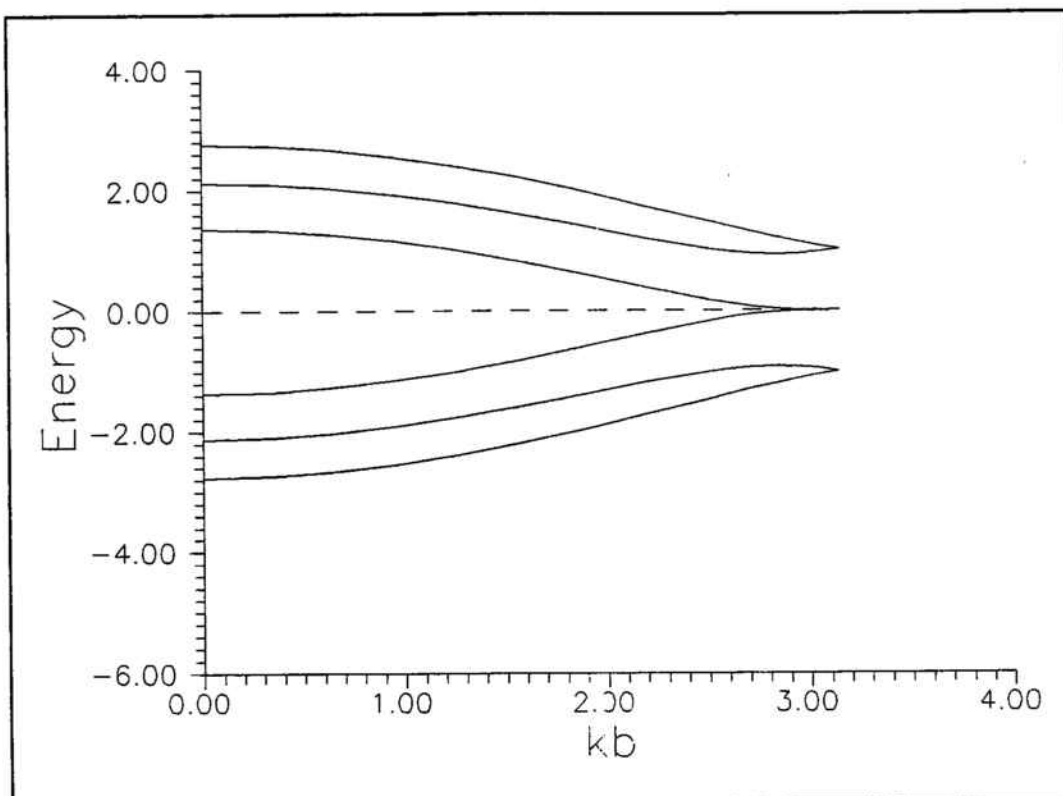
Figure 2: Energy bands for polyacenacene in the Brillouin zone, $(k_b \; \epsilon \; [0, \pi])$. The Fermi energy is represented by a dashed line. The HOMO and the LUMO cross at $k_F = \pi$.

It is a zero-width band gap system. The highest occupied band (HOMO) and the lowest unoccupied one (LUMO) cross at $k_F = \pi$ and they form a "semiloop" shape (see Fig. 2) when undistorted.

Peierls instability (Distortions)

We have studied the different possible distortions that were mentioned for poly-acenacene in section 4 of the Introduction part, by taking into account the pertur-bation δ_{ij} into the Hückel resonance integral, $\beta_{ij} = \beta(1 + \delta_{ij})$.

These distortions where labelled A, B, C depending on which symmetries were broken (a vertical plane, σ_v, and the screw axis, C_s, are the symmetry elements we

considered).

The distortion C_3, i.e. antisymmetric with respect to C_s and σ_v (see Fig. 8(c) in the Introduction part) is the only one that opens a band gap at $k_B = \pi$ when allowing $\delta_1 \neq 0$ and $\delta_0 \neq 0$. But the dependence of the gap energy ΔE versus δ is $\sim \delta^2$ or, what is the same, the orbital response to a distortion of strength δ is $\sim \delta^2$. See Fig. 3 where ΔE has been plotted as a function of δ.
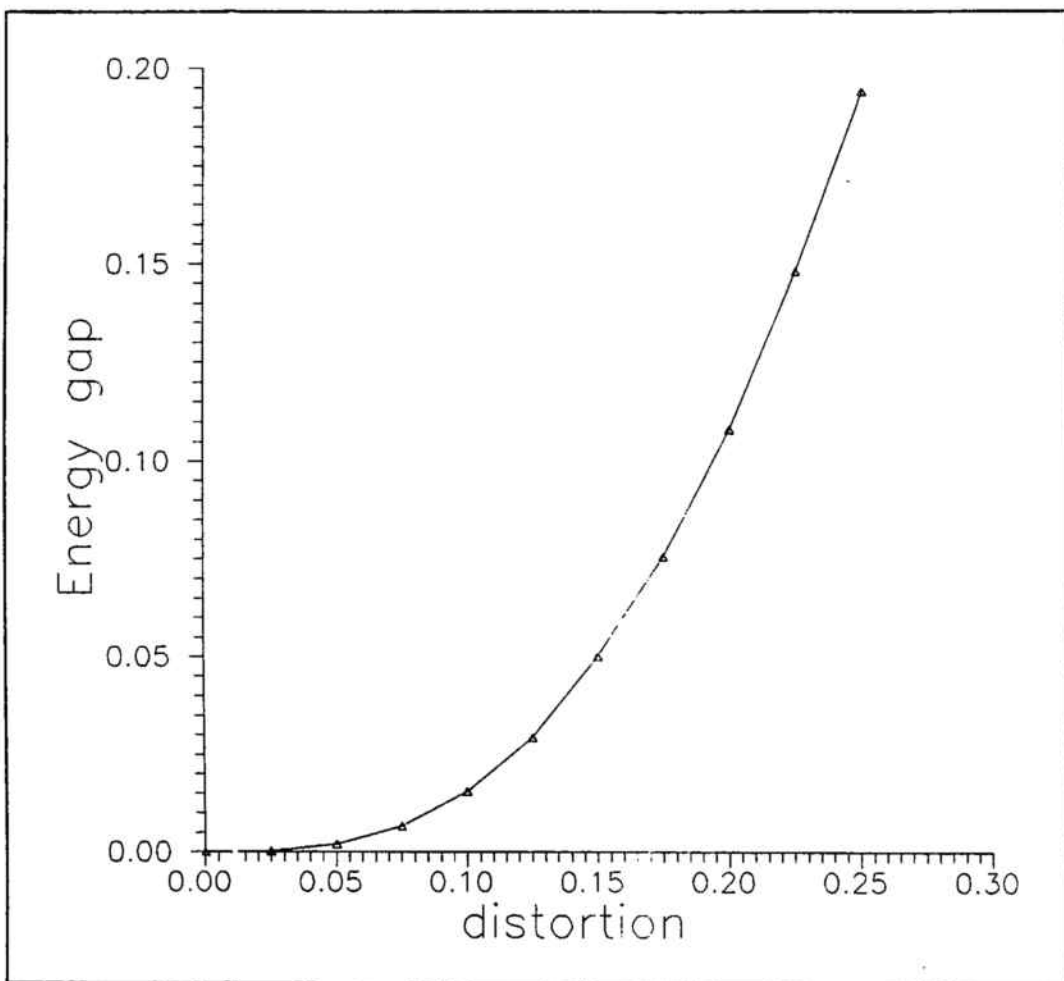
Figure 3: ΔE plot versus δ (Hückel model). These ΔE values correspond to the band gap that is opened when polyacenacene goes into a C_3 distortion. A δ^2 dependence is obtained.

Hückel model doesn't predict, therefore, any distortion for this system.

Nevertheless, going to better approximations in the band theory picture, different

results are obtained. For instance, if interactions within more distant π-centers are included, although small, terms linear in δ arise [Klein2 86].

There exists for polyacenacene a whole bunch of predictions in the band theory picture at different levels of approximation.

Tight-binding SCF-MO method in the level of CNDO (complete neglect of differential overlap) calculations suggest that the Peierls distortion doesn't take place and one can expect the *metallic* behaviour [Yamabe 82].

While Hückel method with second neighbor approximation predicts an energy response $\Delta E \sim \delta^3$ for distortions of the type shown in Fig. 4 [Kertesz 83].

Figure 4: Distortions predicted for polyacenacene by Kertesz *et al.* [Kertesz 83].

Bozović [Bozovic 85] combining tight-binding band structure computations with rigorous line group theoretical arguments predicts B_1 and B_2 distortions as the most favoured (see Fig. 8(b) in the Introduction part) in disagreement to Kertesz results [Kertesz 83]. He allows also the on-site orbital energy to vary linearly upon distortion.

1.1.2 (SPIN-PEIERLS) HEISENBERG MODEL

Undistorted Polyacenacene

The ground state energy for the undistorted polyacenacene has been obtained by the trial wavefunctions proposed in section 3 of the Computations part. Results are given in Table 2 where polyacetylene and the rest of polymers of our interest are also included for the sake of comparison.

E/JN	PCT	PCC	PBA	PPR	PPH
E_1	-.37500	-.37500	-.37500	-.37500	-.37500
E_2	-.37500	-.37500	-.4339(3)	-.4435(2)	-.4494(0)
E_3	-.41100	-.4539(5)	–	–	–
E_4	-.25000	-.333(3)	-.3214(3)	-.32500	-.31250
E_5	-.4279(1)	-.4941(0)	–	-.4906(2)	-.4794(9)
E_6	-.4431(5)	–	–	–	–

Table 2: Ground state Heisenberg energy per site in J units for a family of π-network polymers. PCT stands for Polyacetylene, PCC for Polyacenacene, PPR for Polyperylene and PPH for Polyphenanthrene. E_1 is the energy obtained with a single Kekulé structure. E_4 is the energy of the Néel state and E_2, E_3 and E_5 are the energies obtained with the "short range" RVB Φ_0, the "higher range" RVB Φ_1, and the Néel-state-based ansatz Ψ_0 respectively. E_6 corresponds to the exact value of the energy, only the 1D case is known [Hulthen 38].

The Néel-state-based wavefunction, Ψ_0, gives the lowest upper bound to the ground state energy for polyacenacene.

The energy corresponding to the "short range" RVB ansatz, Φ_0, is exactly the same as the one obtained by considering only one Kekulé structure at a time. This was expected because, as previously mentioned, this system characterizes by no Kekulé structure mixing, i.e. the cyclic boundary conditions of the system determine different non-overlapping Kekulé phases with only *one* state per phase. Therefore, Φ_0 is written in terms of one unique state.

Enlarging the basis set with "higher range" VB states contributes to lower the energy. It can be observed that computations with the "higher range" RVB ansatz, Φ_1, drastically improve the Φ_0 energy.

Φ_1 and Ψ_0, as far as the ground state energy concerns, give a fairly good description of the system when undistorted. Related properties like the spin Peierls instability are studied so as to compare predictions.

The value of the variational parameters associated to the different ansätze is given in Fig. 5. We can observe that they present the symmetries of the system.

(a)

(b)
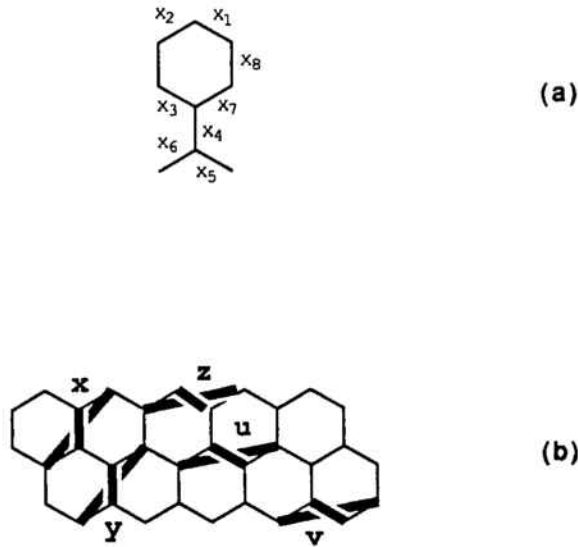
Figure 5: Optimized values for the variational parameters associated to the different trial ansätze in the undistorted polyacenacene. (a) Néel-state-based ansatz. The optimized values are $x_1 = x_2 = x_5 = x_6 = -0.29260(9)$, $x_3 = x_7 = -0.24531(2)$, $x_4 = x_8 = -0.22484(9)$. (b) "Higher range" RVB ansatz $x = y = 0.61590(9)$, $z = v = 0.53784(5)$, $u = 0.69723(1)$, $x_0 = 1$ (parameter associated to n.n. singlets).

Distortions

Spin-Peierls distortions have been studied with the different descriptions of the ground state.

Néel-state-based ansatz

In Fig. 6 the energy of the Néel-state-based ansatz has been plotted as a function of the δ parameter for the different distortions A, B_1, B_2, C_1, C_2, C_3 drawn in Fig. 9 of the Introduction part. A and C_1 are degenerate distortions. The stronger response is given by the C_3 distortion with a dependence in δ of the order $\sim \delta^2$. Fitting the results in a parabolic curve, it is obtained that $\Delta E \simeq 1.923\delta^2$ with a relative error $F = 2.152 \times 10^{-4}$.

A distortion is then not clearly predicted. Comparison of coeficients coming from this part and from the phonon part should be made to decide if the system distorts or not when described by such an ansatz.
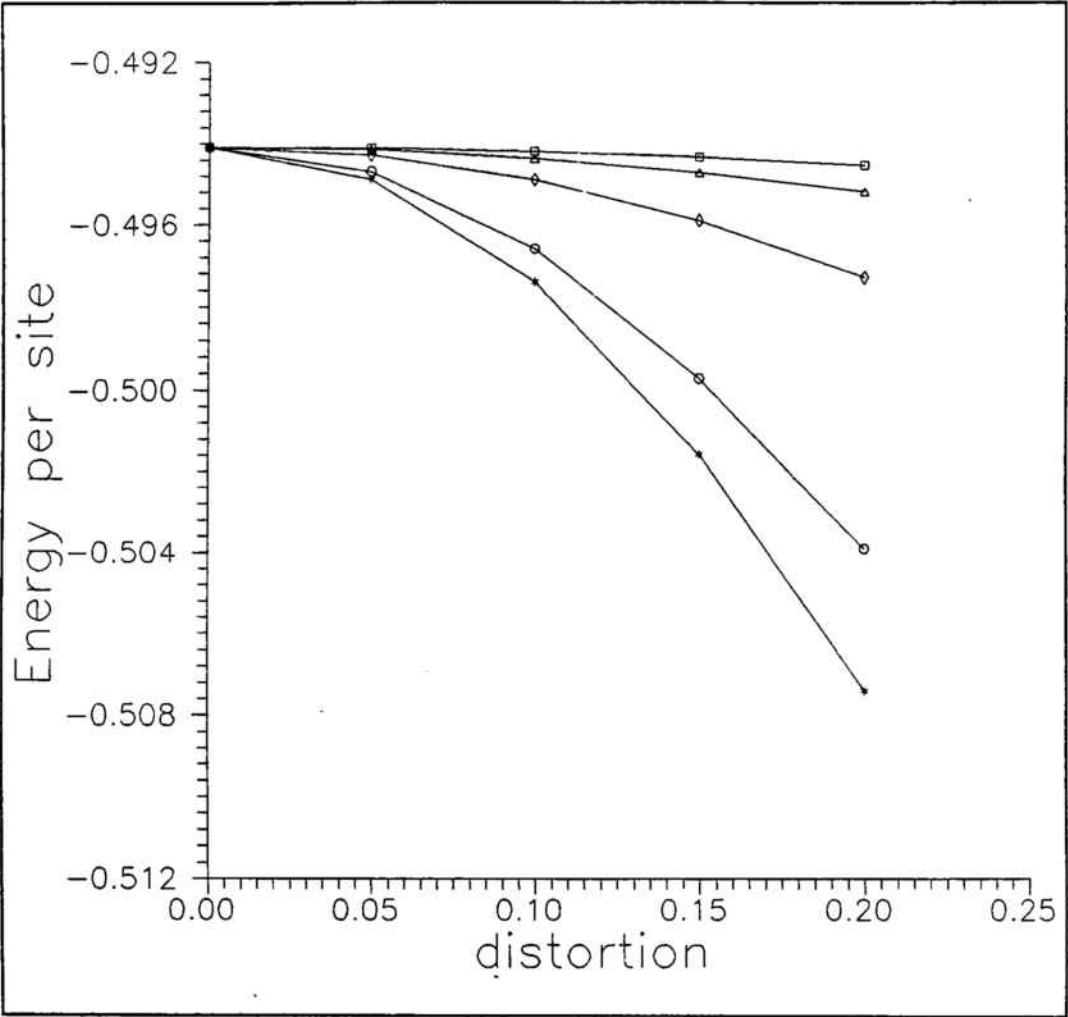
Figure 6: Energy values of the Néel-state-based ansatz in polyacenacene versus the distortion parameter, δ. The curves correspond to the different distortions drawn in Fig. 9 of the Introduction part: ($\square$) B_1, ($\triangle$) B_2, ($\lozenge$) C_2, ($\circ$) A and C_1, ($*$) C_3.

RVB ansätze

The predictions on the favored distortions apparently depend on the reference Kekulé state chosen. It will be shown below that this can be interpreted in a satisfactory way:

"Short range" RVB, Φ_0

For polyacenacene, the energy with Φ_0 can be easily calculated by hand.

As was shown in the section "*Computational example: polyacenacene*" where the reference Kekulé structure chosen to compute the energy corresponded to the $P = 3$ phase, there is *one local* state defined (see Fig. 8(c) in the Computations part). Introducing now the distortion dependence in the C matrix (see eq. (4.10) in the Computations part), we obtain:

$$
\begin{aligned}
C = {} & C^{12}(1 + \delta_{\bar{1}'}) + C^{23}(1 + \delta_2) \\
& + C^{34}(1 + \delta_0) + C^{45}(1 + \delta_{\bar{2}}) \\
& + C^{56}(1 + \delta_{\bar{1}}) + C^{21'}(1 + \delta_1) \\
& + C^{43'}(1 + \delta_{\bar{0}}) + C^{65'}(1 + \delta_{1'})
\end{aligned}
\tag{1.1}
$$

where we have followed the site numbering given in Fig. 8(b) in the Introduction part. For $P = 3$ phase, only $C^{21'}$, $C^{43'}$ and $C^{65'}$ are different from zero.

$$
\begin{aligned}
E/6LJ &= \frac{< \Psi \mid H \mid \Psi >}{< \Psi \mid \Psi > 6LJ} \\
&= \frac{-3}{24}((1 + \delta_1) + (1 + \delta_{\bar{0}}) + (1 + \delta_{1'})) \\
&= \frac{-3}{24}(3 + \delta_1 + \delta_{\bar{0}} + \delta_{1'}).
\end{aligned}
\tag{1.2}
$$

Distortions A and B are not favored because in these cases $\delta_{\bar{0}} = 0$ and $\delta_1 = -\delta_{1'}$. On the other hand, distortion C will definitely lower the energy because $\delta_1 = \delta_{1'}$ and $\delta_{\bar{0}}$ can be taken different from zero.

Therefore, the distortion C is predicted to occur when starting with a $P = 3$ phase with a linear energy dependence in δ, as it is analytically shown in the energy expression (any of the cases C_1, C_2, C_3 is possible. The one that lowers faster the energy is C_3 with $\delta_1 > 0$ and $\delta_{\bar{0}} > 0$).

We repeat the energy calculation choosing now as the Kekulé basis state the one corresponding to the $P = 1$ phase (see Fig. 7(a)), a convenient partition in zones is done (see the dashed lines in Fig. 7(a)), and only one *local state* is defined for the T matrix computation (see Fig. 7(b)).

$$T < e_1 1 \qquad = \qquad 8 < e_1 1$$
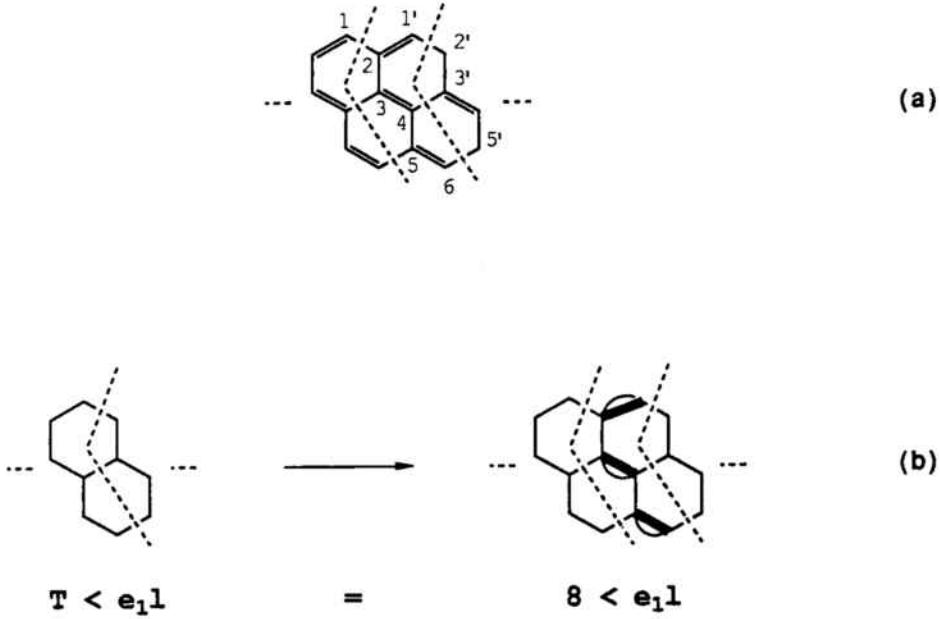
Figure 7: (a) Kekulé state belonging to the $P = 1$ phase in polyacenacene. The dashed lines determine the partition in zones chosen so as to carry out computations for Φ_0. (b) Local state defined for the T matrix. T_{11} matrix element.

In the undistorted case, only $C^{21'}$, C^{34} and C^{56} will give a nonzero contribution and the energy result is the same as the one obtained with the $P = 3$ state. Introducing the corresponding distortion parameters, the energy per site of the system reduces to:

$$E/6LJ = \frac{-3}{24}((1 + \delta_1) + (1 + \delta_0) + (1 + \delta_{\bar{1}}))$$
$$= \frac{-3}{24}(3 + \delta_1 + \delta_0 + \delta_{\bar{1}}). \tag{1.3}$$

Since $\delta_{\bar{0}} = \delta_0$ and $\delta_1 = \delta_{\bar{1}}$ for distortion A, a lowering of $-3\delta_1/12$ is obtained for this case, while distortion C where $\delta_1 = -\delta_{\bar{1}}$, is not favored to occur whenever $\delta_0 = 0$.

Therefore, if $\delta_0 = -\delta_{\bar{0}}$ is equal to zero for distortion C -this particular distortion has been labelled C_1 (see Fig. 9(c) in the Introduction part)-, when starting with $P = 3$ phase, the distortion to be predicted is distortion C_1 while when starting with $P = 1$ phase the distortion to be predicted is distortion A with the same energy

values. This is interpreted so that those two distortions C_1 and A are degenerate in energy, and, in fact, this is what was obtained when the Néel-based ansatz description was considered (although there, the energy dependence was very weak in δ).

Nevertheless, C_3 allows $\delta_0 = -\delta_{\bar{0}} \neq 0$ so that this will be the most favored distortion, with E depending linearly in δ.

"Higher range" RVB, Φ_1

Similar considerations as in the "short range" RVB wavefunction hold for this ansatz. Computations done with a Kekulé structure (taken as reference state to locally build new valence bond states) are equivalent if any other Kekulé structure is chosen. And the distortion behaviour is the same as in the "short range" RVB.

In Fig. 8, the "higher range" RVB energy dependence as a function of the distortion parameter has been plotted for the different distortions A, B_1, B_2, C_1, C_2, C_3 (drawn in Fig. 9 in the Introduction part). A and C_1 are degenerate distortions by the considerations already given for Φ_0.

It can be observed that polyacenacene is unstable to A, B and C distortions with a linear dependence in δ, but C_3 is the most favored one.

Comparing with the Néel-state-based results, equal predictions were obtained, although the energy response there wasn't strong enough so as to be a linear function in δ.

These predictions clearly don't agree with some from band theory results. What is learnt from here is that this system will distort, and no metallic behaviour is expected. Furthermore, that the most favored distortion will be a *totally-antisymmetric* one with respect to C_s and σ_v.

Experimental evidences are necessary to confirm these distortion predictions, but it seems that the efforts to sinthetize this system are not fruitful yet because it is very unstable to air. Nevertheless, the amount of discussion already existing about it in the literature makes its study worthwhile in order to come to a clear conclusion.
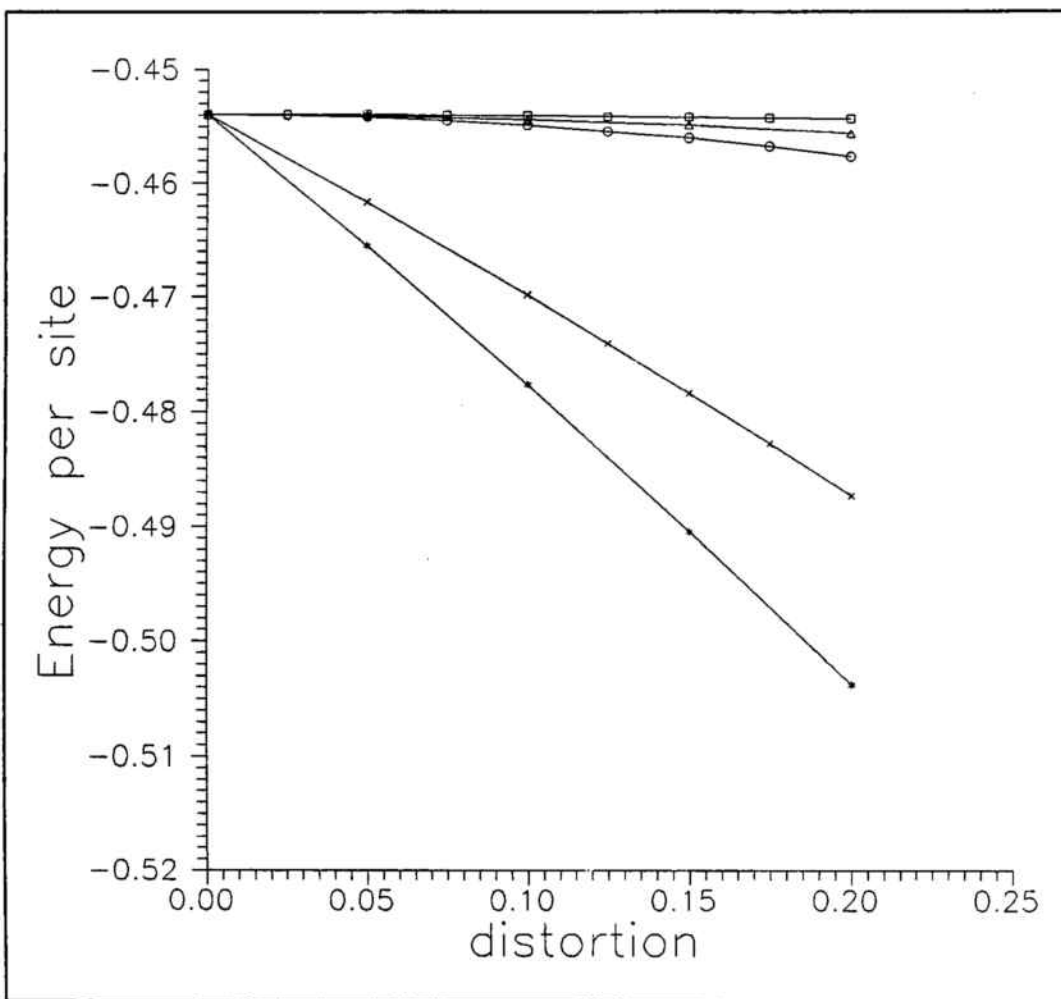
Figure 8: Energy values of the "higher range" RVB ansatz in polyacenacene versus the parameter δ for the different distortions considered in this system. $P = 3$ was the reference Kekulé phase. The various symbols correspond to the different distortions shown in Fig. 9 of the Introduction part: ($\square$) B_1, ($\triangle$) B_2, ($\circ$) A when $P = 3$ and C_1 when $P = 1$, ($\times$) C_1 when $P = 3$ and A when $P = 1$, ($\ast$) C_3.

1.2 PBA

1.2.1 HÜCKEL MODEL

PBA has seven sites per reduced unit cell. It is a half-filled band system. In Fig. 9 the energy bands have been drawn in the Brillouin zone. The lowest occupied band (LOMO) and the highest unoccupied one (HUMO) cross at $k_B = \pi$. It is a zero-width band gap system.
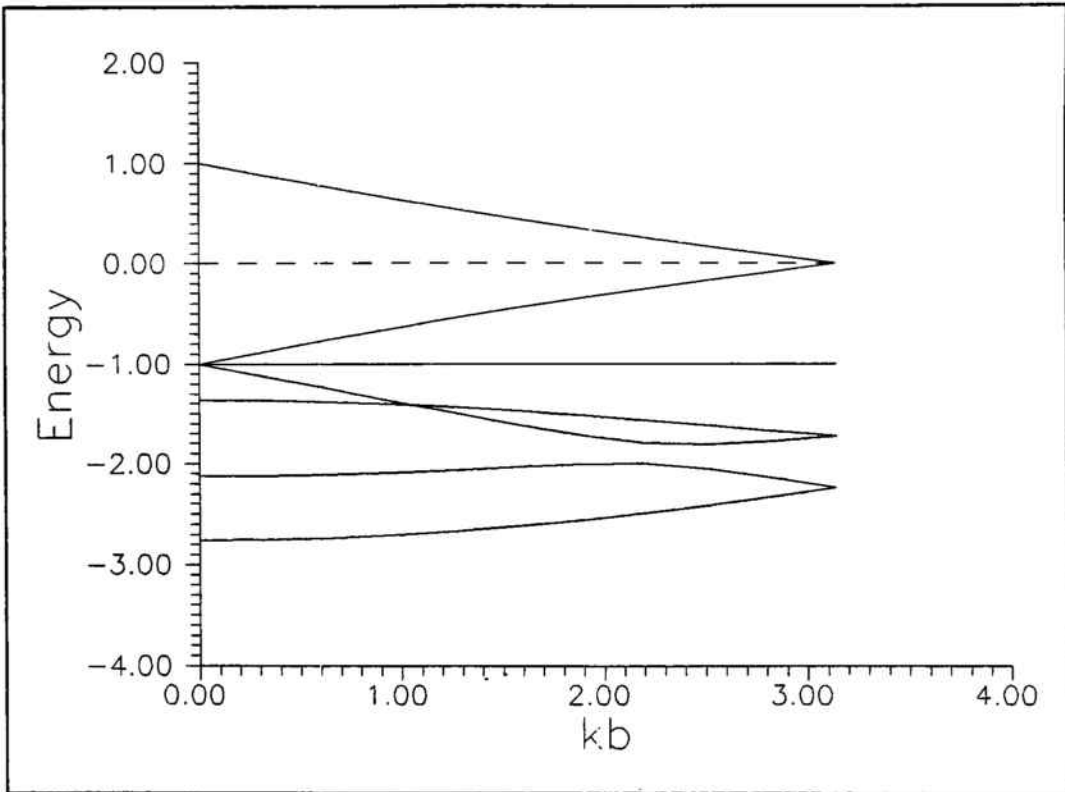
Figure 9: Energy bands for PBA in the Brillouin zone (Hückel model). Only the 8 lowest bands have been drawn. Bands are symmetric at $\epsilon = 0$ with respect to the k axis. The LOMO and HUMO cross at $k_b = \pi$. The Fermi level is represented by a dashed line.

Distortions

The distortions drawn in Fig. 14 in the Introduction part, have been studied for this system. Only the *totally antisymmetric* distortions C_1, C_2 among them all, open the zero-width band gap and with an energy dependence in δ almost linear (see Fig. 10 where ΔE has been plotted versus δ).

93
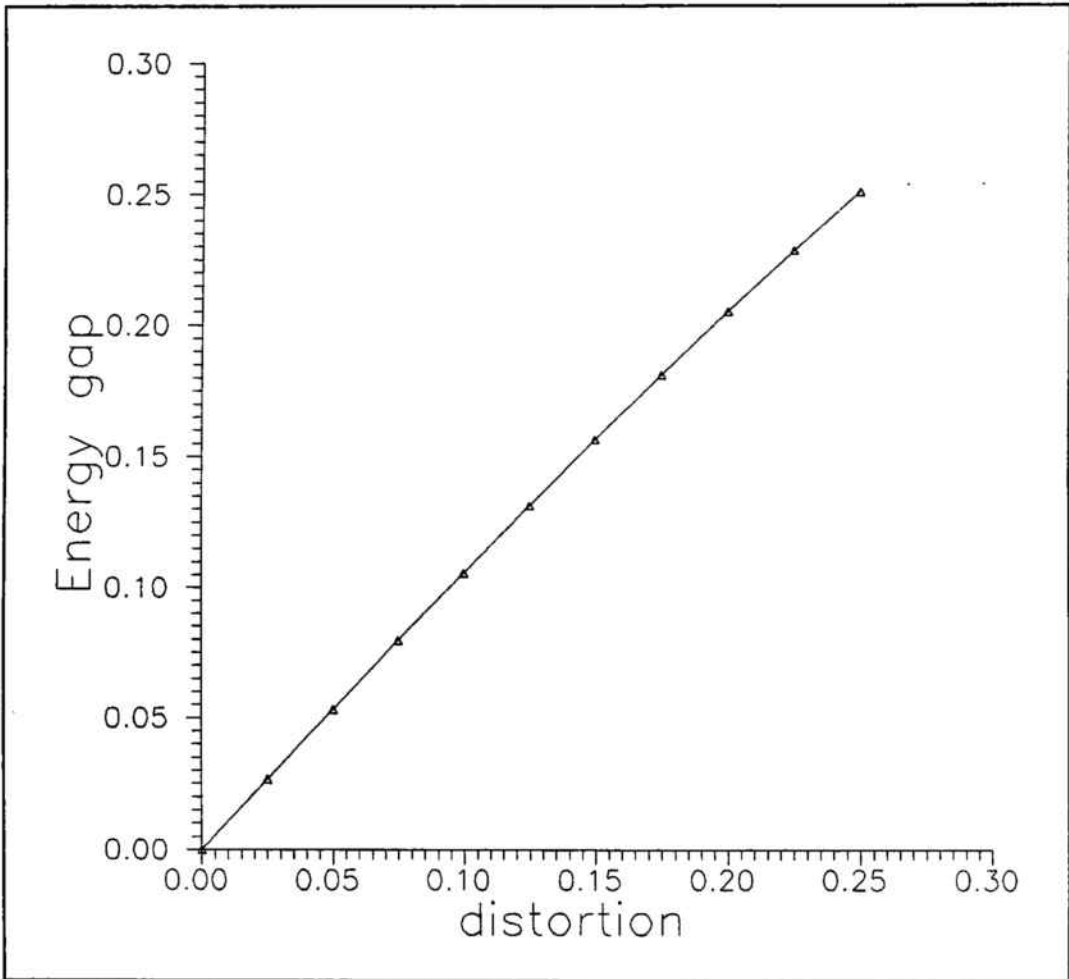
Figure 10: Energy gap dependence in the distortion parameter δ for distortion C_1 in PBA.

1.2.2 (SPIN-PEIERLS) HEISENBERG MODEL

Heisenberg model for this system has been studied with the "short range" RVB ansatz, Φ_0. PBA has two maximal degenerate phases $P = 0$ and $P = 1$ (see Fig. 11 and 12 in the Introduction part). When choosing $P = 0$ phase as the basis set, only one *local state* and 4 variational parameters need to be defined (see Fig. 11).
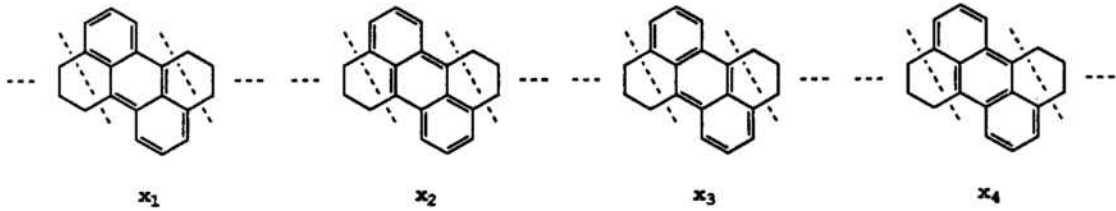
Figure 11: Representation of the 4 variational parameters defined for the Φ_0 computation in PBA. For convenience, instead of assigning a parameter to each possible n.n. singlet pair, the parameter has been associated to the set of singlet pairs in each possible Kekulé configuration in the unit cell. $x_1 = x_2 = 0.17777(3)$, $x_3 = x_4 = 0.22221(6)$.

The energy value is given in Table 2. The lowering experimented by the energy corresponding to only one Kekulé structure is important .

When choosing $P = 1$ phase as the basis set, 3 *local states* and 7 variational parameters are defined and the same ground state energy is obtained.

Distortions

In Fig. 12 the energy of the "short range" RVB ansatz has been plotted as a function of the distortion parameter for the distortions A_1, A_2, C_1, C_2 drawn in Fig. 11 in the Introduction part. The most favored distortions are the *totally-antisymmetric* ones C_1, C_2, in particular C_1, with an energy dependence linear in δ.

This result agrees with the Hückel model predictions.

PBA, as well as polyacenacene, is predicted a *totally-antisymmetric* distortion that breaks the symmetry of the reduced unit cell.

Experimental evidences are still not very clear for this system so as to confirm results. This example, nevertheless, shows that different point of views lead to the same conclusions.
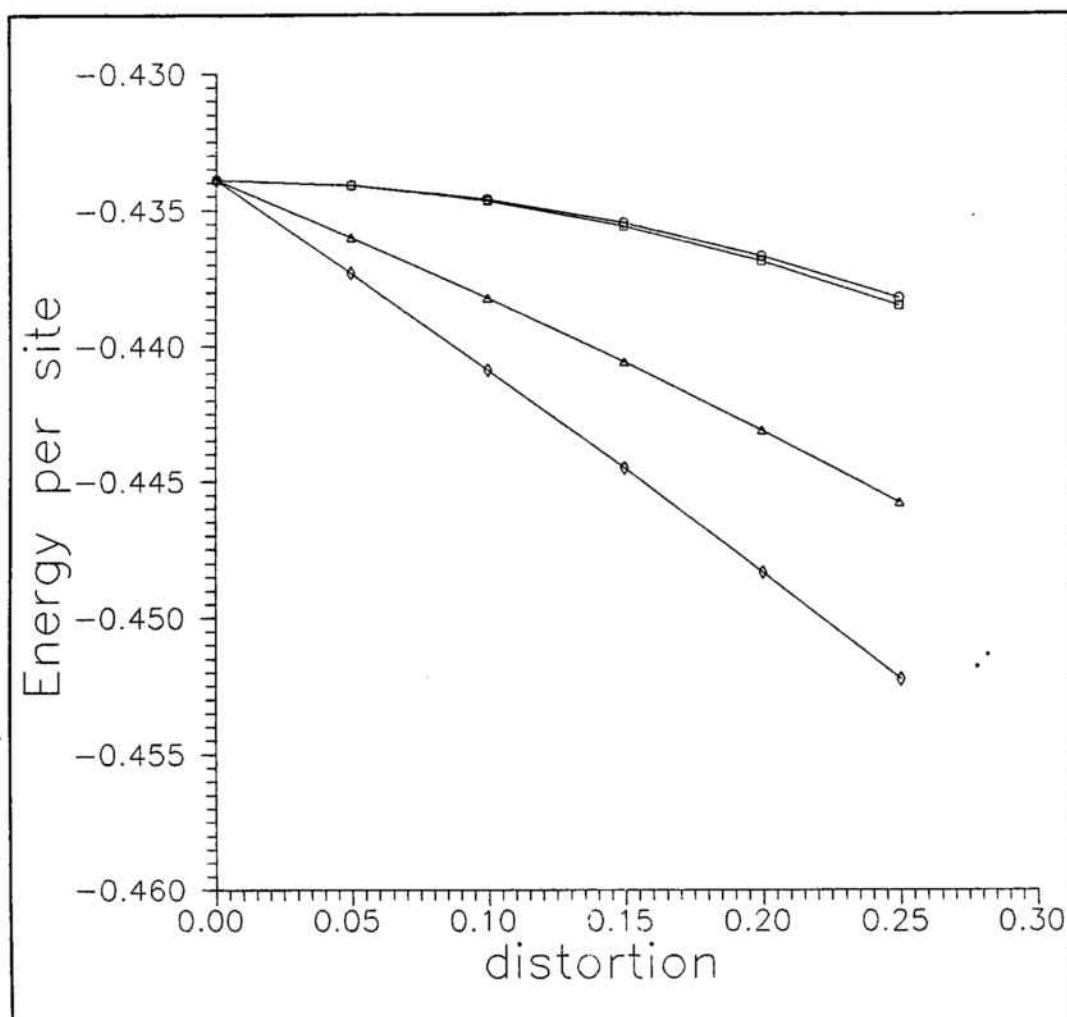
Figure 12: Energy values of the "short range" RVB ansatz plotted as a function of the distortion parameter δ for various possible distortions in PBA: (o) A_1, ($\square$) A_2, ($\triangle$) C_2, ($\diamond$) C_1.

1.3 POLYPERYLENE

1.3.1 HÜCKEL MODEL

Polyperylene has ten sites per unit cell (a reduced unit cell cannot be defined for this system). It is not a half-filled system but Hückel model gives an accidental zero-width band gap at $k_B = 0$.

96

In Fig. 13 the energy bands corresponding to the Brillouin zone have been plotted. The Fermi level is situated at the center of the Brillouin zone and it falls exactly at the accidental crossing point of two bands at $k_B = 0$.
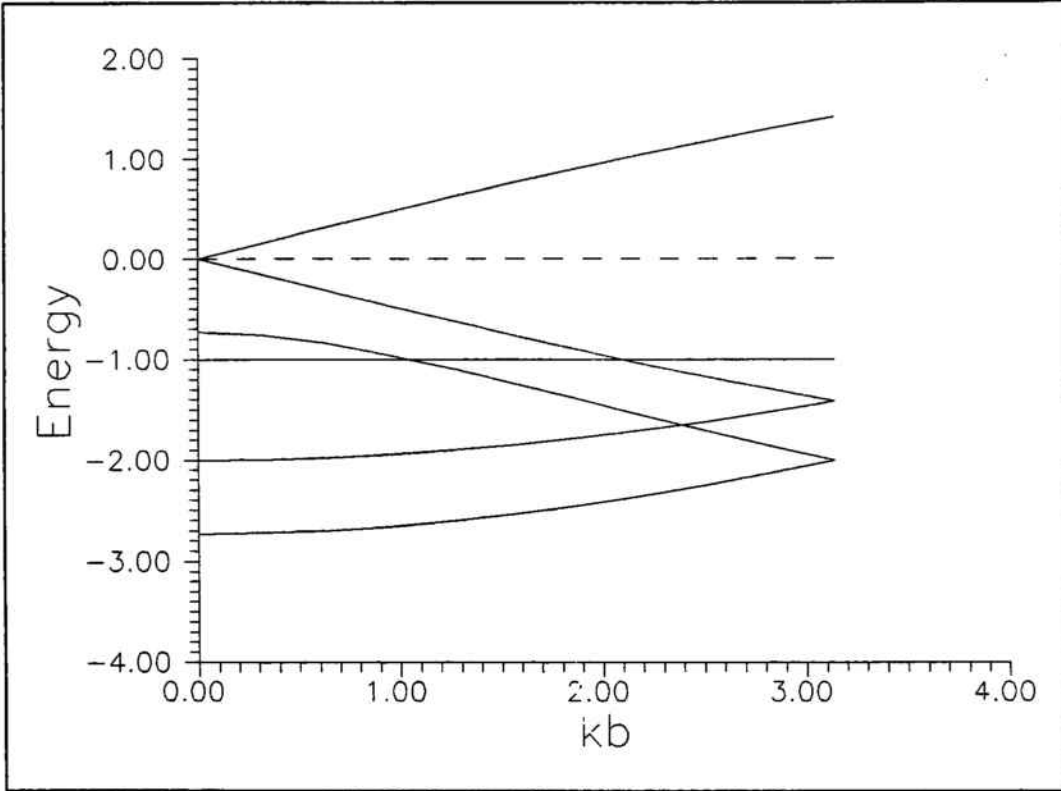
Figure 13: Energy bands for polyperylene in the Brillouin zone (the five lowest occupied bands and the first unoccupied one have been drawn). The Fermi level is represented by a dashed line. An accidental crossing of bands occurs at $k_B = 0$. The system has a zero-width band gap.

Distortions

A, B, C and D distortions have been considered for this system (see Fig. 19 in the Introduction part). The last one consists on a *totally-symmetric* distortion that may remove the crossing at $k = 0$.

Although distortions C_1 and C_2 open a gap at $k = 0$ weakly, the energy dependence in δ is $\Delta E \sim \delta^2$. Only distortion D_1 opens a band gap with an energy response linear in δ. (See Fig. 14 where the gap energy versus the distortion parameter δ has been plotted).
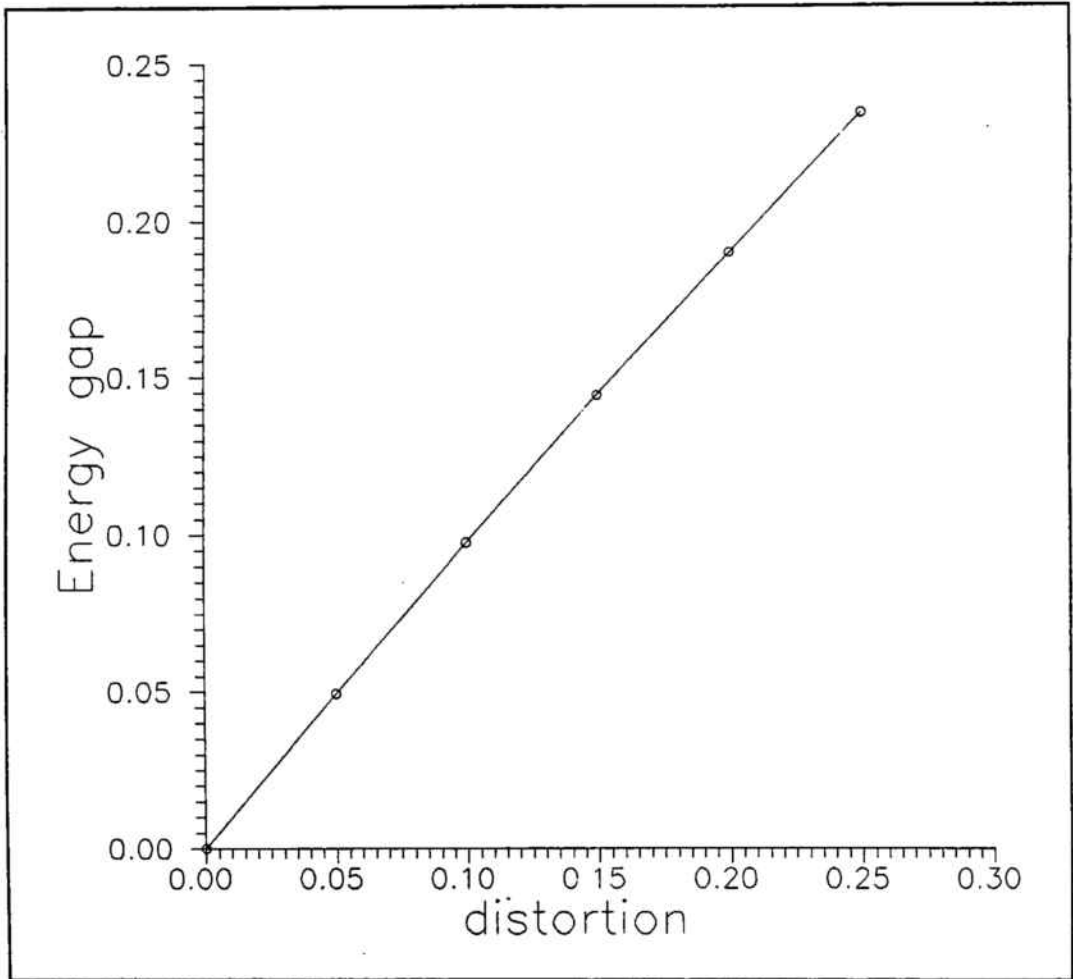
Figure 14: Gap energy plot versus the distortion parameter δ for the D_1 distortion in polyperylene.

Therefore, this system is predicted a totally-symmetric distortion within the band picture and this agrees with Tanaka *et al.* [Tanaka 84] and Bozović [Bozovic 85] results.

1.3.2 (SPIN-PEIERLS) HEISENBERG MODEL

Undistorted polyperylene

In Table 2, the energy results for this system with the different trial ansätze are shown. The lowest upper bound to the ground state energy is given by the Néel-based ansatz as was the case in polyacenacene. Transfer matrices for this computation are 5×5 matrices and 13 variational parameters are needed. In Fig. 15(a) the optimized variational parameters are given.

The "short range" RVB ansatz gives already a good upper bound to the ground state energy because, as in the PBA case, there is mixing of Kekulé states. Polyperylene has two maximal degenerate phases $P = 0$ and $P = 1$ (see Fig. 16 and 17 in the Introduction part). Any of those can be taken as the reference basis set to compute Φ_0. The $P = 0$ phase has been chosen. In that case, only one *local state* has to be defined and 3 variational parameters are needed. (See Fig. 15(b)).
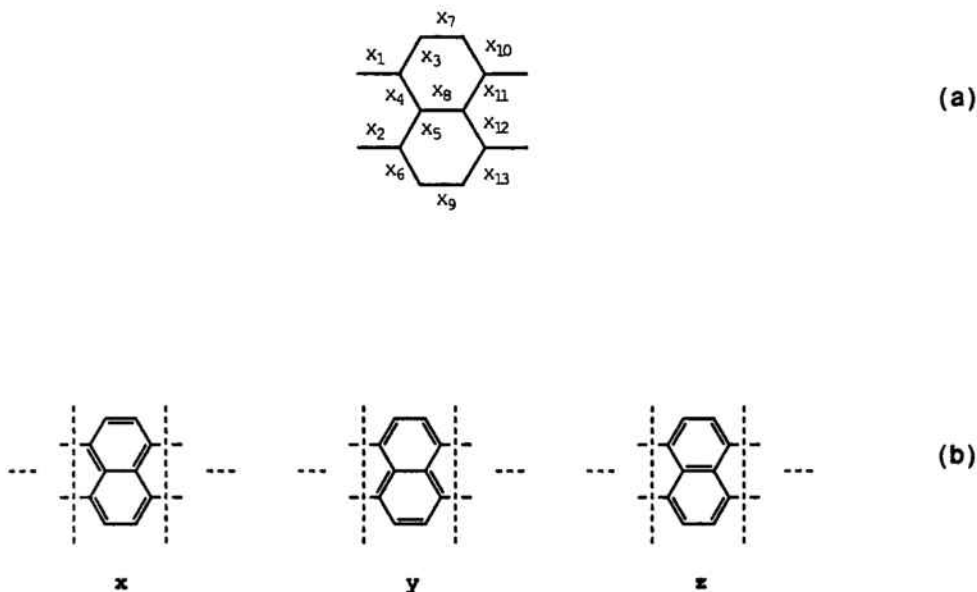
Figure 15: Optimized values for the variational parameters associated to the different trial ansätze in the undistorted polyperylene. (a) Néel-state-based ansatz, $x_1 = x_2 = -0.2369(3)$, $x_3 = x_6 = x_{10} = x_{13} = -0.2901(3)$, $x_4 = x_5 = x_{11} = x_{12} = -0.2427(7)$, $x_7 = x_9 = -0.398(8)$, $x_8 = -0.2453(2)$. (b) "Short range" RVB. The choice of the variational parameters follows the considerations explained in Fig. 11 for PBA, $x = y = 0.8182(5)$, $z = 1$.

Distortions

<u>Néel-state-based ansatz</u>

In Fig. 16 the Néel-state-based energy dependence is plotted as a function of the distortion parameter. Interest has been focused on the *totally-antisymmetric C* distortion and the *totally-symmetric D* distortion. For the rest of the hypothetical distortions, the energy response to the δ perturbation is very weak. Clearly D_1, the symmetric distortion, is favored and with a linear energy dependence on δ.
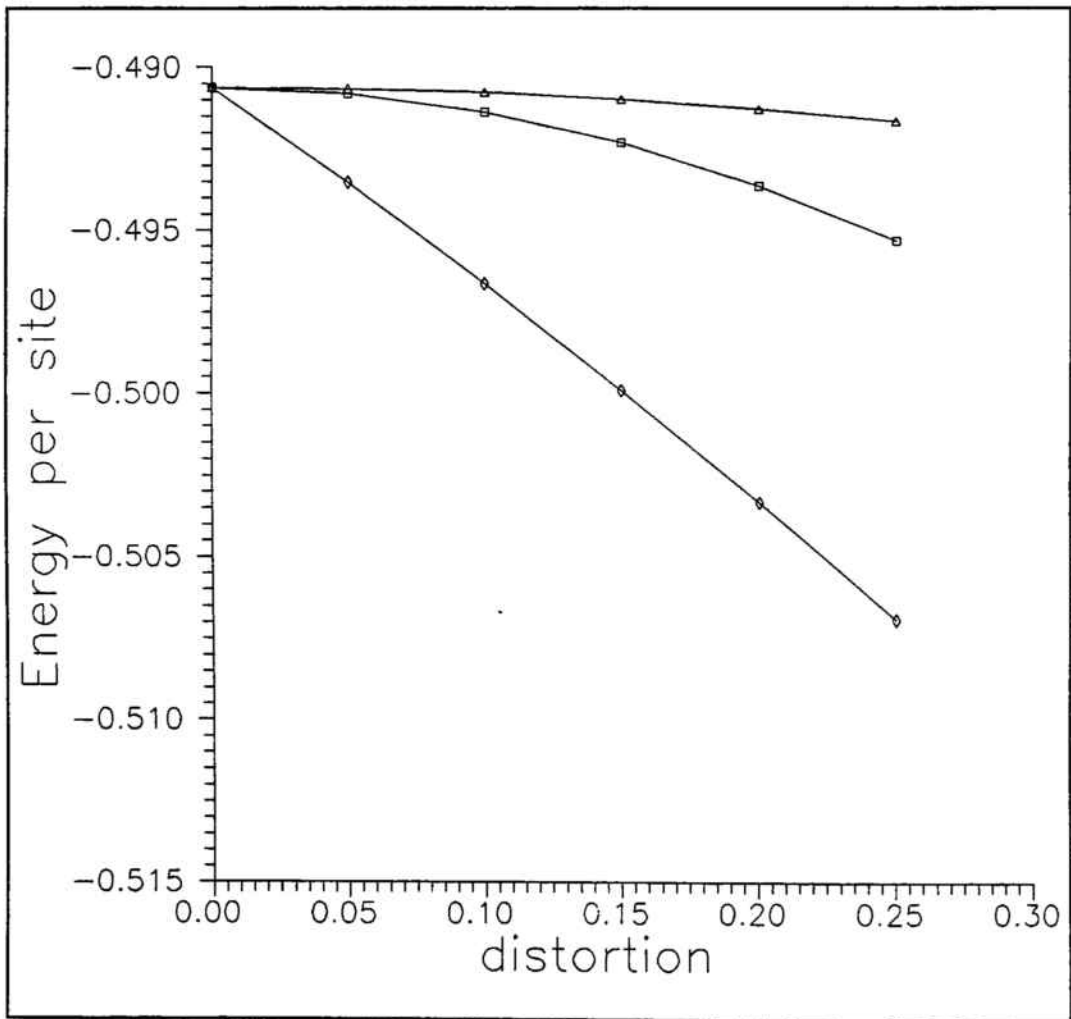
Figure 16: Néel-state-based energy values in polyperylene versus δ for the different distortions considered in this system: ($\triangle$) C_1, ($\square$) C_2, ($\lozenge$) D_1.

100

"Short range" RVB ansatz

The energy given by the "short range" RVB ansatz for the different possible distortions is plotted in Fig. 17 as a function of δ. The *totally-symmetric* distortion D_1 is the most favored. The energy response to that perturbation is linear in δ.

If $P = 1$ phase is chosen as the basis set, the same D_1 distortion is given as the most favored.

Results agree with the Néel-state-based predictions.
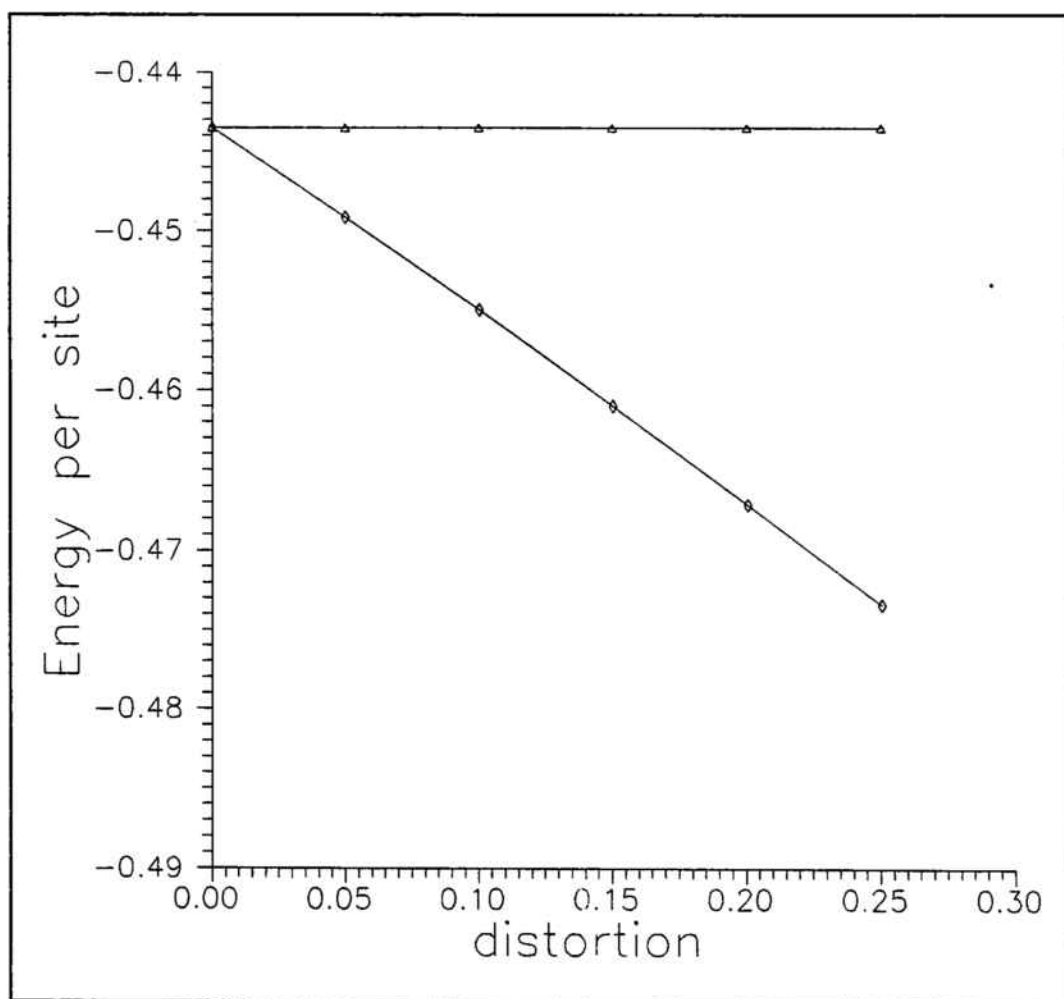
Figure 17: Energy values of the "short range" RVB ansatz plotted as a function of δ. The curves correspond to the various distortions considered for polyperylene: ($\triangle$) C_1 and C_2, ($\diamond$) D_1.

Band theory and Heisenberg model predict the same distortion behaviour for this system, i.e. the system is unstable to a *totally-symmetric* distortion.

Some evidence exists of polyperylene synthesis [Murakami 86], but experimental information on the structure of this system is still needed, such as neutron , electron or X-ray diffraction data in order to confirm the predicted results.

1.4 POLYPHENANTHRENE

1.4.1 HÜCKEL MODEL

Polyphenanthrene has 8 sites per unit cell and, as well as polyperylene, no reduced unit cell can be defined. It is not a half-filled system and Hückel model predicts a band gap. In Fig. 18, the 8 bands for this system have been drawn in the Brillouin zone. The Fermi level is in the middle of the band gap.
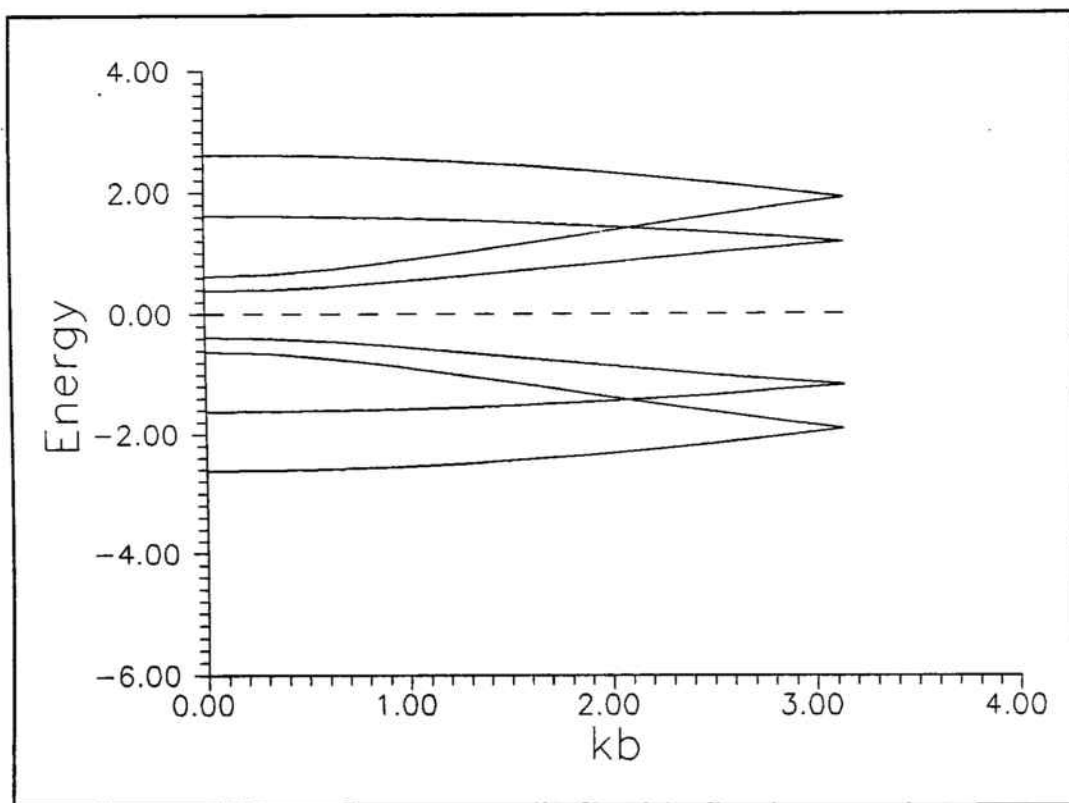
Figure 18: Energy bands for polyphenanthrene in the Brillouin zone. The dashed line corresponds to the Fermi level.

102

This system is not subject to a Peierls instability. A non-metallic behaviour is predicted.

1.4.2 HEISENBERG MODEL

The energy results obtained with the Néel-state-based ansatz and the "short range" RVB wavefunction are given in Table 2. Although the lowest upper bound is given by the Néel-state-based ansatz, the "short range" RVB, which as has been mentioned, constitutes a combination of a subset of all possible n.n. (nearest neighbor) singlet VB states (or Kekulé states), is already an important improvement with respect to the energy of only one Kekulé state.

Néel-state-based ansatz

Three *local states* and 5 variational parameters were defined for the Néel-state-based computation. The optimized values of the parameters are given in Fig. 19.

"Short range" RVB ansatz

This system doesn't have two cardinality-degenerate *maximal* Kekulé phases like the rest of the polymers presented do. Three non mixing phases have been defined (see Fig. 21 and 22 in the Introduction part). In order to obtain the best upper bound to the ground state energy within this ansatz, choice has been made of the phase that had more Kekulé states, and that corresponds to the $P = 1$ phase.

Three *local states* and 5 variational parameters have been defined to carry out computations. They are represented in Fig. 19 with the corresponding optimized values. Like in the rest of the systems, symmetries are mantained in the parameter results. Although we could have worked with less parameters, because normalization allows to set one of the parameters equal to one, we have preferred to let them all vary to make sure that results showed the symmetries they should.

Polyphenanthrene will be discussed in the Third Chapter as well where some interesting excitonic-like excitations will be presented.

103

"Local states"

$\langle e_1 l$ $\langle e_2 l$ $\langle e_3 l$ $\langle e_4 l$ $\langle e_5 l$

(a)

(b)

$\langle e_1 l$ $\langle e_2 l$ $\langle e_3 l$

(c)

x u v y z

(d)
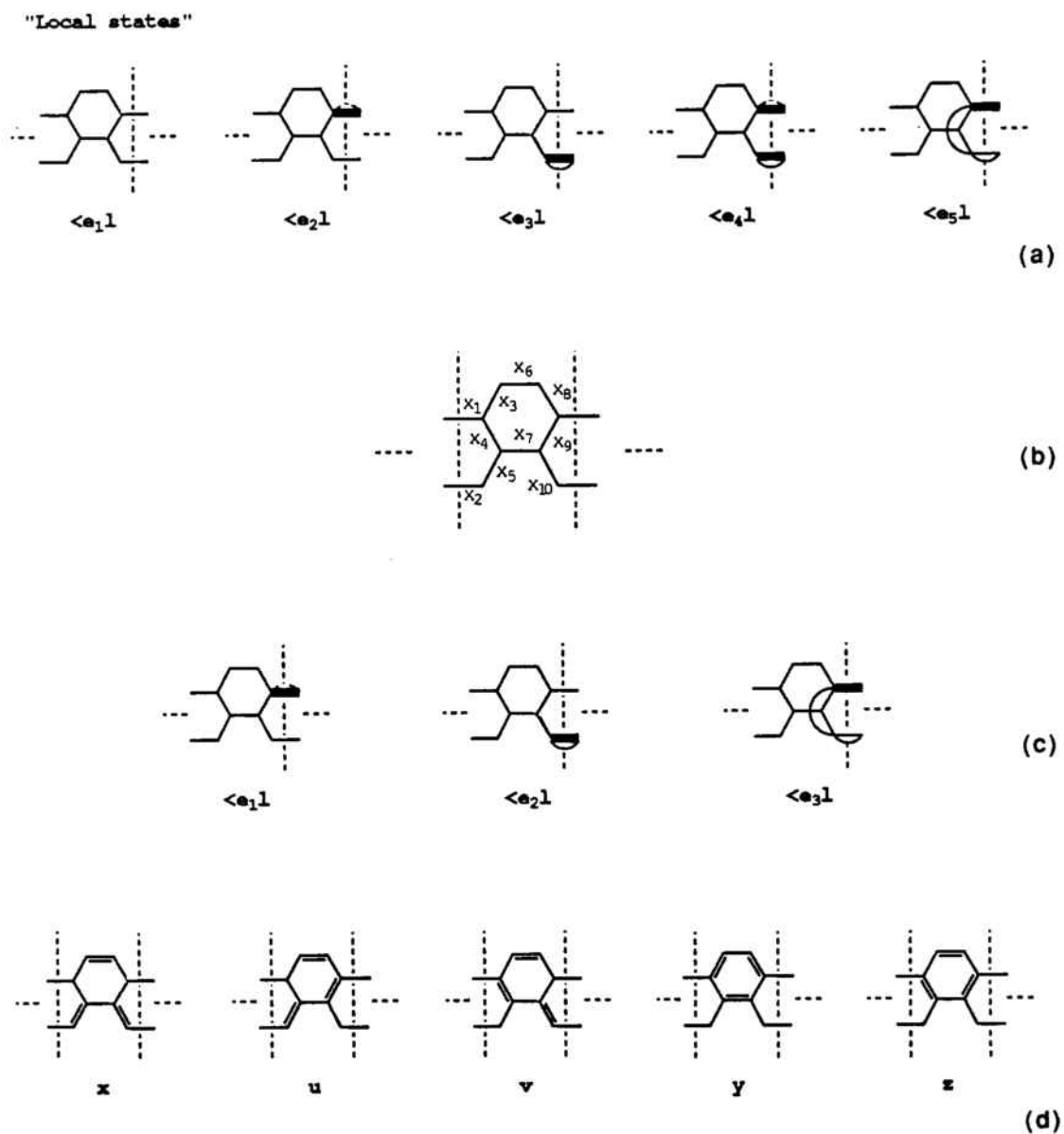
Figure 19: (a) Local states and (b) variational parameters for the Néel-state-based ansatz in polyphenanthrene. The optimized values are, $x_1 = x_7 = -0.2423(3)$, $x_2 = x_6 = -.4002(5)$, $x_3 = x_8 = x_5 = x_{10} = -.2923(3)$, $x_4 = x_9 = -.2473(4)$. (c) Local states and (d) variational parameters for the "short range" RVB ansatz in polyphenanthrene. The optimized values are, $x = 0.4569(3)$, $y = 0.4637(5)$, $z = 0.5551(5)$, $u = v = 0.5114(9)$.

104

2 DISCUSSION

The majority of computations in this chapter have been carried out with the **Transfer matrix technique** which has proven to be very adequate to express the properties of the systems chosen in terms of simple equations.

In this part of the thesis we have presented a study on the ground state nature of a family of conjugated polymers. An important property, **the Peierls instability**, has been explored.

Various alternative descriptions have been discussed. We have contrasted predictions of two opposite points of view:

- a **Localized scheme** where electron correlation is considered an important interaction. Within this picture, **Néel-state-based** descriptions have been compared to **RVB** (Resonating Valence Bond) descriptions.

- **Band theory**, that neglects electron correlation.

Néel-state-based ansatz

In all the undistorted π-network systems considered, and, among the various trial ansätze chosen, the best upper bound to the ground state energy is given by the Néel-state-based ansatz.

It is observed that this wavefunction is relatively efficient for those systems with low average coordination number, $\bar{z}$, i.e. the lowering in energy from the Néel energy, when adding to the Néel state other states where neighboring spins are flipped (as in the Néel-state-based ansatz), is greater if $\bar{z}$ is very small. Ordering the systems by decreasing $\bar{z}$ values,

- polyacenacene, $\bar{z} = 2.66$
- polyperylene, $\bar{z} = 2.6$
- polyphenanthrene, $\bar{z} = 2.5$
- polyacetylene, $\bar{z} = 2$ the corresponding lowering in energy with respect to the Néel energy is, respectively: -0.1611, -0.1656, -0.1669, -0.1779.

Also it is observed (see Fig. 5, 15, 19) that the absolute value of the optimized variational parameters is greater , when they are associated to spin flips that occur in **boundary** positions and for systems with low $\bar{z}$.

Furthermore, being x_i the variational parameter associated to the flip in position i between two neighboring spins a_i and b_i, the Néel- state-based wavefunction could

be partitioned,

$$| \Psi > = \frac{x_i}{\sqrt{1 + x_i^2}} |i \; flip > + \frac{1}{\sqrt{1 + x_i^2}} |no \; i \; flip > \qquad (2.1)$$

where $\frac{x_i^2}{1+x_i^2} \equiv c_i^2$ gives the probability of having a spin-flip on bond i. It is very interesting to observe that there exists a clear relation among all c_i^2 associated to bond positions with equal conditions on both ends, and this is almost independent of the system where they belong, i.e. given a bond i between sites a_i and b_i, if site a_i has n nearest neighbors and site b_i has m nearest neighbors, all bonds with n and m neighboring sites in any system have almost equal probability of having a spin-flip. See Table 3 where the c_i^2 values for the different systems have been given, they have been classified according to n-m values (see Fig. 5, 15, 19 for x_i positions).

POLYMER	$(z=2)$ - $(z=2)$	$(z=2)$ - $(z=3)$	$(z=3)$ - $(z=3)$
Polyacelylene	0.1313(9)	–	–
Polyacene	–	$[x_1]$ 0.0832(1)	$[x_5]$ 0.0460(3)
Polyacenacene	–	$[x_1]$ 0.0788(7)	$[x_7]$ 0.0567(6)
			$[x_8]$ 0.0481(2)
Polyphenanthrene	$[x_6]$ 0.1380(8)	$[x_3]$ 0.0787(3)	$[x_4]$ 0.0576(5)
			$[x_7]$ 0.0554(6)
Polyperylene	$[x_7]$ 0.1372(4)	$[x_3]$ 0.0776(4)	$[x_8]$ 0.0567(7)
			$[x_4]$ 0.0556(6)
			$[x_1]$ 0.0531(6)

Table 3: The values $c_i^2 \equiv \frac{x_i^2}{1+x_i^2}$, i.e. the probability of having a spin- flip on bond i, are given for the different bonds of the systems (indicated by [ ]). The c_i^2 are grouped by the number of nearest- neighbor sites on both ends of the bond. Results for polyacene have been provided by García-Bach *et al.* [Garcia-Bach2 89].

The reason of the little discrepancies observed among the c_i^2 parameters in a given column follows the same explanation. Namely, given a bond with n-m neighbors, the probability of a spin-flip decreases if the number of corresponding second neighbors increases and the same holds going to third, fourth,... neighbors. This can be observed in Table 3 by checking the x_i positions in Fig. 5, 15, 19.

We conclude then from these observed results that, the more nearest neighbors a given pair of spins has, the lesser the probability of having a spin-flip is.

More information about the nature of the systems with the Néel- state-based description can be obtained if the wavefunction is partitioned in a different way. It can be expressed:

$$|\Psi> = \sum_i^* \frac{x_i}{\sqrt{1+\sum_j^* x_j^2}}|flip \; on \; site \; l> + \frac{1}{\sqrt{1+\sum_j^* x_j^2}}|no \; flip \; on \; site \; l> \quad (2.2)$$

where $\sum_j^*$ means a sum over all neighbors of a given spin on site l. $d_l^2 \equiv \frac{1}{1+\sum_j^* x_j^2}$ is the probability of no spin-flip on **site** l.

While in the previous partition (2.1) we were interested in the probability of a spin-flip for a **pair** of neighboring spins, here (2.2) attention is focused on the behaviour of only one spin as a function of the number of neighbor spins. In Table

4, the parameters d_l^2 have been given for the various systems we studied. They have been classified in terms of the $z\bar{z}$ values, namely, for a given site l, z is the number of nearest neighbors of this site and $\bar{z}$ is the average number of nearest neighbors of the z neighbors of site l. In Fig. 20 the positions of the l spins for the different $z\bar{z}$ cases have been drawn.

	$z\bar{z} = 4$	$z\bar{z} = 5$	$z\bar{z} = 6$	$z\bar{z} = 7$	$z\bar{z} = 8$	$z\bar{z} = 9$
PCT	0.7677(3)	–	–	–	–	–
PCA	–	–	0.8463(6)	0.81311(5)	–	–
PPH	–	0.8027(8)	–	–	0.8296(3)	–
PPR	–	0.8043(5)	–	–	0.8338(5)	0.8488(5)
PCC	–	–	0.8537(9)	0.8184(6)	–	0.8540(3)

Table 4: Values of the parameter $d_l^2 \equiv \frac{1}{1+\sum_j z_j^2}$ for the various $z\bar{z}$ values and systems. PCT denotes Polyacetylene, PCA is Polyacene, PPH is Polyphenanthrene, PPR is Polyperylene and PCC stands for Polyacenacene. d_l^2 is the probability of no spin-flip for a given spin on site l.

Interesting relations can be deduced from Table 4. It is observed that, the probability of **no flip** for a particular site increases whenever the coordination number of this site and of its nearest neighbors increases. This holds for all $z\bar{z}$ values in our systems except for $z\bar{z} = 6$, where the probability of no spin flip is extraordinarily high. An explanation of this irregularity could be found in the fact that the location of the site l with these $z\bar{z}$ conditions (see Fig. 20) is somewhat special. It is a totally symmetric position, its neighbors have equal probability of spin interchange with it. An interchange with one of its neighbors would break this symmetry forcing the equivalent positions of the whole system to have the same interchange (because of the periodic boundary conditions), that would explain the reason why the spin prefers not to flip. This fact could be related with the instability of polyacene and polyacenacene that makes them difficult to be synthesized.

Apart from the $z\bar{z} = 6$ case, the conclusions reached by the study of Tables 3 and 4 are in agreement with the fact that 3D spin systems tend to show antiferromagnetic order, while in 1D systems, the probability of spin-flips is much higher and no Néel ordering is observed.
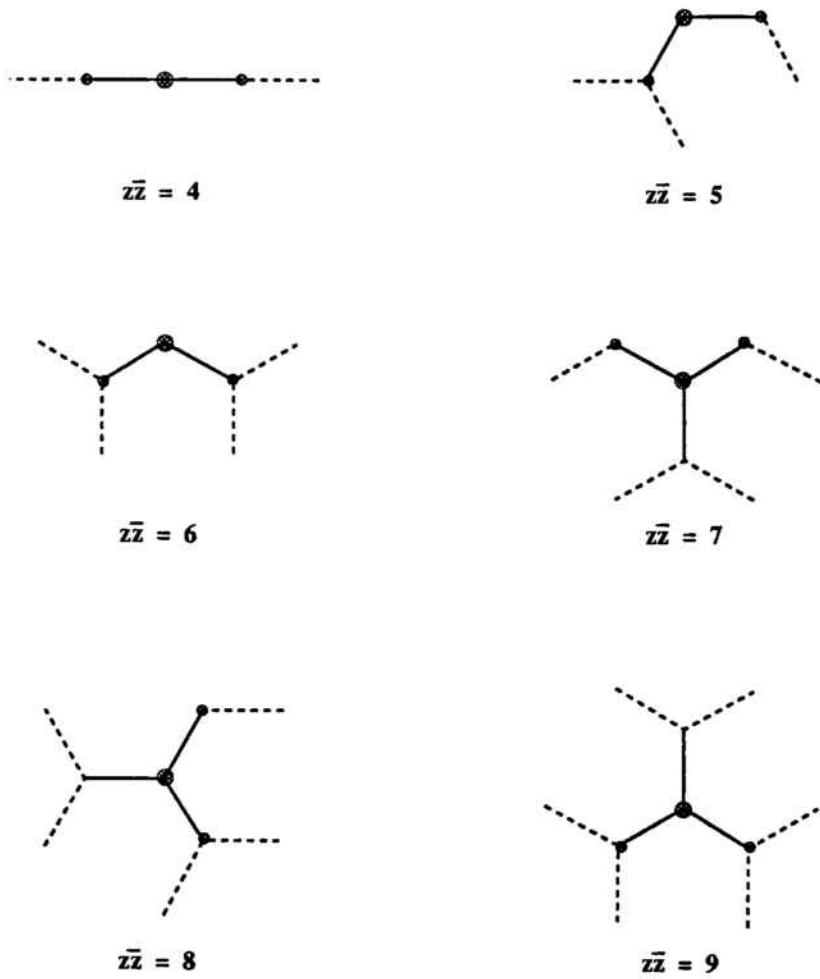
Figure 20: Possible positions for a spin l classified according to the corresponding $z\bar{z}$ values. The big circles denote spin l and the small ones its neighbors.

RVB description

Some interesting conclusions can also be reached from the RVB ansätze results, although they don't give the best upper bound to the ground state energy.

Two ansätze have been proposed, the "short range" RVB and the "higher range" RVB.

The "short range" RVB wavefunction, Φ_0, proves to be appropiate for those π-networks with **low** mean coordination number, $\bar{z}$, and with **many** Kekulé structures per site, n_K. A balance of these two factors is observed in the results of our π-network systems.

- polyacetylene, $\bar{z} = 2$, $n_K = 1$
- polyphenanthrene, $\bar{z} = 2.5$, $n_K \simeq 2.6$
- PBA, $\bar{z} = 2.57$, $n_K = 4$
- polyperylene, $\bar{z} = 3$, $n_K = 3$
- polyacenacene, $\bar{z} = 2.66$, $n_K = 1$

Whenever $n_K = 1$, as it happens for polyacetylene and polyacenacene, the energy obtained from Φ_0 is the energy corresponding to only one Kekulé structure. From the rest of the systems (see Table 2), polyphenanthrene is the one where Φ_0 provides the best upper bound, though the Néel-based ansatz still gives the lowest energy.

The "higher range" RVB, Φ_1, has been proposed for those systems where Φ_0 didn't improve the energy of only one Kekulé structure, namely polyacetylene and polyacenacene.

It is usually expected that adding new states to a basis set will always lower the energy value, but the question is what sort of states should be added. What is clear is that from the set of all singlet VB states, those that contribute the most is the subset of n.n. valence bond states (or Kekulé structures) where spins that are nearest neighbors are paired to singlet (Φ_0 is an example). This basis can be enlarged by those states that have pairings between non n.n. spins but still in the nearby, like Φ_1 definition, as was explained in the Computations part. Results confirm that the energy is fastly lowered (see Table 2), though not enough to reach the Néel-state-based energy.

It remains to be asked whether adding states with spins paired to singlet between sites further apart, will improve the energy result. The fact is that when

studying the variational parameters in Φ_1, those that weight more are the associated to short bonds (pairings) and longer bond contributions are much smaller (see Fig. 5). Therefore, an important lowering in the ground state energy wouldn't be expected.

Though the Néel-state-based ansatz gives better energy results for the ground state, one would expect that when taking into account interactions between second nearest neighbors, the energy corresponding to the Néel-state-based ansatz would increase frustrating somewhat the antiferromagnetic order, while, the one obtained by the RVB ansätze wouldn't.

Furthermore, these RVB descriptions play an important role when different type of excitations are considered for the systems, like *excitonic* excitations as will be seen in the Third Chapter for polyphenanthrene, or *hole* excitations commented in next chapter in the framework of Hi-Tc superconductors.

RVB is also an efficient description for studying the Peierls instability in these π-network systems. In all the extended polymers we studied, the energy response to a linear perturbation has always been linear, so that this ansatz is very sensitive to instabilities. With this ansatz it can be unambigously predicted that there always exists a distortion for any of the systems that lowers the energy linearly in δ, being this term dominant in front of vibrational energy that shows a δ^2 dependence. It is worthwhile to observe that in polyacenacene case, the Néel-state-based description was unable to predict whether the distortion was going to take place or not.

Finally, it is interesting to note that the behaviour of the variational parameters in any ansatz, when distortions are considered, seems to follow some rules. In all the systems, it has been observed that the variational parameters associated to every ansätze vary in the same way upon distortion, i.e., their absolute value always increase if a positive perturbation between sites l and p is introduced, either if a parameter is associated to a spin-flip of neighboring sites l and p (in Néel-state-based ansatz) or to a singlet pair l and p (in RVB ansätze). The explanation of that fact is that whenever $\delta_{lp} > 0$, sites l and p will tend to be closer, facilitating consequently either a spin-flip or a singlet coupling to occur, so that the weight of that operation will be more important.

Band theory ↔ Localized Scheme

When comparing band theory results with the localized description of the studied systems, we conclude that predictions of the two opposite limits seem to lead to similar consequences under similar structural circumstances, i.e. both approaches predict the same instability behaviour for the polymers when band theory is able to give a clear answer.

Band theory results depend enormously on the level of approximation, while this isn't so much the case for the localized description. This can be observed in the study of polyacenacene where band theory, at different levels of approximation, gives rise to different results.

On the contrary, the localized approach has proven to give non-contradicting predictions even if better descriptions were considered.

The analogy that is observed could be interpreted as that it is not necessary at all to neglect electron correlation in order to predict a Peierls-like transition. Contrary to the results obtained including correlation as a perturbation that leads to a lowering of the distortion [Dixit 84].

The analysis that has been carried out in this chapter would require experimental testing. Though the synthesis of some of the systems considered like polyacenacene seems quite difficult to achieve, hopes are put in this direction.

Heisenberg model on the square lattice. Relation with high-Tc superconductors.

Contents

Another interesting problem to be studied that needs the inclusion of electron correlation is the understanding of high-Tc superconductors and their mother compounds.

Our aim in this chapter is to explore the **ground state nature** of these systems in order to be able to build elementary excitations upon it, spin-like as well as hole-like excitations.

1   HISTORICAL SUMMARY ON SUPERCONDUCTIVITY

The superconductivity field started when Kammerlingh Onnes in 1911 observed that mercury had zero resistance at a temperature below $4.2K$. Later, the same superconducting behaviour was found in other metals like Sn, Al, Pb,... and compounds. Pioneering work on this field was done by London and London [London 35], Ginzburg and Landau [Ginzburg 50], Cooper [Cooper 56].

In 1957 Bardeen, Cooper and Schrieffer [Bardeen 57] proposed the **BCS** theory. This theory explains the superconductivity mechanism as a result of **electron pairing** due to the **lattice vibrations** (phonons). It is a consistent proposal that basically accounts for the properties of all the superconductors known before 1986. It was thought for a long time, that with BCS theory the superconductivity origin was completely stablished and that obtaining quantitative agreement between theory and experiment was only a question of details and not of principles.

From the beginning, it was considered of technological interest to have superconductors with high transition temperatures to the superconducting state, so that a great effort was done in the search of these kind of systems. In 1986, the list of superconductors was enormous but the transition temperatures were still below $20K$ and already some of them, like organic systems, A-15 compounds (e.g. Nb_3Sn, Nb_3Ge), Chevrel phases (e.g. $TrMo_6S_8$) presented some deviations with respect to strict BCS predictions.

The discovery of $La_{2-x}Ba_xCuO_4$ [Bednorz 86] and later $YBa_2CuO_{7-\delta}$ [Wu 87], compounds that become superconductors at temperatures around $68K$ (Lanthanum

compound) and $90K$ (Ytrium compound) respectively, represented an important issue in the search of high-Tc superconductors. It was observed that they were oxides with perovskite structure and that the experimental results couldn't honestly be fitted to conventional BCS theory predictions.

The manifest disagreement between the new superconductors and BCS theory predictions affects its fundamental aspects and a new theory to explain the experimental results in a satisfactory way is needed.

2 PROPERTIES
OF THE HIGH-Tc SUPERCONDUCTORS

The experimental characteristics of these new materials (see Bednorz *et al.* [Bednorz 88] for a review) are quite different from those of "classical" superconductors. We shall enumerate some of the most important features:

- They show *high* transition temperatures to the superconducting phase ranging from $60K$ to $120K$.

- X-ray measures and photoemission studies indicate that the electron correlation is *important* in these systems.

- The normal-superconductor state energy-gap is *anisotropic*.

- The carriers are *holes* (at least confirmed in the copper- oxide compounds we are discussing).

- The superconductor-metal tunneling effect is *anomalous*.

- As well as classical superconductors, quantized-flux measures through a ring $\Phi = n\Phi_0$, with $\Phi_0 = hc/q$ the elemental quantized-flux and n natural, show that there exists pairing between carriers, i.e.

$$q = 2e \qquad (2.1)$$

e being the electron charge.

- The coherence-length ξ of the pair is *small* and *anisotropic* contrary to that of classical superconductors.

- The Fermi energy, E_F, is of the order of the energy gap, Δ, $E_F \sim \Delta$ so that nearly all carriers participate in the superconductivity phenomenon.

This last feature, as commented in the introduction to this chapter, will play an important role when studying which is the mechanism of superconductivity in these

materials. This property distinguishes definitely the new superconductors from the classical ones where only a small fraction of the carriers are near the Fermi level and participate in superconductivity.

2.1   Structure and Electronic Properties

A starting point towards the understanding of the behaviour of these systems can be obtained from structure and electronic properties.

We restrict ourselves to the copper-oxides, in particular, $La_{2-x}Sr_xCuO_4$ and its corresponding mother compound, La_2CuO_4, shall be studied.

La_2CuO_4 is an insulator with three dimensional antiferromagnetic order. When it is doped with a small percentage of Ba or Sr, it becomes superconductor.

A common characteristic of the novel copper-oxide superconductors is that they are perovskite-like materials. Ideally, a perovskite is a compound formed by three kind of atoms in composition ABX_3 where A and B are metallic donors and X is a non-metallic acceptor (see Fig. 1 (a)). Often, in order to understand the great variety of perovskites, it is useful to regard their unit cell not as a cube but as a set of octahedra (see in Fig. 1 (b) the dashed lines).

The different piling and octahedra orientation give rise to the known perovskite variants, among them, La_2CuO_4 where $A = La$, $B = Cu$ and $X = O$ (see Fig. 2).

In this compound, the copper-oxigen, $Cu - O$, planes are electronically well separated, the distance between any two of them is approximately $6A$. This is a fundamental feature for the two dimensional behaviour of the system.

The La atoms donate three electrons to the neighbor oxigens, also the Cu atoms donate two electrons, remaining Cu^{2+} with a $3d^9$ configuration. This $3d$ level splits in a $3d_{x^2-y^2}$ and a $3d_{z^2-r^2}$ level due to the fact that the octahedra are elongated along the c axis. The copper-oxigen distance in the plane is, approximately, $1.9A$, while in the perpendicular direction is $2.4A$. An explanation of the elongation of octahedra could be found in the Jahn-Teller effect, in Cu^{2+} with $3d^9$ configuration, the ground state is degenerate, and a spontaneous distortion of the octahedron occurs to remove this degeneracy. The copper $3d_{x^2-y^2}$ orbitals and the oxigen $2p_x$ and $2p_y$ orbitals strongly hybridize.

ABX₃

A, B - metallic cations

X - non metallic anion

(a)   (b)
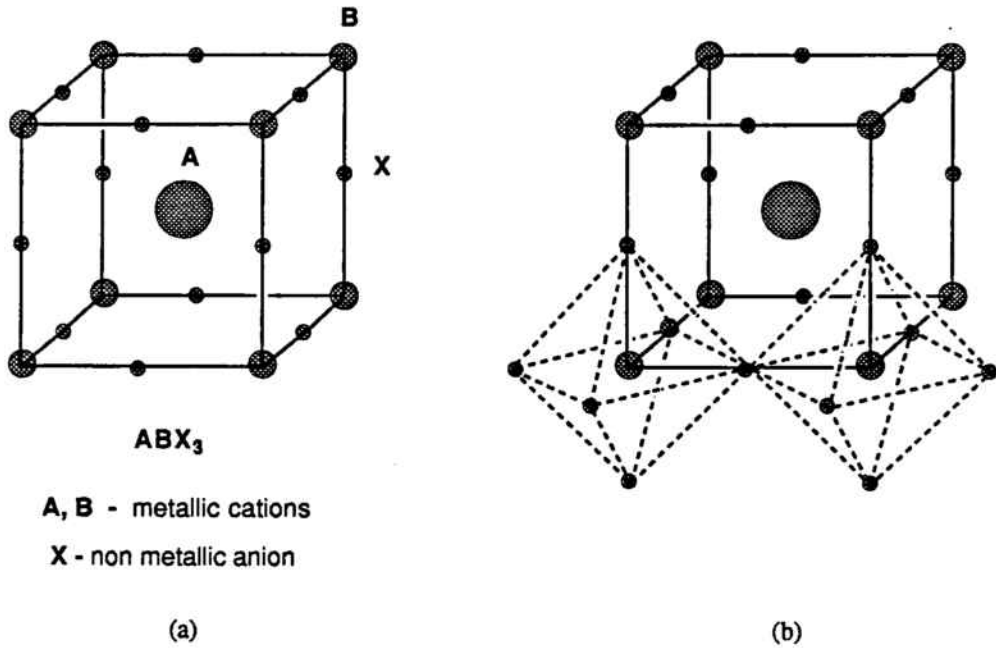
Figure 1: Perovskite structure. A and B are metallic donors and X is a non-metallic acceptor.

The structure is, then, $Cu - O$ planes with highly hybridized orbitals in the plane and the interaction among these planes fairly weak, conferring a bidimensional behaviour to the system. A $Cu - O$ plane can be represented as a square lattice where each lattice-point is occupied by a block $O - Cu - O$ as drawn in Fig. 3.

La$_2$CuO$_4$

La, Ba

Cu

O
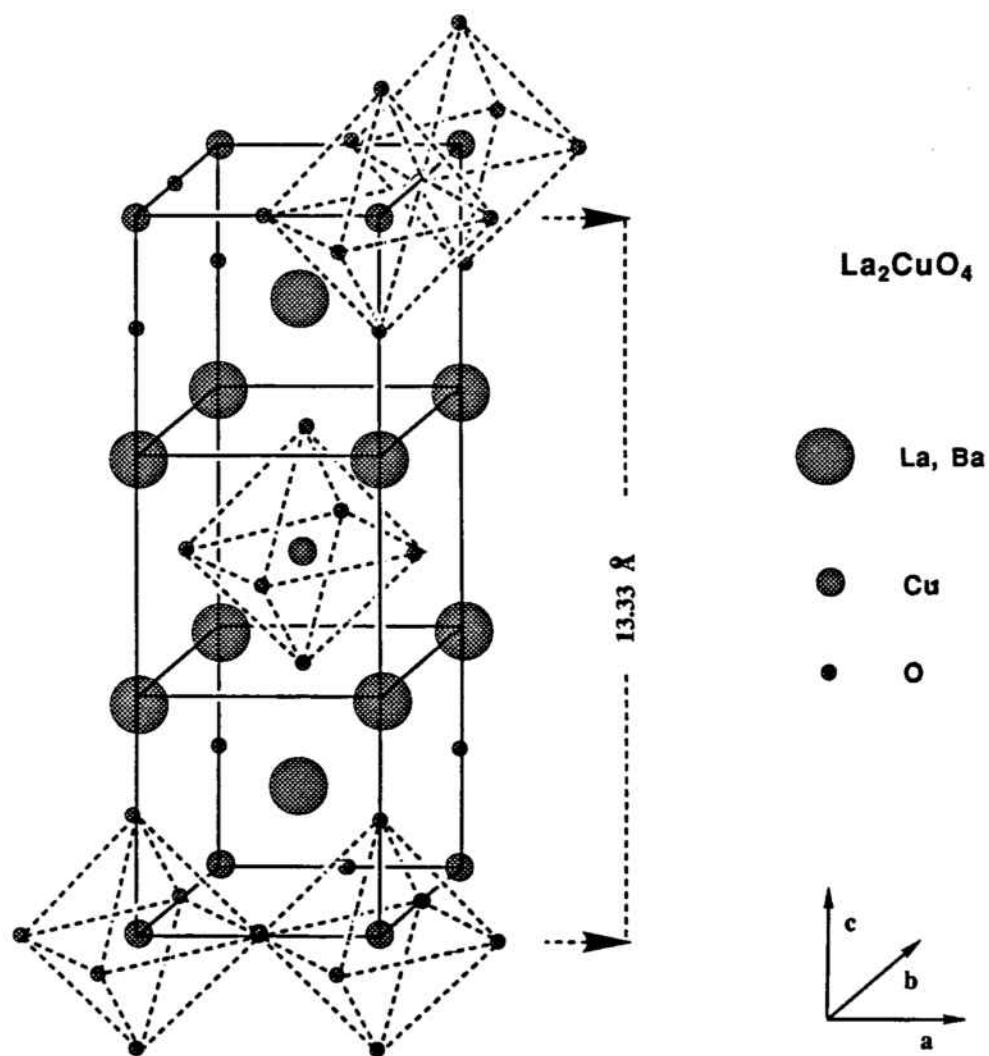
Figure 2: Perovskite structure corresponding to the $La - Cu - O$ compound. It differs from the ideal perovskite in that alternated octahedra planes are displaced.

119
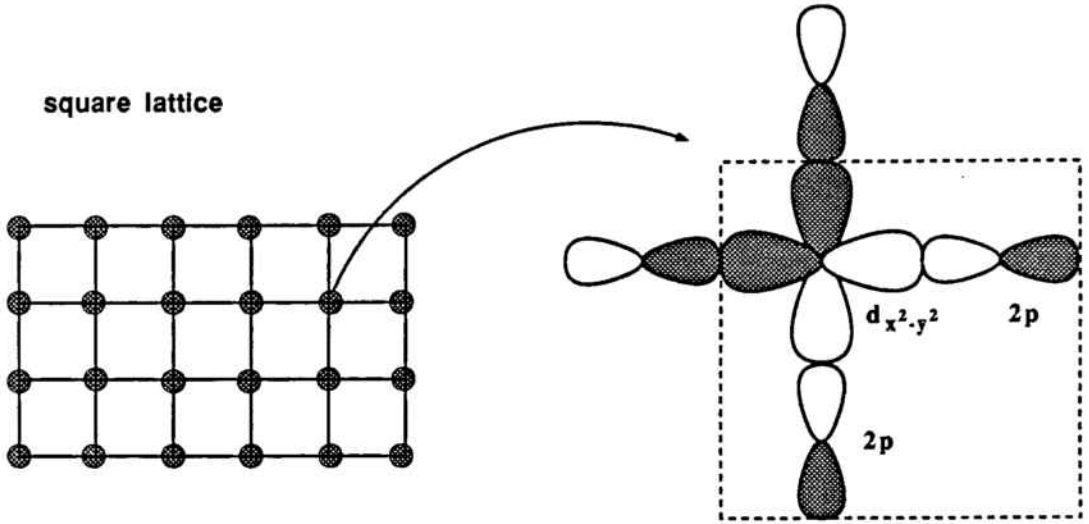
Figure 3: Square lattice. Every lattice point stands for the set $O - Cu - O$.

2.2 Tight-Binding Model

Within the band theory picture, the tight-binding approximation consists on assuming that in the vicinity of each lattice point, the full periodic crystal hamiltonian, H, can be approximated by the hamiltonian of a single atom located at a lattice point, H_{at}, and an additional term, $\Delta H(\bar{r})$ ($\bar{r}$ position vector), that contains the corrections to the atomic potential required to produce the full periodic potential of the crystal, i.e.,

$$H = H_{at} + \Delta H(\bar{r}). \tag{2.2}$$

Eigenfunctions of H,

$$H\Psi(\bar{r}) = \epsilon(\bar{k})\Psi(\bar{r}), \tag{2.3}$$

are Bloch orbitals. Periodicity of Bloch orbitals in k space ensures that they can be expressed as a linear combination of functions centered on lattice points, or *Wannier*

120

functions, Φ,

$$\Psi(\bar{r}) = \sum_R e^{i\bar{k}\bar{R}}\Phi(\bar{r} - \bar{R}). \tag{2.4}$$

In the LCAO approximation, Wannier functions, $\Phi(\bar{r} - \bar{R})$, can be approximated by a linear combination of atomic orbitals Ψ_n,

$$\Phi(\bar{r}) = \sum_n b_n \Psi_n(\bar{r}), \tag{2.5}$$

with

$$H_{at}\Psi_n = E_n\Psi_n. \tag{2.6}$$

The eigenvalue problem (2.3) can be solved using (2.4) and (2.5). And the Bloch energies, $\epsilon(\bar{k})$, are obtained.

A tight-binding calculation can be done with the $2p_x$, $2p_y$ orbitals of the oxigen and the $3d_{x^2-y^2}$ of the copper. Solving the tight-binding model, where the hopping integral t_α is between the copper orbital (with E_1 energy) and the neighboring oxigen orbital (with E_2 energy), the energies obtained are:

$$\epsilon_{k\pm} = \frac{(E_1 - E_2)}{2} \pm \frac{1}{2}[(E_1 - E_2)^2 + 8t_\alpha^2(1 + \cos k_x a + \cos k_y a)]^{1/2}$$

$$\epsilon_{k_0} = 0 \tag{2.7}$$

where a is the distance between sites and k subindexes $" + "$, $" - "$ and $"0"$ refer, respectively, to the antibonding, bonding and nonbonding bands.

We have, for the insulator compound (La_2CuO_4), five electrons per unit cell, then the Fermi level, E_F, is in the antibonding band. For simplicity, only this band will be considered.

This antibonding band can be reproduced, approximately, by a tight-binding model with hopping integrals between Wannier orbitals centered on copper atoms. These Wannier orbitals are to have the same symmetry as the copper $3d_{x^2-y^2}$ orbital with contributions from the neighboring oxigen $2p_x$ and $2p_y$ orbitals.

When the La_2CuO_4 compound is considered, this model has one electron per Wannier orbital and the rest of the four electrons are in the bonding and nonbonding bands that we are not taking into account.

As previously mentioned, it is observed experimentally that the La_2CuO_4 is an insulator and when it is doped, i.e., a La atom is substituted by Ba or Sr, the system becomes superconductor. Ba and Sr donate only two electrons to the neighboring oxigens, that means that one of these oxigens receives one electron instead of two. As oxigen is a very electronegative atom, it gets the missing electron from the $Cu-O$ planes. The doping process is equivalent, then, to introde *holes* on the square lattice.

$La_{2-x}Ba_xCuO_4$ remains insulator until the doping fraction, x, is of order ~ 0.05. In Fig. 4 the phase diagram *critical Temperature-doping fraction*, $T_c - x$, has been drawn.

Phase Diagram $La_{2-x}Ba_xCuO_4$
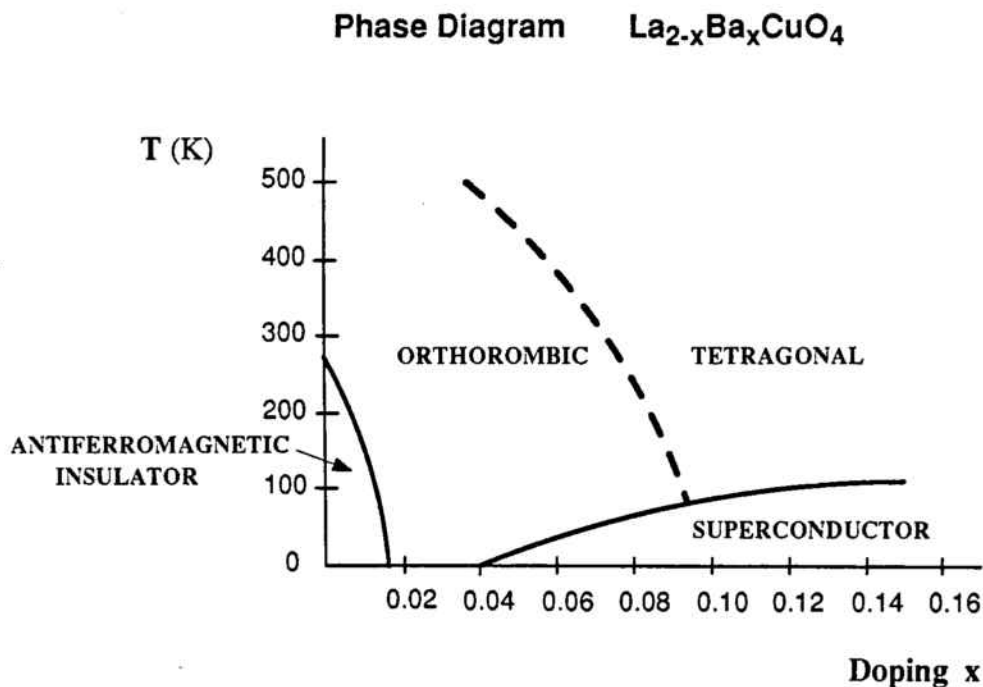
Figure 4: Phase diagram *critical Temperature - doping fraction* for the Lanthanum compound. (Note: It is only a qualitative picture).

It can be observed that, apart from the insulator-superconductor transition with an intermediate spin-glass zone, this compound shows also a structural phase transition.

Then these systems can be described, in a simple way, as a square lattice with one electron per site in the insulating phase that goes into a superconducting phase

when a small amount of holes is introduced.

In Fig. 5 a whole family of superconducting ceramic (i.e. oxides) materials is shown. They all have a structure of well separated $Cu-O$ planes and present similar properties.
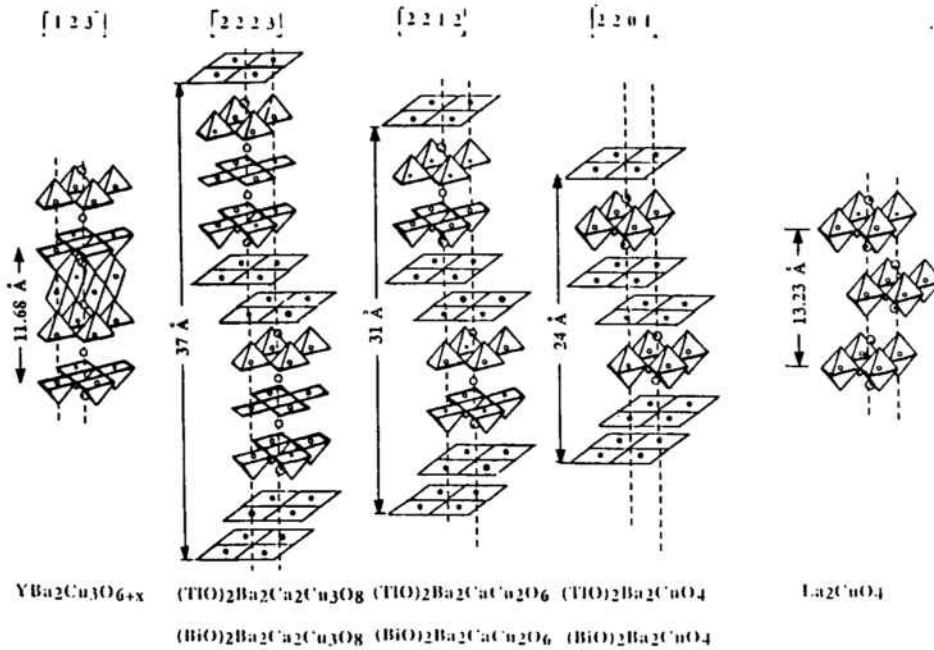
Figure 5: Copper-oxide superconductors.

Important interactions in these systems are now of interest. For simplicity, we shall continue centering the discussion on the $La - Sr - Cu - O$ compound unless expressed explicitly otherwise.

2.3 Important Interactions. Magnetism and Mott Insulators

The undoped compound La_2CuO_4, has one electron per site and, according to the tight-binding model presented above, the system should be a metal because it corresponds to a half-filled-band system. Experiments show, on the contrary, that La_2CuO_4 is a good insulator with an energy gap of $2eV$. In fact, there are many oxides like NiO, MnO, ... that, according to a band theory picture, should be conductors and they turn out to be insulators. The reason of this inconsistency is that in all these systems the *electron correlation* is an *important* interaction and, as tight-

123

binding calculations neglect it, the results obtained by this model are wrong. This strong electron correlation is what is also observed in these new superconductors.

All these systems are known as *Mott-insulators* [Mott 49]. They have one electron per Wannier orbital, the strong electron repulsion doesn't allow the electrons to gain delocalization energy and they remain localized with one electron per orbital. Taking into account the *screening* effect, the dominant electrostatic interaction is the *onsite* Coulomb repulsion, U. In oxides of transition metals U is of the order of 5 to 10 eV.

As the electrons hop between the transition metals through the oxigen orbitals, the hopping integral, t, is small $t \sim 0.5eV$. The delocalization energy of the electrons will then be $0.5eV \times z \sim 2.0eV$ where z is the coordination number of the lattice, and this energy is small compared to U. That forces the electrons to localization, i.e. to a Mott-insulating phase. Any excitation that requires charge transfer will need an energy of the order $E \sim U - zt$. This is the so-called *Mott-Hubbard gap*.

The suitable model hamiltonian for these systems is the *Hubbard* hamiltonian. Hubbard introduced it in 1963 [Hubbard 63] to study the properties of Mott insulators. It is the simplest model that takes into account electron correlation on a site and hopping between neighboring orbitals.

3   HUBBARD AND RELATED MODELS

3.1   Hubbard Model

We consider the one-band Hubbard model,

$$H_{Hu} = -t \sum_{<i,j>} [c_{i\sigma}^+ c_{j\sigma} + c_{j\sigma}^+ c_{i\sigma}] + U \sum_i n_{i\uparrow} n_{i\downarrow} \qquad (3.1)$$

where $c_{i\sigma}^+$ $(c_{i\sigma})$ is the operator that creates (destroys) an electron with spin σ on site i, $n_{i\sigma}$ is the number operator, i.e. $n_{i\sigma} = c_{i\sigma}^+ c_{i\sigma}$, it counts the number of electrons with spin σ on site i. t is the hopping integral between n.n. sites $(t > 0)$ and U is the onsite Coulomb repulsion. The first term is a kinetic term where an electron with spin σ is destroyed on site j and created on site i. And the second term, is the onsite electrostatic repulsion.

In the $U \ll t$ limit, the tight-binding model is recovered, and when $U \gg t$ we are in the strong electron-correlation regime.

Once the important interactions of the systems we are considering have been included in this model, one should proceed to solve it. It has been solved exactly only in one dimension (1D) by Lieb and Wu [Lieb 68] for all values of U and t. But, apart from the 1D case, no other analytic solution of the model has been achieved.

Different approaches have been carried out in order to obtain approximate solutions to more general cases than the 1D model. Some examples are,

- Cluster expansion method [Klein2 76]

- Monte Carlo numerical simulations [Hirsch 85], [Sorella 88] (2D model)

- Mean-field theories using different techniques. They provide a nice picture of the physical system but they are difficult to handle for this hamiltonian because electron correlation is important and cannot be simply averaged. Some of the techniques are, (*a*) slave-boson technique [Inui 86], [Ruckenstein 87], [Anderson2 87], [Baskaran 87], [Kopp 88], [Kotliar 88]. (*b*) Gauge theories and quantum-field theory techniques [Anderson 88], [Dzyaloshin. 88].

- Green-functions techniques. They are interesting because response functions can be studied [Schmitt-R 88], [Kane 89] among others.

For the description of high-Tc superconductors, a Hubbard model on the square lattice in the strong electron-correlation limit ($U \gg t$) and near the half-filled band (i.e. $1 - n_f \ll 1$ where n_f is the occupation number per site) can be considered. The last condition is used because the cases of interest correspond to one electron per site with a small number of holes.

3.2   Effective Hamiltonian. $t - J$ Model

The Hubbard hamiltonian, in the limit of strong electron correlation and near the half-filled band can be reduced to a simpler effective hamiltonian, the $t - J$ model. Let's consider then, the Hubbard hamiltonian (3.1) in the large U/t limit and $1 - n_f \ll 1$. Up to order t/U, it can be reduced, by canonical transformation, to two contributions. One, coming from the hopping term, that takes into account the mobility of the holes, and disappears for $n_f = 1$. The second contribution can be interpreted as a "virtual hopping" between pairs of singly occupied sites. Such a contribution can be expressed by a *Heisenberg term*,

$$\bar{S}_i \bar{S}_j, \tag{3.2}$$

with i and j nearest neighboring sites, that follows the virtual process,

$$|\uparrow,\downarrow> \longrightarrow |\uparrow\downarrow,-> ^{virt} \longrightarrow |\downarrow,\uparrow> \tag{3.3}$$

on sites i and j. It consists on the exchange of spins of a pair of singly occupied neighboring sites through a virtual hole-doubly occupied intermediate state. A real process of this kind is negligible because an energy of the order of U is needed.

The two contributions to this model are comparable when $U \sim t/(1 - n_f)$.

In order to derive the $t - J$ model, let's rewrite the Hubbard model as a sum:

$$H_{Hu} = T_h + T_d + T_{mix} + V \tag{3.4}$$

where T_h describes the hopping of the holes onto singly occupied sites,

$$|-,\uparrow> \longrightarrow |\uparrow,->, \tag{3.5}$$

$$T_h = -t \sum_{<i,j>,\sigma} (1 - n_{i,-\sigma}) c_{i\sigma}^+ c_{j\sigma} (1 - n_{j,-\sigma}) + H.c. \tag{3.6}$$

$H.c.$ stands for the hermitian conjugate.

T_d describes the hopping of doubly occupied sites onto singly occupied sites,

$$|\uparrow,\uparrow\downarrow> \longrightarrow |\uparrow\downarrow,\uparrow>, \tag{3.7}$$

$$T_d = -t \sum_{<i,j>,\sigma} n_{i,-\sigma} c_{i\sigma}^+ c_{j\sigma} n_{j,-\sigma} + H.c. \tag{3.8}$$

T_{mix} describes the processes where transitions from singly to doubly occupancy are considered,

$$|\uparrow,\downarrow> \longrightarrow |\uparrow\downarrow,->, \tag{3.9}$$

$$T_{mix} = -t \sum_{<i,j>,\sigma} n_{i,-\sigma} c_{i\sigma}^+ c_{j\sigma}(1 - n_{j,-\sigma}) + H.c.$$

$$-t \sum_{<i,j>,\sigma} (1 - n_{i,-\sigma}) c_{i\sigma}^+ c_{j\sigma} n_{j,-\sigma} + H.c. \tag{3.10}$$

And V is the Coulomb repulsion term,

$$V = U \sum_i n_{i\uparrow} n_{i\downarrow}. \tag{3.11}$$

The effective hamiltonian will be obtained after applying a unitary transformation onto H_{Hu},

$$H_{eff} = e^{iS} H_{Hu} e^{-iS}$$

$$= (1 + iS + ...) H_{Hu}(1 - iS + ...)$$

$$= H_{Hu} + i[S, H_{Hu}] + ... \tag{3.12}$$

where S is chosen so that the term T_{mix} disappears at lowest order in t/U. The aim of that is to remove real mixing processes between different Hubbard bands, i.e. double occupancy.

This choice translates into the following condition:

$$i[S, T_h + T_d + V] = -T_{mix} \tag{3.13}$$

which is equivalent to:

$$S = \sum_{n,m} | \phi_n > \frac{< \phi_n | T_{mix} | \phi_m >}{i(\epsilon_n - \epsilon_m)} < \phi_m | \tag{3.14}$$

where ϕ_n and ϕ_m are eigenstates of $T_h + T_d + V$ with the number of doubly occupied sites differing in one and with eigenvalues ϵ_n and ϵ_m respectively. ϵ_n and ϵ_m are not known exactly except for the one dimensional case but, in the large U limit, their difference will be of the order of U. Then, to first order in t/U, the value of S will be

$$S = -\frac{it}{U} \sum_{<i,j>,\sigma} n_{i,-\sigma} c_{i\sigma}^+ c_{j\sigma}(1 - n_{j,-\sigma})$$

$$-\frac{it}{U} \sum_{<i,j>,\sigma} (1 - n_{i,-\sigma}) c_{i\sigma}^+ c_{j\sigma} n_{j,-\sigma}. \tag{3.15}$$

127

The effective hamiltonian after eliminating the doubly occupied sites reduces to,

$$H_{eff} = -t \sum_{<i,j>,\sigma} (c_{i\sigma}^+ c_{j\sigma} + c_{j\sigma}^+ c_{i\sigma})$$

$$+t^2/U \sum_{j,\tau,\tau'} (c_{j+\tau\uparrow}^+ c_{j\downarrow}^+ c_{j\downarrow} c_{j+\tau'\uparrow} + c_{j\uparrow}^+ c_{j+\tau\downarrow}^+ c_{j+\tau'\downarrow} c_{j\uparrow}$$

$$+c_{j+\tau\uparrow}^+ c_{j\downarrow}^+ c_{j+\tau'\downarrow} c_{j\uparrow} + c_{j\uparrow}^+ c_{j+\tau\downarrow}^+ c_{j\downarrow} c_{j+\tau'\uparrow}) \qquad (3.16)$$

where $j + \tau$ and $j + \tau'$ are nearest neighbors of j, and creation and annihilation operators are restricted to the space without double occupancy. The t^2/U terms describe a hop from $j + \tau$ to $j + \tau'$ via a "virtual" intermediate state with a doubly occupancy at j. We now keep only the two-site contributions ($\tau = \tau'$) and make use of the spin operators $\bar{S}_i$,

$$\bar{S}_i = c_{is}^+ \bar{\sigma}_{ss'} c_{is'} \qquad (3.17)$$

$\bar{\sigma}_{ss'}$ are Pauli matrices. Then, the final $t - J$ hamiltonian can be written:

$$H_{eff} = T_h + \frac{4t^2}{U} \sum_{<i,j>} (\bar{S}_i \bar{S}_j - 1/4) \qquad (3.18)$$

where T_h is the hole-transport contribution (3.6) and the second term is the *Heisenberg* interaction term between spins.

We have obtained a simpler effective hamiltonian than the starting Hubbard model that reproduces the main characteristics of this one in the strong electron correlation limit near the half-filled band region as corresponds to high-Tc materials.

3.3   Heisenberg Model

We devote ourselves to the exactly one electron per site case on the square lattice system which is a suitable model to describe mother compounds of high-Tc superconductors.

When there is one electron per site, $n_f = 1$, the T_h term in (3.18) disappears. In this case the effective $t - J$ hamiltonian reduces to the **Heisenberg hamiltonian**,

$$H_{Heis} = J \sum_{<i,j>} \bar{S}_i \bar{S}_j \qquad (3.19)$$

with $J > 0$.

128

The way the Heisenberg hamiltonian has been obtained here from the Hubbard model is not unique. We have followed Gros *et al.* [Gros 87] development but there are also other very interesting derivations in the literature (see [Klein 74], [Zaanen 88], [Poshusta 89], [Ramsak 89]).

This hamiltonian, as commented in the First Chapter, while simpler than the Hubbard model, has not been solved exactly yet, except in the one dimensional case [Hulthen 38] with the Bethe ansatz and for small systems where diagonalization is computationally feasible.

Different approaches have been done in order to have solutions for more general cases than the 1D Heisenberg model. We enumerate here some of them:

- Spin-wave theory [Anderson 52].

- A search for exact analytic results and fundamental theorems [Haldane 88], [Mattis 88], [Shastry 88].

- Monte Carlo numerical simulations [Reger 88], [Barnes 88]. Very accurate results of the ground state energy have been obtained, but still, the ground state wavefunction cannot be calculated by this method.

- Exact diagonalization of small systems [Oitmaa 78], [Dagotto 88], [Bonca 89], [Poilblanc 89], [Zivkovic 89], [Hasegawa 89], [Figueirido 89]. Although providing exact information, the systems that have been diagonalized are very small (4×4). When going to bigger systems the basis set increases considerably making computations almost impossible. Nevertheless, these results are of great value because approximations may be more rigorously tested than is otherwise possible.

- Scaling and real-space renormalization group techniques. They are very powerful in obtaining the ground state energy [Dasgupta 81], [Zivkovic 89].

- Finally, the variational method. This approach is very useful because, contrasting to most of the rest, it provides information about the ground state nature through the wavefunction. [Klein2 76], [Klein1 79], [Klein2 79], [Klein 83], [Oles 87], [Gros 87], [Becker 88], [Huse 88], [Liang 88], [Horsch 88], [Sachdev 89].

Our main interest in this work is the ground state nature of the Heisenberg model on the square lattice. We have used the variational method.

We will present in the next section our calculation .

4 SPIN-1/2 ANTIFERROMAGNETIC HEISENBERG MODEL FOR SQUARE LATTICE STRIPS

Following the same scheme as in the First Chapter, we consider here alternative *variational localized-site cluster-expanded wavefunctions* to study the nature of the ground state of our systems.

Although what is relevant for the high-Tc superconductors is the square lattice system, we have chosen **square lattice strips** of different **widths** for various reasons. These systems are interesting by themselves because they are a means of studying the evolution of some properties from one dimensional to the two dimensional case. Information of the 2D square lattice will be obtained as an **infinite-width** limit of our finite-width systems. And the **transfer matrix** technique, as shown previously for polymers, proves to be computationally very powerful whenever the systems are strips.

Then, the systems under study are $w \times L$ strips of different widths and cyclic boundary conditions along L (strip-length), with L very large, tending to infinity. (see Fig. 6).

In order to make a good choice of ground state trial wavefunctions, the reasoning given for polymer systems in Chapter 1, where comparison was made between 1D and 3D results, is valid here for square lattice strips because of their quasi-1D nature. We shall work with the same ansätze in a different framework.

We examine two Resonating Valence Bond (RVB) ansätze -Φ_0 and Φ_1- in close relation to 1D systems defined in eq. (3.11) and (3.13) respectively, in the *Computations* part of the First Chapter, and a Néel-based ansatz, Ψ_0, more related to antiferromagnetic order given by eq. (3.9) in the same section.

Two physical magnitudes have been computed for these systems. First, the ground state energy is evaluated as in the preceding chapter, using equations (4.1) and (4.8) of the *Computations* part. Also, an Antiferromagnetic Spin Long-Range-Order (AFLRO) correlation function,

$$\rho = \frac{1}{w^2} | \sum_{i,j=1}^{w} (-1)^i (-1)^j \frac{<\Psi | \bar{S}_i \bar{S}_j | \Psi>}{<\Psi | \Psi>} | \tag{4.1}$$

is computed, where Ψ is the corresponding trial ground state wavefunction, w is the

strip-width and i and j are sites taken very far apart. This function measures the average of finding the spin on site j oriented antiferromagnetically according to a spin on site i. It is an interesting magnitude because provides information about the magnetic nature of the state described by the wavefunctions considered.

We have, then, organized this chapter as follows. In section 4.1 we briefly explain the computation of the AFLRO correlation function based on the transfer matrix technique. In section 4.2 calculation of the transfer matrix is indicated. In section 4.3 results for the ground state of our systems are presented, discussed and compared with other known results, and the correlation function for the ansätze proposed is studied.
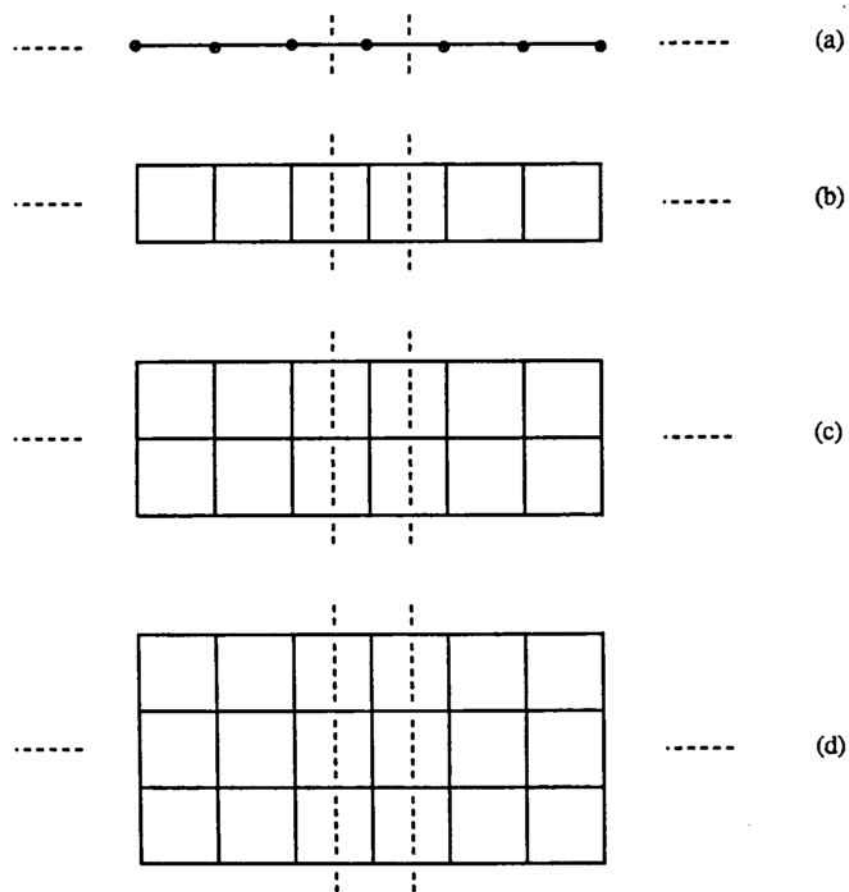
Figure 6: Portion of the strips studied with unit cells located between the two dashed lines. (a) linear chain, (b) square ladder strip, (c) 3-site wide strip, (d) 4-site wide strip.

4.1 Correlation Function

Apart from the ground state energy, we are interested in studying whether our trial wavefunctions have Antiferromagnetic Long Range Order (AFLRO).

The magnitude given by eq. (4.1) has been computed for our strip-sytems.

For the RVB-type ansätze, i.e. the "short range" RVB, Φ_0, and the "higher range" RVB, Φ_1, ρ obviously tends to zero because, as they have been defined, there are no VB structures with spins singlet-paired at long distances.

In the case of the Néel-state-based ansatz, Ψ_0, this magnitude reduces to a simple expression using the transfer matrix technique. Defining (i,j) as the transposition operator between sites i and j, the following equality holds,

$$\bar{S}_i \bar{S}_j = \frac{1}{2}(i,j) - \frac{1}{4} \tag{4.2}$$

substituting it into (4.1), ρ reduces, for w **even**, to:

$$\rho = \frac{1}{2w^2} | \sum_{i,j=1}^{w} (-1)^i (-1)^j \frac{< \Psi \mid (i,j) \mid \Psi >}{< \Psi \mid \Psi >} | \tag{4.3}$$

and, for w **odd**:

$$\rho = \frac{1}{w^2} | \sum_{i,j=1}^{w} ((-1)^i (-1)^j \frac{1}{2} \frac{< \Psi \mid (i,j) \mid \Psi >}{< \Psi \mid \Psi >}) - \frac{1}{4} | \tag{4.4}$$

We proceed now to analyze the matrix element $< (i,j) > \equiv \frac{<\Psi|(i,j)|\Psi>}{<\Psi|\Psi>}$ depending on i, j parity and with $i - j = n$ very large.

(a) $i - j$ is **even**. In this case the terms that will contribute will be those where i and not j is affected by a spin-flip (coming from the action of the *pair-excitation operator* in the definition of Ψ_0), and the symmetric case, i.e. j but not i is affected by a spin-flip.

We define $U(i)$ as the transfer matrix on site i unit cell that accounts for the contributions coming from the *bra* and *ket* part of $< \Psi \mid (i,j) \mid \Psi >$, where site i is affected by a spin-flip. And $W(i)$ is the corresponding matrix that contains all the terms where i is not affected by any spin-flip. Then, the transfer matrix for this unit cell,

$$T(i) = U(i) + W(i) \tag{4.5}$$

with $T(i) \equiv T$ because of translational invariance.

In terms of these matrices,

$$< (i,j) >= \frac{1}{tr(T^L)} \{ tr[T^{L-i-1}U(i)T^{i-j-1}W(i)T^j]$$
$$+ tr[T^{L-i-1}W(i)T^{i-j-1}U(j)T^j] \}. \tag{4.6}$$

For L tending to infinity and $i - j$ very large, it reduces to:

$$< (i,j) >= \frac{1}{\Lambda^2 < \Lambda,l \mid \Lambda,r >^2} \{ < \Lambda,l \mid U(i) \mid \Lambda,r >< \Lambda,l \mid W(j) \mid \Lambda,r >$$
$$+ < \Lambda,l \mid W(i) \mid \Lambda,r >< \Lambda,l \mid U(j) \mid \Lambda,r > \}. \tag{4.7}$$

Using (4.5), relation (4.7) simplifies to:

$$< (i,j) >= \{ \Lambda < \Lambda,l \mid \Lambda,r >$$
$$\times (< \Lambda,l \mid U(i) \mid \Lambda,r > + < \Lambda,l \mid U(j) \mid \Lambda,r >)$$
$$-2 < \Lambda,l \mid U(i) \mid \Lambda,r >< \Lambda,l \mid U(j) \mid \Lambda,r > \} / (\Lambda^2 < \Lambda,l|\Lambda,r >^2) \tag{4.8}$$

(b) $i - j$ is **odd**. The terms to contribute will be those where i and j are both affected by spin-flips and, those where none of them are.

Then, as in the previous case,

$$< (i,j) >= \frac{1}{\Lambda^2 < \Lambda,l \mid \Lambda,r >^2} \{ < \Lambda,l \mid U(i) \mid \Lambda,r >< \Lambda,l \mid U(j) \mid \Lambda,r >$$
$$+ < \Lambda,l \mid W(i) \mid \Lambda,r >< \Lambda,l \mid W(j) \mid \Lambda,r > \}$$
$$= \frac{1}{\Lambda^2 < \Lambda,l \mid \Lambda,r >^2} \{ \Lambda^2 < \Lambda,l \mid \Lambda,r >^2$$
$$+2 < \Lambda,l \mid U(i) \mid \Lambda,r >< \Lambda,l \mid U(j) \mid \Lambda,r >$$
$$- \Lambda < \Lambda,l \mid \Lambda,r > [< \Lambda,l \mid U(i) \mid \Lambda,r > + < \Lambda,l \mid U(j) \mid \Lambda,r >] \} \tag{4.9}$$

Substituting this expression into (4.3), when w is **even**:

$$\rho = \frac{1}{2w^2 < \Lambda, l \mid \Lambda, r >^2 \Lambda^2}$$

$$\times | \sum_{i=1}^{w} \{ \sum_{j}^{i+j=\overset{.}{2}} [\Lambda < \Lambda, l \mid \Lambda, r > (< \Lambda, l \mid U(i) \mid \Lambda, r > + < \Lambda, l \mid U(j) \mid \Lambda, r >)$$

$$-2 < \Lambda, l \mid U(i) \mid \Lambda, r >< \Lambda, l \mid U(j) \mid \Lambda, r >]$$

$$- \sum_{j}^{i+j\neq\overset{.}{2}} [2 < \Lambda, l \mid U(i) \mid \Lambda, r >< \Lambda, l \mid U(j) \mid \Lambda, r > +\Lambda^2 < \Lambda, l \mid \Lambda, r >^2$$

$$-\Lambda < \Lambda, l \mid \Lambda, r >$$

$$(< \Lambda, l \mid U(i) \mid \Lambda, r > + < \Lambda, l \mid U(j) \mid \Lambda, r >)]\} |. \quad (4.10)$$

Carrying out summations it simplifies to,

$$\rho = \frac{1}{w^2 \Lambda^2 < \Lambda, l \mid \Lambda, r >^2} (\frac{\Lambda w < \Lambda, l \mid \Lambda, r >}{2} - \sum_{i=1}^{w} < \Lambda, l \mid U(i) \mid \Lambda, r >)^2 \quad (4.11)$$

or, equivalently, using (4.5),

$$\rho = \frac{1}{w^2 \Lambda^2 < \Lambda, l \mid \Lambda, r >^2} (\frac{\Lambda w < \Lambda, l \mid \Lambda, r >}{2} - \sum_{i=1}^{w} < \Lambda, l \mid W(i) \mid \Lambda, r >)^2 \quad (4.12)$$

valid for w **even**.

When w is **odd**, ρ in eq. (4.4) has a $-\frac{1}{4w^2}$ term that cancels with a factor $\frac{1}{4w^2}$ coming from the $\sum_{i=1}^{w} \sum_{j}^{i+j\neq\overset{.}{2}} 1$ in (4.10), so that the same expressions (4.11) and (4.12) hold for w **odd**.

We have considered in this derivation that $U(i)$ and $W(i)$ are matrices defined on *one* unit cell on the strip. For our square lattice strip systems, it was more convenient to define these matrices on a cell twice the unit cell. The expression (4.12) changes to

$$\rho = \frac{1}{w^2 \Lambda^4 < \Lambda, l \mid \Lambda, r >^2} [\frac{\Lambda^2 < \Lambda, l \mid \Lambda, r > w}{2} - \sum_{i=1}^{w} < \Lambda, l \mid W(i) \mid \Lambda, r >]^2. \quad (4.13)$$

The same holds for (4.11).

135

4.2 Construction of Transfer matrices

4.2.1 Néel-based ansatz

As in the preceding chapter, the wavefunction Ψ_0 can be represented by drawing lines between neighbor spins $< i, j >$ that are flipped due to the action of the *pair-excitation operator*. Each of these lines has a variational parameter x_{ij} associated. By translational invariance, these parameters will be independent of the unit cell and only a few relevant ones will remain.

When computing the overlap, *thick lines* are drawn for the *bra* contributions and *curved thin lines* for the *ket* contributions. For orthogonality reasons, only the cases where the same spins are flipped in *bra* and *ket* will contribute to the overlap.

We consider, as an example, the square ladder strip. Given a unit cell, sites are enumerated as shown in Fig. 7, the variational parameters corresponding to these positions are x_{12}, x_{13}, x_{24}, that we redefine as x_1, x_2, x_3 respectively. And by symmetry x_3 will be equal to x_2. In Fig. 8 we draw the possible *local states* that can be defined in a particular zone in terms of the *bra* and *ket* contributions. ·
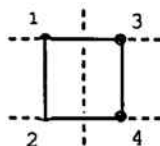
Figure 7: Enumeration of sites within a unit cell of the square ladder.

136
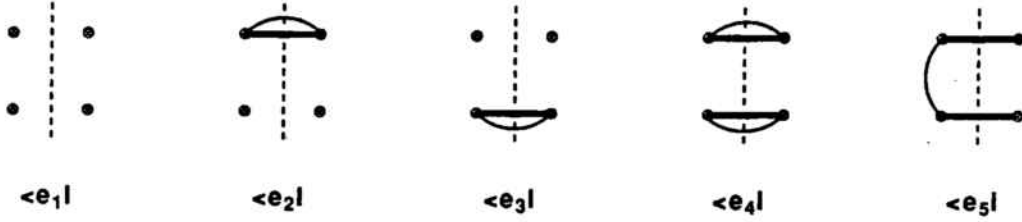
Figure 8: Local states defined in a zone of the square ladder strip for $< \Psi \mid \Psi >$ and $< \Psi \mid H \mid \Psi >$ computation when Ψ is the Néel-based ansatz.

Now, given a *local state* in a zone, all the local states that are compatible with it in the next zone, are studied. And the transfer matrix elements can readily be defined (see Fig. 9).

For this system, the transfer matrix is a 5×5 matrix, and $< \Psi \mid \Psi >$ reduces to expression (4.3) given in the *Computations* part of the First Chapter.

In the calculation of $< \Psi \mid H \mid \Psi >$, considerations are analogous to the polyacenacene example shown in the First Chapter.

Other width strips give rise to similar considerations. Only local states and variational parameters are to be analyzed for any case. For the 3-width strip, all calculations are done with 14×14 matrices. And, for the 4-width strip, matrices 44×44 are needed.

Figure 9: Matrix elements of T associated to the Néel-based ansatz for the square ladder.

138

4.2.2 RVB ansätze

Also, in this calculation, analogous considerations as in the polyacenacene example given in the First Chapter hold.

For the square lattice strip, when Ψ is the "short range" RVB ansatz, Φ_0, three different *local states* can be drawn (see Fig. 10). When Ψ is the "higher range" RVB ansatz, Φ_1, a total of 132 *local states* are defined for the same system.

Studying now for wavefunction Φ_0 the evolution of each *local state* from one zone to the next, both, the variational-parameter contribution and the island counting (Rümer rules) are taken into account (see Fig. 11). As in the Néel-based ansatz, the parameters are independent of the unit cell, so that only x_{12}, x_{13}, x_{24} are relevant and are redefined x_1, x_2, x_3, with $x_3 = x_2$.

Within this ansatz, for the 3-width strip, those matrices are 11×11, and for the 4-width strip, they are 44×44.
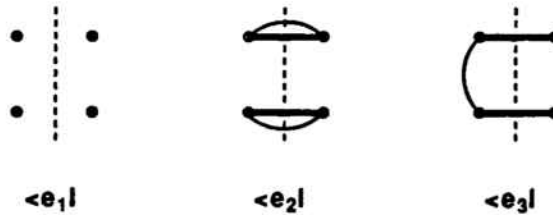
Figure 10: Local states defined when Ψ is the "short range" RVB ansatz for the square ladder strip.
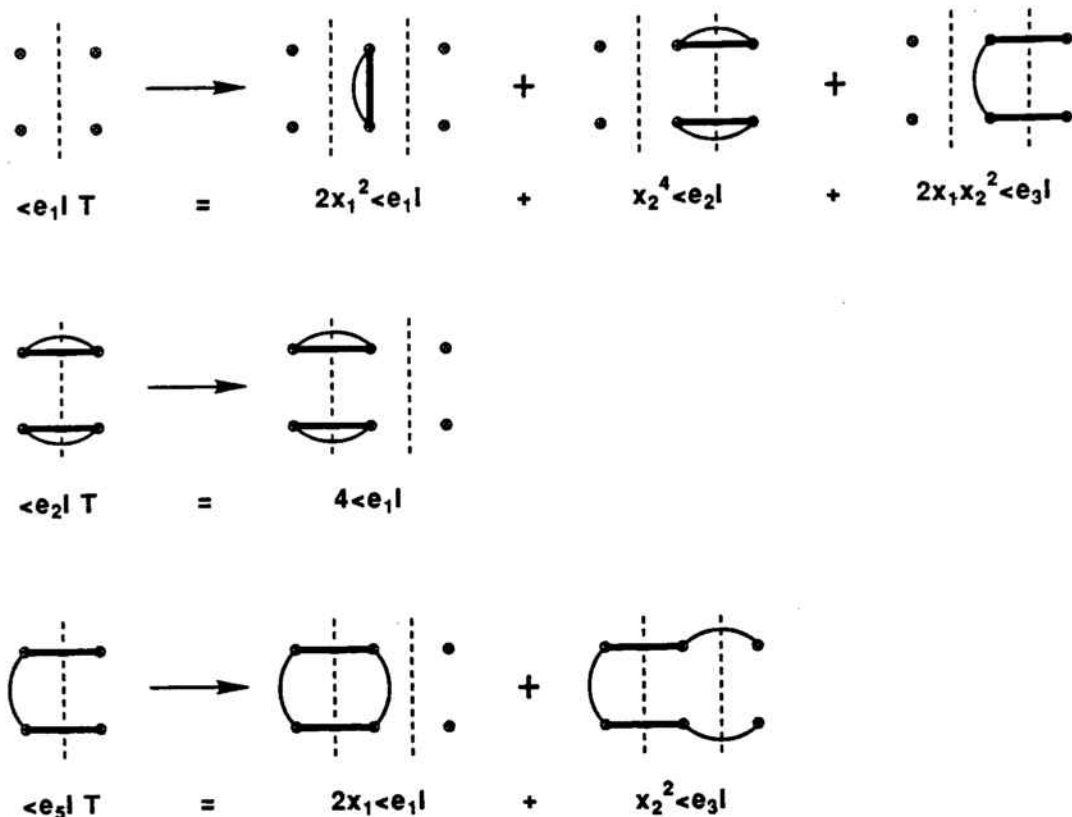
Figure 11: Transfer matrix elements associated to the "short range" RVB ansatz for the square ladder strip.

4.3 RESULTS AND DISCUSSION

4.3.1 Ground State Energy

We have computed the ground state energy, E, with the trial wavefunctions Ψ_0 (Néel-based ansatz) and Φ_0 ("short range" RVB ansatz) for infinite-length strips with periodic boundary conditions and finite widths up to four sites wide (see Fig. 6). Calculation of E with the "higher range" RVB ansatz, Φ_1, has been carried out for the one-dimensional case and for the square-ladder strip.

In Table 1 we show the results obtained and compare with exact results and

results obtained by other authors [Fan 88], [Sachdev 89], [Zivkovic 89].

w x L	1 x ∞	2 x ∞	3 x ∞	4 x ∞
E_1	-0.375	-0.5560(2)	-0.5414(8)	-0.573
E_2	-0.375	-0.5569(6)	-0.5682(4)	-0.5722(1)
E_3	-0.411	-0.5731(7)	–	–
E_4	-0.250	-0.375	-0.416	-0.437
E_5	-0.4279(1)	-0.5507(4)	-0.5833(8)	-0.6025(3)
E_6	-0.4431(5)	-0.578	-0.594	-0.618

Table 1: Ground state energy per site in J units for infinite-length strips of widths 1, 2, 3, 4 sites. E_1 is the energy obtained by [Zivkovic 89] considering a ground state wavefunction as a combination of nearest-neighbor valence bond states equally weighted. E_2, E_3 and E_5 are the energies obtained with Φ_0, Φ_1 and Ψ_0 respectively. E_4 is the energy of the Néel state. E_6 is the energy obtained [Zivkovic 89] extrapolating from exact results for finite $w \times L$ strips. In the $1D$ case, the exact result [Hulthen 38] is given by E_6.

In the one dimensional case, we can compare the ground state energy with the exact value. Although from Table 1 we learn that the best upper bound is given by a Néel-based ansatz, it has been shown [Valenti 87], [Garcia-Bach 88] that when VB states with spins paired at longer distances than nearest neighbors are added to the RVB ansätze, the ground state energy improves drastically ($E \simeq -0.440(1)J$). Nevertheless, the results for the 1D case when Φ_0, Φ_1 and Psi_0 are used, were included in the Table for completeness.

The **RVB ansätze** we have worked with are of "short range type" (Φ_1 being an improvement of Φ_0) and, as we can see, the corresponding energy is far from the best upper bound to the ground state energy of these systems. But, they are considered here because they may be useful when building hole excitations upon the ground state. When a small amount of holes are introduced in the system, it has been suggested [Anderson2 87], [Kivelson 87] and lately experimentally observed that there is no long range order. Also, from the preceding chapter discussion, we observe that the introduction of holes is going to reduce the average number of neighbors per site, $\bar{z}$, and, since the number of Kekulé states is high, we can expect a RVB type ground state. Then, the background of spins can be well described as a "short range" RVB, provided there is no local momentum. If a nonzero local momentum were observed, it would mean that the system would be non-localized and RVB description wouldn't be appropriate. Up to now, this doesn't seem the case.

141

Our computation has also been useful for checking the effectiveness of the transfer matrix method. Fan and Ma [Fan 88] obtained the ground state energy of the square ladder with a "short range" RVB wavefunction using a generating function approach. Their results agree completely with our calculation, which is easily carried out with a 3 × 3 transfer matrix, as shown in the previous section.

It is worthwhile to mention that the "higher range" RVB ansatz gives a very good upper bound to the ground state energy of the square ladder, basically due to the great number of valence bond states that mix, so that the energy is fastly lowered. Still, studying the values of variational parameters (see Fig. 12) we observe that those associated to longer bonds are much smaller than those associated to dimers (i.e. nearest neighbors singlet pairs).
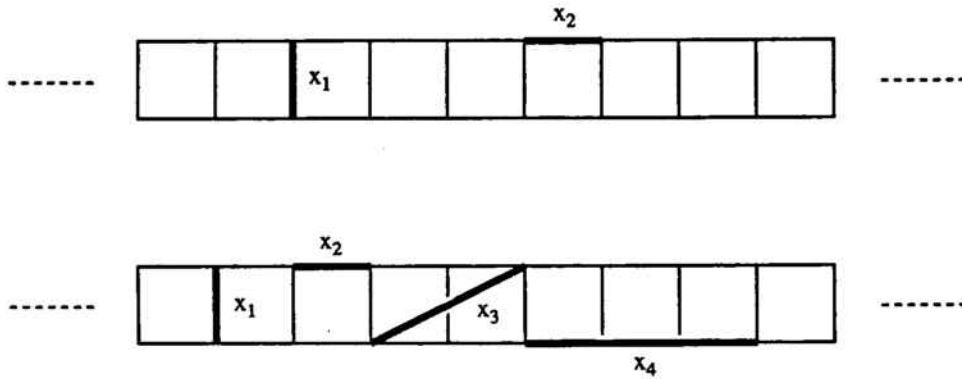
Figure 12: Value of the variational parameters associated to singlet pairs in Φ_0 and Φ_1 for the square ladder. Only non symmetrically-equivalent parameters are presented. A singlet-pair is represented by a bond between the two paired spins. (a) for Φ_0, $x_1 = 1$, $x_2 = 1.0899(7)$. (b). for Φ_1, $x_1 = 1$, $x_2 = 0.8849(4)$, $x_3 = 0.3993(0)$, $x_4 = 0.2508(5)$.

Eventually, we expect that **longer** singlet pairs are going to contribute less and less to lower the ground state energy although they will be important for the **long range order nature** of the wavefunction. In fact, Liang *et al.* [Liang 88] have shown that a long-range RVB-like wavefunction describes fairly well the ground state of the Heisenberg model on the square lattice but the best upper bound to the ground state energy is given by a Néel-like wavefunction.

A **Néel-state-based ansatz** similar to Ψ_0, was also proposed independently by other authors [Sachdev 89]. We obtain in the one dimensional case, by the transfer matrix technique already described, a ground state energy in agreement

with Sachdev's result [Sachdev 89], which has been obtained with a Jordan-Wigner transformation.

Within this ansatz, the energy per site scales fairly well as a function $E_\infty + b/w$, w being the strip-width, to the result $E_\infty = -0.6626(9)J$ for the 2D square lattice ($w \longrightarrow \infty$ limit) (see Fig. 13).
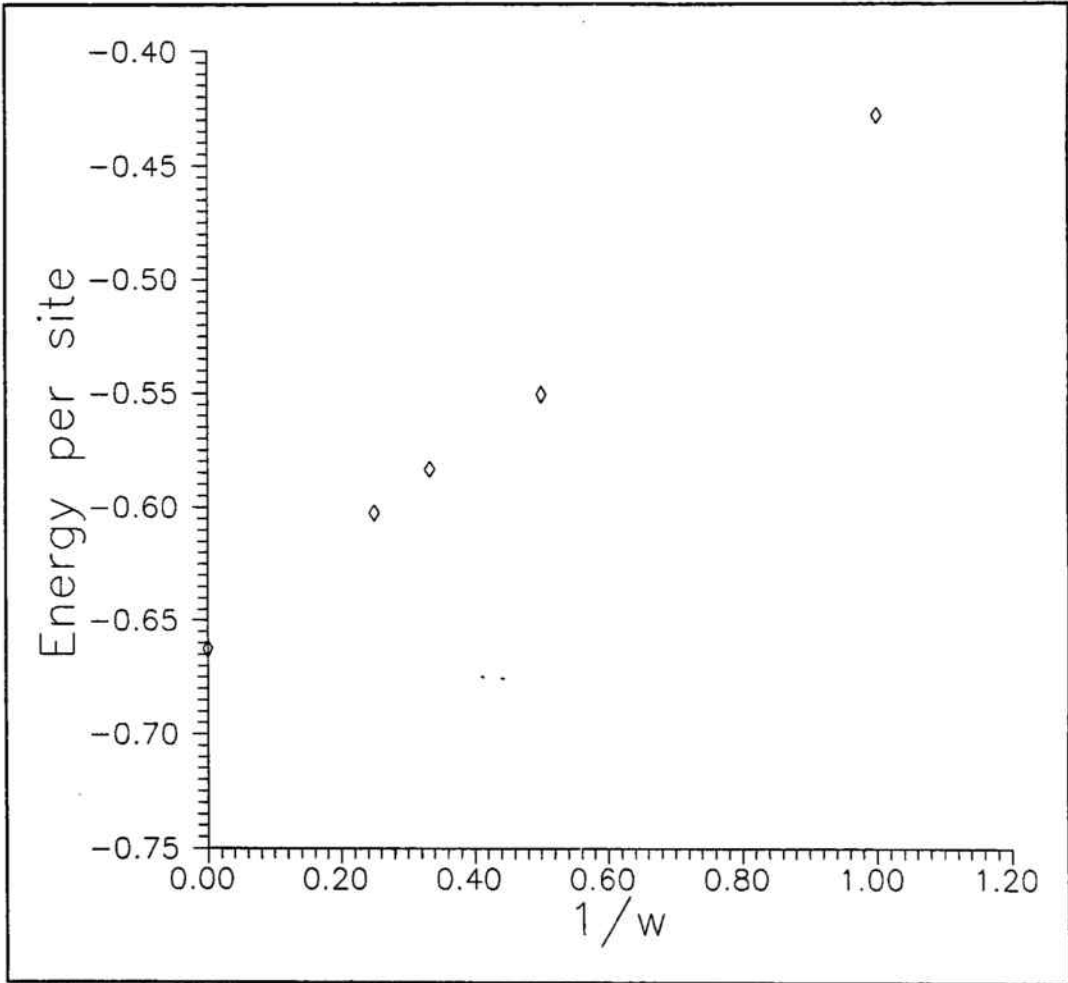
Figure 13: Plot $E - 1/w$ for the strip systems with the Néel-based ansatz, Ψ_0. The ($\Diamond$) correspond to the computed energies.

In spite of being a four-point extrapolation, E_∞ compares with Sachdev's energy

[Sachdev 89], $E_\infty = -0.663(4)J$, obtained developing a renormalized perturbation series in terms of the unique, by symmetry, variational parameter associated to neighbor-pair spin-flips, g (see Fig. 14(e)). But still, this value is far from the best energy values obtained up to now [Liang 88] $E_\infty \simeq -0.668(8)$ by a Monte Carlo Néel-like wavefunction, see also Zivković et al. [Zivkovic 89] and references therein.

This extrapolation is only indicative. In Fig. 14 we show the values of the variational parameters involved in the Néel-based ansatz for the different systems studied.

We conclude that up to 4-site wide, boundary effects are still important (those parameters associated to edges contribute the most) but, at the same time, a gradual decrease is observed when increasing the number of sites per width. The parameters associated to non-edge flips have values around Sachdev's, $g = 0.1878$, for the 2D square lattice.
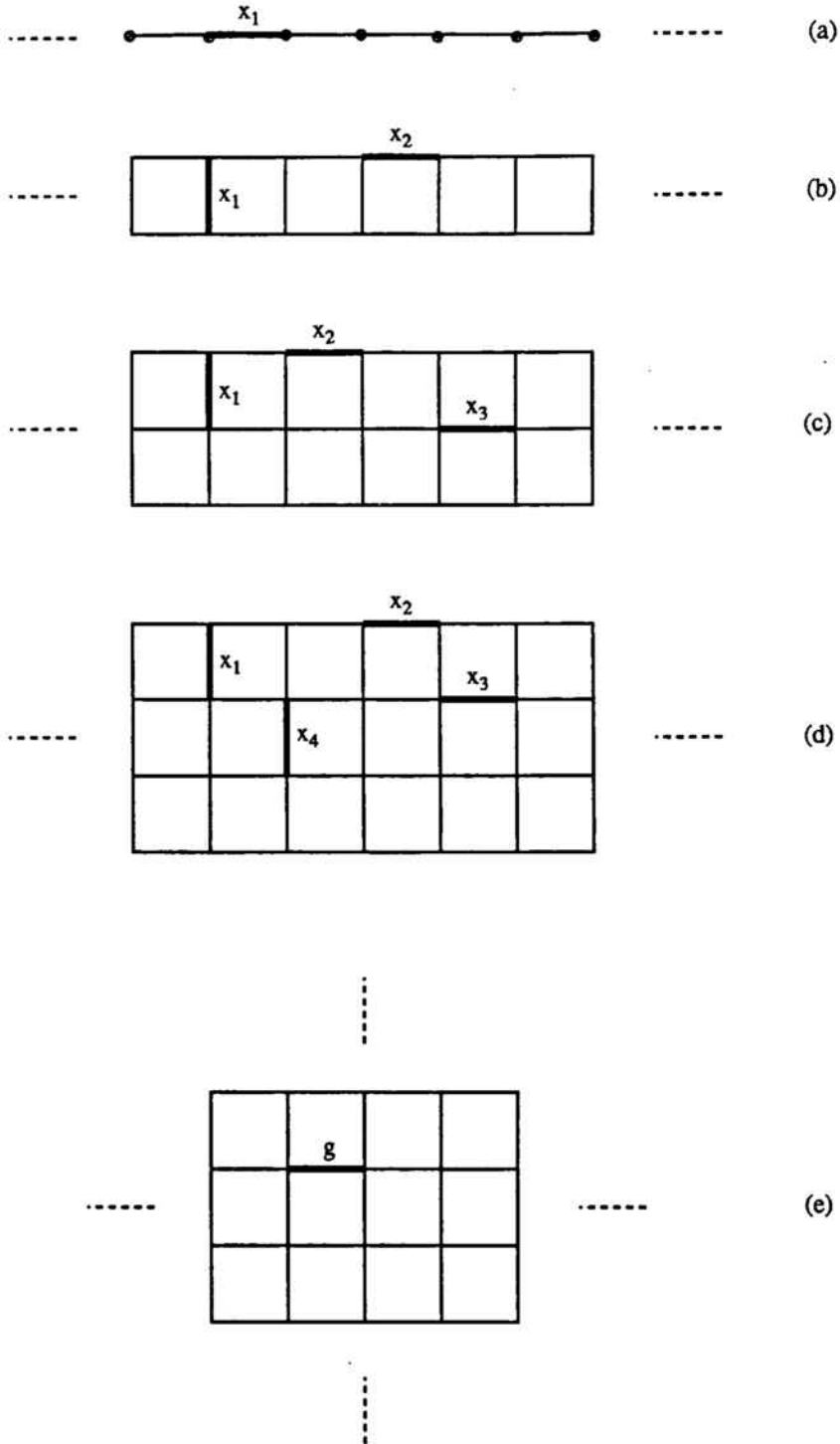
Figure 14: Value of the variational parameters associated to the spins-flips in Ψ_0 for the systems studied. A spin-flip is drawn as a bond between the two flipped spins. (a) linear chain $x_1 = -0.3889(4)$. (b). square ladder $x_1 = -0.3004(3)$, $x_2 = -0.2656(2)$. (c) three-site wide square strip $x_1 = -0.2229(2)$, $x_2 = -0.2501(8)$, $x_3 = -0.1903(0)$. (d). four-site wide square strip $x_1 = -0.2212(5)$, $x_2 = -0.2457(7)$, $x_3 = -0.1861(2)$, $x_4 = -0.18153(3)$. (e) square lattice [Sachdev 89] $g = -0.1878$

4.3.2 Correlation Function

ρ has been computed with the Néel-based ansatz using expression (4.12) for our strips. Results are presented in Table 2.

wxL	ρ
$1x\infty$	0.0837(0)
$2x\infty$	0.1008(0)
$3x\infty$	0.1274(1)
$4x\infty$	0.1340(8)

Table 2: Values of ρ for our systems.

This ansatz shows AFLRO for these systems as we would expect from the fact that it is a Néel state dominated ansatz, known to have LRO. We observe that AFLRO increases with w.

Neutral Excitations in quasi-1D electron systems. systems. Application to extended polymer systems. Polyphenanthrene.

Contents

In this chapter, some novel neutral spin-0 excitations for quasi-1D systems with one electron per site are presented within a **localized scheme**. The ground state wavefunction is defined by a **variational localized-site cluster-expanded ansatz** and these excitations are naturally built upon it [Klein1 89], [Garcia-Bach1 89].

All computations are easily carried out by the **transfer matrix technique** that enables explicit inclusion of **electron-correlation effects** and, at the same time, provides a **quasi-particle band-theoretic picture** of these excitations.

This treatment is applied, in particular, to a polyphene strip (polyphenanthrene).

1   INTRODUCTION

Following the discussion of the First Chapter about the two complementary approaches to describe conjugated polymer systems, i.e. band theory at different levels of approximation and valence bond (VB) localized scheme, it was mentioned there that, usually, molecular orbital (MO) band-theoretic schemes have been used to describe these systems, namely, the Hückel MO (which is the simplest one), extended Hückel and MNDO models, and, occasionally, SCF (Self-Consistent-Field) solutions to Hubbard and Parisier-Parr-Pople models. On the other hand, much less work has been done utilizing resonance-theoretic or valence-bond models.

VB-based schemes were, in fact, long ago introduced [Rumer 32], [Pauling 58] in a chemical context but, for some time, they have been considered not very useful in favour of delocalized mean-field views (MO, band theory), mainly because the number of basis states increases considerably when dealing with large systems.

Nevertheless, for systems where electron correlation is an important interaction, like polymer systems and the new Hi-Tc superconductors, a mean-field treatment is difficult to handle due to the important two-body Coulomb interaction in a many body problem, and different levels of approximation can lead to different results (as seen in the First Chapter). While a localized description has been proven adequate. Though little, some existing results with this description [Klein1 76], [Klein2 76], [Klein1 79], [Klein2 86], [Liang 88] reveal novel ground state long-range ordering, implicating in some cases, distortions and solitonic excitations, often for the same structures for which similar predictions are made from MO models, as has been also shown in the First Chapter.

149

However, up to now, much of the quantitative work within this localized scheme has focused on ground states and little has been done on excitations. Usually, mean-field theories, i.e. band-theoretic approaches where Coulomb repulsion is averaged, are developed, though one has to be very careful with uncontrolled approximations.

Motivated by the possibility of exploiting localized descriptions for excitations, low-lying excited states are built within a *localized valence bond scheme* that avoids mean-field approach problems [Valenti 87], [Klein1 89], [Garcia-Bach1 89], [Garcia-Bach3 89].

We restrict ourselves to translationally-symmetric infinite strips with one electron per site (polymer strips, square-lattice strips of different widths, etc.) (see Fig. 1),
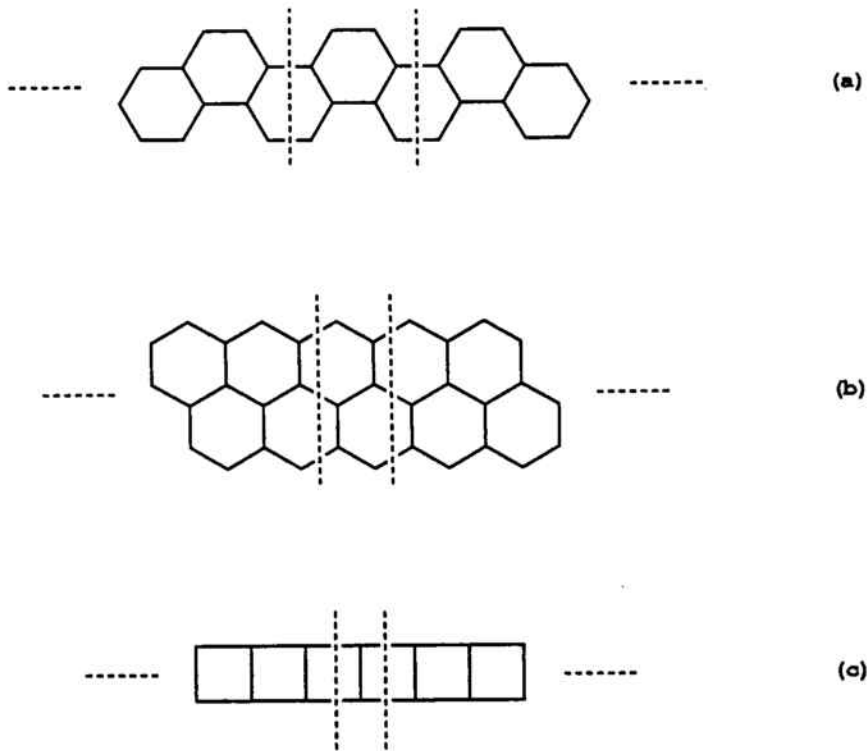

Figure 1: Portion of strips with unit cells located between the two dashed lines. (a) polyphene chain, (b) polyacenacene, (c) square ladder strip.

and with short range "effective" interactions. Current interesting model hamil-

tonians like the Heisenberg model, already introduced in Chapter 1, or the Herndon-Simpson model [Herndon 73], [Herndon1 74], [Herndon2 74], which will be described below, fullfil this condition. All calculations will be done in terms of the transfer matrix technique that deals with the systems locally.

The ground state is defined by a variational localized-site cluster-expanded ansatz and the excitations studied can be termed as *elementary* excitations upon the ground state. They are built involving changes in one of the ground state variational parameters in a way that the generalized Brillouin theorem [Epstein 74] is accomplished, i.e. the ground and excited state wavefunctions are to be orthogonal and non-interacting. A quasi-particle band-theoretic picture including correlation is obtained.

2   EXCITED STATES

Within the scheme of the localized description and the transfer matrix technique, excitations can be obtained modifying the ground state wavefunction locally, i.e. introducing a local perturbation on the ground state background. A simple way to construct a special class of excited states is in terms of **single excitations**, $\Psi(x_n)$, that are the same as Ψ except that the variational parameter x_n associated with a monomer n is replaced by x'_n. This new parameter is chosen to satisfy a generalized Brillouin condition [Epstein 74]:

$$< \Psi \mid \Psi(x_n) >= 0 \qquad (2.1)$$

that together with the assumption of ground state optimization implies:

$$< \Psi \mid H \mid \Psi(x_n) >= E_0 < \Psi \mid \Psi(x_n) >= 0 \qquad (2.2)$$

i.e. the ground and single excitation wavefunctions are to be orthogonal and non-interacting. The **excited states** are then expanded in terms of these single excitations. They characterize for being **neutral** and **spin zero**.

By definition, these excitations are localized-site cluster expansions, therefore the transfer matrix technique can be used in order to obtain the energy gap. Computations will be similar to the case of the ground state energy, with extra contributions due to the replacement of some variational parameters.

When computing (2.1) by the transfer matrix technique, a local parameter x'_n instead of x_n appears in the transfer matrix T_n, therefore this will be the only matrix modified, it can be labelled by $T_n(x_n)$, the expression (2.1) reduces to:

$$< \Psi \mid \Psi(x_n) > = tr\{T_n(x_n) \prod_j^{\neq n} T_j\} \qquad (2.3)$$

A matrix T_n can be viewed as a function of x_n and $\bar{x}_n$, both parameters arising, respectively, from the *ket-* and *bra-* part of the local matrix element. And $T_n(x_n)$ is defined to have all the x_n (but not $\bar{x}_n$) of T_n replaced by x'_n. $T_n(x_n)$ is linear in x'_n. The same holds for $T_n(\bar{x}_n)$ where the x_n from the *bra*, $\bar{x}_n$, have been replaced by x'_n. A more general modified T matrix will be $T_n(\bar{x}_n, y_n)$ where the variational parameters x_n arising from the *bra* are replaced by x'_n and the parameters y_n arising from the *ket* are replaced by y'_n.

2.1 Matrix elements

In order to build the excited states and calculate the excitation energy, matrix elements between the various wavefunctions introduced above are to be evaluated.

Any overlap and Hamiltonian matrix elements between the ground state wavefunction Ψ and the single excitation wavefunctions $\Psi(x_n)$ is zero by (2.1) and (2.2). Only matrix elements between pairs of single excitations $\Psi(x_m)$ and $\Psi(y_n)$ remain to be computed. A nice way to express these wavefunctions is in terms of *parameter-space shift operators* $S(x_m)$, which automatically replace x_m by x'_m:

$$S(x_m) = 1 + (x'_m - x_m)\frac{\partial}{\partial x_m} \qquad (2.4)$$

This definition can be used not only for expressing $\Psi(x_m)$ but also for transfer matrices and matrix elements because of their linear dependence on the variational parameters:

$$|\Psi(x_m) > = S(x_m)|\Psi >$$
$$T_m(x_m) = S(x_m)T_m$$
$$T_m(\bar{x}_m, y_m) = S(\bar{x}_m)S(y_m)T_m \qquad (2.5)$$

152

And

$$< \Psi(x_m)|\Psi(y_n) > = S(\bar{x}_m)S(y_n) < \Psi|\Psi >$$

$$= S(\bar{x}_m)S(y_n)tr \prod_{q=1}^{L} T_q \qquad (2.6)$$

$$< \Psi(x_m)|H|\Psi(y_n) > = \sum_{c}\sum_{p=1}^{L} S(\bar{x}_m)S(y_n)tr\{C_{p+1\rightarrow p+c} \prod_{q}^{\neq p+1\rightarrow p+c} T_q\} \qquad (2.7)$$

2.2 Translational Symmetry

Making use of the translational invariance of our systems, variational parameters will be independent of the monomer unit and, subsequently, we can drop monomer unit subscripts on T and x.

Following previous definitions, $T(x)$ is a transfer matrix where the parameter x coming from the *ket*-part of the local overlap is replaced by x'. In $T(\bar{x})$ the parameter x arising from the *bra*-part is replaced by x', and $T(\bar{x}, y)$ is a transfer matrix where the variational parameter x arising from the *bra*-part is replaced by x' and the parameter y coming from the *ket*-part is replaced by y'. Still, $\Psi(x_n)$ characterizes for having the parameter x corresponding to the nth monomer unit replaced by x' subjected to condition (2.1). In that sense $\Psi(x_n)$ depends upon n and it can be written as $\Psi_n(x)$. Then, equation (2.3) is

$$< \Psi \mid \Psi_n(x) > = tr\{T(x)T^{L-1}\}. \qquad (2.8)$$

In the limit of long strips, the largest eigenvalue Λ of T dominates, and the Brillouin condition (2.1) simplifies to

$$(\Lambda, l \mid T(x) \mid \Lambda, r) = 0 \qquad (2.9)$$

where $(\Lambda, l|$ and $|\Lambda, r)$ are the left and right eigenvectors for Λ such that $(\Lambda, l|\Lambda, r) = 1$.

This is a simple expression independent of the monomer unit and the value of x' can be straightforward obtained from it.

By the translational invariance of our systems, the excited states are to exhibit cyclic translation-group symmetries. From single excitations, **symmetry adapted singly excited states** can be defined

$$| x \; k > \equiv \frac{1}{\sqrt{L\Lambda^L}} \sum_{n=0}^{L} e^{ikn} \mid \Psi_n(x) >, \tag{2.10}$$

labelled by wavevectors k,

$$k = \frac{2\pi m_k}{L} \tag{2.11}$$

with $m_k = 1, 2, ..., L$. The normalization factor of these vectors is only approximated. We will have, for each wavevector k, *mutually interacting excitations in correspondence with the different variational parameters in* Ψ.

In order to obtain the energy gap of these excitations, one needs to determine the mutual overlap of these symmetry adapted states

$$< x \; k \mid y \; k' > = \frac{1}{L\Lambda^L} \sum_{n,d} e^{ik'(n+d)-ikn} < \Psi_n(x) \mid \Psi_{n+d}(y) >$$
$$= \delta(k, k')\Lambda^{-L} \sum_d e^{ikd} < \Psi_n(x) \mid \Psi_{n+d}(y) > \tag{2.12}$$

and the "excitation-energy" matrix elements

$$< x \; k \mid H - E_0 \mid y \; k' > =$$
$$\delta(k, k')\frac{1}{L}\Lambda^{-L} \sum_{m,n=1}^{L} e^{ik(n-m)} < \Psi_m(x) \mid (H - E_0) \mid \Psi_n(y) > \tag{2.13}$$

where E_0 is the ground state energy.

2.3   Overlap Matrix elements

The mutual overlap between two symmetry adapted states will be expressed in terms of transfer matrices,

$$< x \; k \mid y \; k' > = \delta(k, k')\Lambda^{-L} \sum_d e^{ikd} < \Psi_n(x)|\Psi_{n+d}(y) > \tag{2.14}$$

where

$$< \Psi_n(x)|\Psi_{n+d}(y) > = [S(\bar{x}_n)S(y_{n+d})Tr \prod_{q=1}^{L} T_q]_0. \tag{2.15}$$

The subscript '0' indicates that the parameters in T_q are to be distinguished when applying the shift operators and, afterwards, the site dependence will be eliminated.

When $L \longrightarrow \infty$, the largest eigenvalue Λ of T dominates and the previous expression reduces to:

$$< \Psi_n(x)|\Psi_{n+d}(y) > = [S(\bar{x}_n)S(y_{n+d})(\Lambda,l| \prod_{q=n}^{n+d} T_q|\Lambda,r)]_0\Lambda^{L-d-1} \tag{2.16}$$

when $d \geq 0$ and finite.

A similar expression holds for $d \leq 0$.

Then,

$$\begin{aligned}
< x\ k\ |\ y\ k' > = \delta(k,k')\{&(\Lambda,l|T(\bar{x},y)|\Lambda,r)\Lambda^{-1} \\
&+ \sum_{d\geq 1} e^{ikd}(\Lambda,l|T(\bar{x})T^{d-1}T(y)|\Lambda,r)\Lambda^{-d-1} \\
&+ \sum_{d'\geq 1} e^{-ikd'}(\Lambda,l|T(y)T^{d'-1}T(\bar{x})|\Lambda,r)\Lambda^{-d'-1}\}
\end{aligned} \tag{2.17}$$

d' corresponds to $d \leq -1$ with $d' = -d$.

Assuming that T is diagonalizable and λ refers to any eigenvalue of T with $(\lambda,l|$ and $|\lambda,r)$ the corresponding biorthonormal left- and right-eigenvectors, every term of the previous expression can be analyzed as a function of them. Terms of the kind,

$$e^{ikd}(\Lambda,l|T(\bar{x})|\lambda,r)(\frac{\lambda}{\Lambda})^{d-1}(\lambda,l|T(y)|\Lambda,r) \tag{2.18}$$

are obtained.

Those terms where $\lambda = \Lambda$ may be eliminated because of equation (2.9).

In the limit $L \longrightarrow \infty$, the overlap matrix element finally reduces to:

$$< x\ k\ |\ y\ k' > = \delta(k,k')\{T_{\Lambda\Lambda}(\bar{x},y) + \sum_{\lambda}^{\neq\Lambda}[T_{\Lambda\lambda}(\bar{x})\lambda_k T_{\lambda\Lambda}(y) + T_{\Lambda\lambda}(y)\lambda_{-k}T_{\lambda\Lambda}(\bar{x})]\} \tag{2.19}$$

where

$$T_{\lambda\mu}(*) \equiv (\lambda,l\ |\ T(*)\ |\ \mu,r)\Lambda^{-1}, \tag{2.20}$$

$(*)$ stands for $(\bar{x})$, (y), or $(\bar{x},y)$, and

$$\lambda_k \equiv \sum_{d\geq 1}(\frac{\lambda}{\Lambda})^{d-1}e^{ikd} = \frac{\Lambda e^{ik}}{\Lambda - \lambda e^{ik}} \tag{2.21}$$

with $|\lambda| < \Lambda$.

In (2.19) a compact expression for the overlap in terms of transfer matrices has been reached.

2.4 "Excitation-Energy" Matrix elements

A similar analytic result will be obtained for the "excitation-energy" matrix elements between two symmetry adapted states:

$$< x \ k \mid (H - E_0) \mid y \ k' >=$$

$$\delta(k, k')\frac{1}{L}\Lambda^{-L} \sum_{m,n=1}^{L} e^{ik(n-m)} < \Psi_m(x)|(H - E_0)|\Psi_n(y) > \qquad (2.22)$$

For $L \longrightarrow \infty$, it reduces:

$$< \Psi_m(x)|(H - E_0)|\Psi_n(y) >=$$

$$(S(\bar{x}_m)S(y_n)) \sum_c \{\sum_{p=1}^{L} trC_{p+1 \rightarrow p+c} \prod_{q}^{\neq 1 \rightarrow c} T_{p+q} -$$

$$L(\Lambda, l|C_{1 \rightarrow c}|\Lambda, r)\Lambda^{-c} tr \prod_{r=1}^{L} T_r\})_0 \qquad (2.23)$$

That can be rewritten as:

$$< x \ k \mid (H - E_0) \mid y \ k' >=$$

$$\delta(k, k')\Lambda^{-L} \sum_{m,n=1}^{L} e^{ik(n-m)}[S(\bar{x}_m)S(y_n) \sum_c \sum_{p=1}^{L} trD_{p+1 \rightarrow p+c} \prod_{q}^{\neq 1 \rightarrow c} T_{p+q}]_0 \qquad (2.24)$$

where the matrices

$$D_{p+1 \rightarrow p+c} \equiv C_{p+1 \rightarrow p+c} - (\Lambda, l \mid C_{1 \rightarrow c} \mid \Lambda, r)\Lambda^{-c} \prod_{q=1}^{c} T_{p+1} \qquad (2.25)$$

contain all the information of the interaction part that takes place in the monomer units from $p + 1$ to $p + c$.

Note that in (2.24) there are three sets of distinguished monomers $\{m\}$, $\{n\}$ and $\{p + 1 \rightarrow p + c\}$. m labels the monomer unit where the parameter x_m coming from the *bra* part of the matrix element, is replaced by x'_m, n labels the monomer unit where the parameter y_n coming from the *ket* part of the matrix element, is replaced by y'_n, and $p + 1 \rightarrow p + c$ correspond to the set of unit cells where the interaction is taking place. As this equation is a sum over m, n, and p, it has been separated into various contributions depending on the ordering and/or overlapping of these set of monomers. A total of thirteen contributions consisting on transfer and connection

156

matrices products are obtained. They are given explicitly in Table 1 where the definitions in (2.20) and (2.21) have been used together with the following ones:

$$D_{\lambda\mu}^{c,0} \equiv (\lambda, l|[D_{1\to c}]_0|\mu, r)\Lambda^{-c}$$

$$D_{\lambda\mu}^{c,\pm k}(z) \equiv \sum_{p=1}^{c} e^{\pm ikp}(\lambda, l|[S(z_p)D_{1\to c}]_0|\mu, r)\Lambda^{-c}$$

$$D_{\lambda\mu}^{c,k}(\bar{x}, y) \equiv \sum_{p,q=1}^{c} e^{ik(q-p)}(\Lambda, l|[S(\bar{x}_p)S(y_p)D_{1\to c}]_0|\mu, r)\Lambda^{-c} \qquad (2.26)$$

The $+$ or $-$ of exponents in the second equation depend on if z is either y or $\bar{x}$ respectively.

Ordering of sites	Contribution
$m = n < p+1 \to p+c$	$\sum_c \sum_\lambda T_{\Lambda\lambda}(\bar{x}, y)\lambda_o D_{\lambda\Lambda}^{c,o}$
$p+1 \leq m, n \leq p+c$	$\sum_c D_{\Lambda\Lambda}^{c,k}(\bar{x}, y)$
$p+1 \to p+c < m = n$	$\sum_c \sum_\lambda D_{\Lambda\lambda}^{c,o}\lambda_o T_{\lambda\Lambda}(\bar{x}, y)$
$p+1 \to p+c < m < n$	$\sum_c \sum_{\lambda\mu} D_{\Lambda\lambda}^{c,o}\lambda_o T_{\lambda\mu}(\bar{x})\mu_k T_{\mu\Lambda}(y)$
$p+1 \leq m \leq p+c < n$	$\sum_c \sum_\lambda D_{\Lambda\lambda}^{c,-k}(\bar{x})e^{ikc}\lambda_k T_{\lambda\Lambda}(y)$
$m < p+1 \to p+c < n$	$\sum_c \sum_{\lambda\mu} T_{\Lambda\lambda}(\bar{x})\lambda_k e^{ik(c-1)} D_{\lambda\mu}^{c,o} T_{\mu\Lambda}(y)$
$m < p+1 \leq n \leq p+c$	$\sum_c \sum_\lambda T_{\Lambda\lambda}(\bar{x})\lambda_k D_{\lambda\Lambda}^{c,k}(y)e^{-ik}$
$m < n < p+1 \to p+c$	$\sum_c \sum_{\lambda\mu} T_{\Lambda\lambda}(\bar{x})\lambda_k T_{\lambda\mu}(y)\mu_o D_{\mu\Lambda}^{c,o}$
$n < m < p+1 \to p+c$	$\sum_c \sum_{\lambda\mu} T_{\Lambda\lambda}(y)\lambda_{-k} T_{\lambda\mu}(\bar{x})\mu_o D_{\mu\Lambda}^{c,o}$
$n < p+1 \to p+c < m$	$\sum_c \sum_{\lambda\mu} T_{\Lambda\lambda}(y)\lambda_{-k} D_{\lambda\mu}^{c,o} e^{-ik(c-1)}\mu_{-k} T_{\mu\Lambda}(\bar{x})$
$n < p+1 \leq m \leq p+c$	$\sum_c \sum_\lambda T_{\Lambda\lambda}(y)\lambda_{-k} D_{\lambda\Lambda}^{c,-k}(\bar{x})e^{ik}$
$p+1 \leq n \leq p+c < m$	$\sum_c \sum_\lambda D_{\Lambda\lambda}^{c,k}(y)e^{-ikc}\lambda_{-k} T_{\lambda\Lambda}(\bar{x})$
$p+1 \to p+c < n < m$	$\sum_c \sum_{\lambda\mu} D_{\Lambda\lambda}^{c,0}\lambda_o T_{\lambda\mu}(y)\mu_{-k} T_{\mu\Lambda}(\bar{x})$

Table 1: Contributions to $< x\ k|(H - E_0)|y\ k >$

The sums over λ and μ in the Table are over all eigenvalues of T other than the largest eigenvalue, Λ.

Once these matrix elements are calculated, we proceed to solve the generalized eigenvalue problem with energy-difference and overlap matrices. The dimension of these matrices is equal to the number of different variational parameters in the

157

ground state ansatz. A number of bands, equal to this dimension, that specify the excitation energies as a function of the wavevector k will be obtained.

We have neutral, spin-0 excitations that include correlation effects because of the correlated nature of the ground state upon which they are built. At the same time a band picture is obtained. . These excitations can be thought as **bosonic quasiparticle-elementary excitations**, like phonons or Frenkel-exciton excitations. They can be treated as independent and multiple occupancy of these bands is possible. In this case, their excitation energies should add. Therefore, such features as thermodynamic properties can be developed from the usual single-(quasi)particle partition functions.

3 APPLICATION TO A POLYPHENE STRIP

In order to give more insight to the interpretation of the excitations just presented, we have applied the method to a polyphenanthrene strip (see Fig. 1(a)) and compared the gap energies with experimental results obtained for finite-length polyphene chains.

3.1 Herndon-Simpson Model

The hamiltonian we have used is the Herndon-Simpson model [Herndon 73], [Herndon1 74], [Herndon2 74] which is defined on a space with a basis of orthogonal Kekulé structures $| K)$. To every Kekulé structure $| K >$ a corresponding orthogonal one, $| K)$, has been defined so that

$$(K \mid K') = \delta(K, K'). \tag{3.1}$$

Though originally this hamiltonian was, somehow, empirically obtained, it can be deduced [Rokshar 88], [Klein2 89] from the Heisenberg model by transforming away the overlap matrix $\hat{S}$ in the subspace of Kekulé states, i.e.

$$\mathcal{H} \equiv \hat{S}^{-1/2} \hat{H} \hat{S}^{-1/2} \tag{3.2}$$

where

$$\hat{H} = \sum_{K,K'} < K \mid H \mid K' >| K)(K' | \tag{3.3}$$

$$\hat{S} = \sum_{K,K'} < K \mid K' >| K)(K' | \tag{3.4}$$

The desired hamiltonian results from (3.2) upon expression in powers of a parameter s with no more than second order terms. $s \equiv 1/4$ for a benzenoid system, that is, any system that can be obtained as a cut from the honeycomb lattice. Polyphenanthrene and all the systems studied in the First Chapter are benzenoids.

Finally, the Herndon-Simpson hamiltonian can be expressed,

$$\mathcal{H} = R_1 V_1 + R_2 V_2. \qquad (3.5)$$

This model can be understood to define interactions between pairs of Kekulé states K, K' differing only on a local region. V_1 and V_2 are operators so that $(K|V_i|K')$ is different from zero, if and only if, K and K' differ by an alternate pattern of conjugation around a 6 or 10 cycle of the polymer backbone respectively, and R_i are scalars.

These V_1 and V_2 operators can be introduced in a very convenient way [Klein3 89] as follows; let's define $\hat{\nu}_C$ as an operator associated to a cycle, C, of the polymer backbone, such that $\hat{\nu}_C$ acts on a Kekulé structure state K to give either zero, if cycle C is not conjugated, or reverses the conjugation pattern around C giving K_C, if otherwise (see Fig. 2).

Then V_1 and V_2 are sums of $\hat{\nu}_C$ over all 6 and 10 cycles in the polymer backbone, respectively.
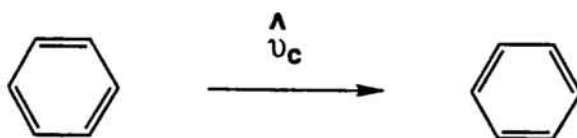

Figure 2: Effect of $\hat{\nu}_C$ operator when C is a 6-cycle.

159

3.2 Ground State wavefunction

The ground state ansatz is a weighted superposition of orthogonal Kekulé states or "short range" RVB (Resonating Valence Bond) wavefunction

$$| \Psi > = \sum_K \prod_{<i,j>}^{K} x_{ij} \, | K)$$

(3.6)

where the weighting factor is a product of variational parameters x_{ij} associated to every singlet pair ij of $| K)$, each Kekulé structure is weighted in terms of their local features. By symmetry and normalization considerations it will be shown that the number of relevant variational parameters for the polyphene strip reduces to one.

We have chosen this model hamiltonian and ground state ansatz for various reasons. Planar polymer systems have proven to be well described by the short range RVB (see First Chapter results and references therein). Also, working with orthogonal states makes computations easier and for this particular hamiltonian, R_1 and R_2 are already parameterized [Klein3 89] so that comparison with experimental results is possible. Furthermore, the excited states of this model will consist on different combinations of the various possible nearest-neighbor singlet spin pairings.

The general method presented in the previous sections is now applied.

3.3 Polyphenanthrene

3.3.1 Herndon-Simpson Model

For the polyphenanthrene strip (see Fig. 1 (a)), the Herndon-Simpson hamiltonian can be rewritten in a more suitable way following Klein et al. [Klein3 89] in terms of "pseudospin" operators. In Fig. 3, the four types of translational symmetry equivalent bonds in this polymer are drawn and labelled 1, 2, α, β.

In the First Chapter, it was shown that polyphenanthrene has three different non-interacting phases $P = 0$, $P = 1$, $P = 2$. A bond between two neighboring sites is defined as *single* if, talking in terms of their π-electron spins, they are not paired, and as *double* if those two sites form a singlet pair.

Phase $P = 0$ contains a unique Kekulé structure in which every α and β bonds is single. Phase $P = 1$ contains numerous Kekulé structures and characterizes by the

fact that in every ring one of the bonds (α and β) is single and the other is double. And $P = 2$ phase has a unique Kekulé structure in which every α and β bond is double. (See Fig. 21 and 22 in the Introduction part of the First Chapter).
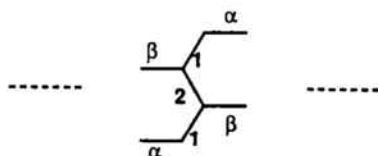

Figure 3: 1, 2, α and β label the four types of symmetry equivalent bonds in polyphenanthrene.

Configuration mixing between Kekulé structures occurs only in $P = 1$ phase, then, it is expected that the ground state will belong to this phase. In this phase, every ring on the polyphenanthrene strip has either bond α or bond β as a double bond, so that two different *local states* can be defined for that ring, $|\alpha\rangle$ or $|\beta\rangle$. And a sequence of such *local states* along the strip defines a Kekulé structure belonging to the $P = 1$ phase, with the restriction that no two $|\beta\rangle$ *local states* can be adjacent. For instance, in Fig. 4, a L=10 strip has been drawn, and the Kekulé structure represented corresponds to the sequence $\alpha\alpha\beta\alpha\beta\alpha\alpha\beta\alpha$.

Figure 4: A typical Kekulé structure on a $L = 10$ polyphenanthrene strip. This Kekulé state is specified by the sequence $\alpha\alpha\beta\alpha\beta\alpha\alpha\beta\alpha$.

Note that the definition of a *local state* that is given in this chapter differs from that in the previous chapter. There, a *local state* defined on a few-site zone accounted for the contributions of the *bra* and *ket* part of an overlap matrix element, while here

the local states have been introduced to define the wavefunction, in particular, the Kekulé structures.

Then, a Kekulé structure for an L-length strip is represented:

$$\sigma(L) = \sigma_1\sigma_2...\sigma_L \tag{3.7}$$

where σ is α or β with the restriction of no two $|\beta\rangle$ adjacent local states.

If these *local states* are considered as "pseudospins", associated "pseudospin" operators s_j^z, s_j^+, s_j^- can be introduced for ring j.

Then, $\hat{\nu}_C$ for a six-site ring, j, interchanges α and β local states at that ring. This can be expressed by the action of $s_j^+ + s_j^-$. Furthermore, the constraint that no two neighboring rings are both in a β local state can be fulfilled in terms of projectors, which, for ring n, are defined:

$$\hat{p}_n = \frac{1}{2} + s_n^z \tag{3.8}$$

V_1 is, then, expressed as

$$V_1 = \sum_j \hat{\rho}_j = \sum_j \hat{p}_{j-1}(s_j^+ + s_j^-)\hat{p}_{j+1}. \tag{3.9}$$

When $\hat{\nu}_C$ acts on a 10-site cycle around two neighboring rings j and $j+1$, it interchanges $\alpha\beta$ and $\beta\alpha$ local structures. This can be reproduced by the effect of the operator $s_j^+ s_{j+1}^- + s_j^- s_{j+1}^+$. And states for rings $j-1$ and $j+2$ are restricted to be α states. Therefore, the V_2 operator is expressed:

$$V_2 = \sum_j \hat{\rho}_{jj+1} = \sum_j \hat{p}_{j-1}(s_j^+ s_{j+1}^- + s_j^- s_{j+1}^+)\hat{p}_{j+2}. \tag{3.10}$$

The Herndon-Simpson hamiltonian reduces, then, to:

$$\mathcal{H} = \sum_{j=1}^L \{R_1\hat{p}_{j-1}(s_j^- + s_j^+)\hat{p}_{j+1} + R_2\hat{p}_{j-1}(s_j^+ s_{j+1}^- + s_j^- s_{j+1}^+)\hat{p}_{j+2}\} \tag{3.11}$$

3.3.2 Ground State ansatz

As previously mentioned, the trial ground state wavefunction is chosen as a weighted superposition of Kekulé structures where the weighting factor is a product of variational parameters associated to every *singlet pair* or bond. In principle, we

162

have 4 possible variational parameters for the polyphenanthrene system corresponding to the 4 possible bonds on the backbone of the system: x_α, x_β, x_1, x_2 (see Fig. 3). They can be redefined:

$$x'_\alpha = x_\alpha x_2,$$
$$x'_\beta = x_\beta x_1^2 / x_2,$$
$$x'_1 = 1,$$
$$x'_2 = 1. \tag{3.12}$$

This is so because the occurrence of double bonds at the bond positions 1 and 2 is completely determined by the pattern of double bonds at the adjacent bond positions α and β. Then, without loss of generality, x_1 and x_2 can be chosen equal to 1 . Normalization of Ψ enables to fix the value of one of the remaining parameters, we take $x_\alpha = 1$. Finally only one relevant parameter remains, which is the one associated to a double bond (singlet pair) at the position β, x_β. For simplicity the β subscript is going to be dropped.

The ground state wavefunction (3.6) is then:

$$|\Psi> \equiv \sum_K \prod_j x_j^{\delta(\sigma_j(K),\beta)} |K) \tag{3.13}$$

where $\sigma_j(K) = \alpha$ or β, and the subindex j labels the ring. By the translational invariance of the system, the variational parameters will be independent of j. Therefore, all calculations will be done in terms of only one variational parameter, though, for keeping generality, this won't be considered until the energy optimization is carried out.

3.3.3 Ground State Energy

An upper bound to the exact ground state energy will be obtained upon optimization of the expression,

$$E \leq \frac{<\Psi|\mathcal{H}|\Psi>}{<\Psi|\Psi>}. \tag{3.14}$$

The overlap and the hamiltonian matrix elements are to be expressed in terms of transfer matrices (as shown in the general case).

163

Overlap:

$$< \Psi | \Psi >= \sum_K \prod_j^K (\bar{x}_j x_j)^{\delta(\sigma_j(K),\beta)} \tag{3.15}$$

$\bar{x}_j$ refers to the variational parameter associated to the *bra* part of the overlap corresponding to ring j, and x_j is that associated to the *ket* part. Note that $(K|K') = 0$ whenever $|K) \neq |K')$ because of orthogonal Kekulé structures. Therefore, only $(K|K)$ overlaps contribute to the previous equation.

Using the definition of Kekulé structures in terms of sequences of σ_j *local states*, the overlap reduces to:

$$< \Psi | \Psi >= \sum_{\sigma_1 \sigma_2 ... \sigma_L} \prod_j \{(\bar{x}_j x_j)^{\delta(\sigma_j,\beta)} \eta(\sigma_j, \sigma_{j+1})\} \tag{3.16}$$

where

$$\eta(\sigma_m, \sigma_n) \equiv \begin{array}{ll} 0 & \sigma_m = \sigma_n = \beta \\ \\ 1 & otherwise \end{array} \tag{3.17}$$

takes into account the restriction that no two β *local states* can be adjacent.

The definition of $|\Psi>$ in terms of *local states* enables the use of the **transfer matrix technique** to compute the overlap and Hamiltonian matrix element.

The transfer matrix, T, elements are defined between two consecutive rings j and $j + 1$ in the following way,

$$(\sigma_j|T|\sigma_{j+1}) \equiv (x_j \bar{x}_j)^{\delta(\sigma_j,\beta)} \eta(\sigma_j, \sigma_{j+1}). \tag{3.18}$$

And the overlap reduces,

$$< \Psi | \Psi >= \sum_{\sigma_1 \sigma_2 ... \sigma_L} \prod_{j=1}^L (\sigma_j|T|\sigma_{j+1}) = tr T^L. \tag{3.19}$$

The evaluation of transfer matrix elements is shown in Fig. 5. The T matrix is then, for ring j:

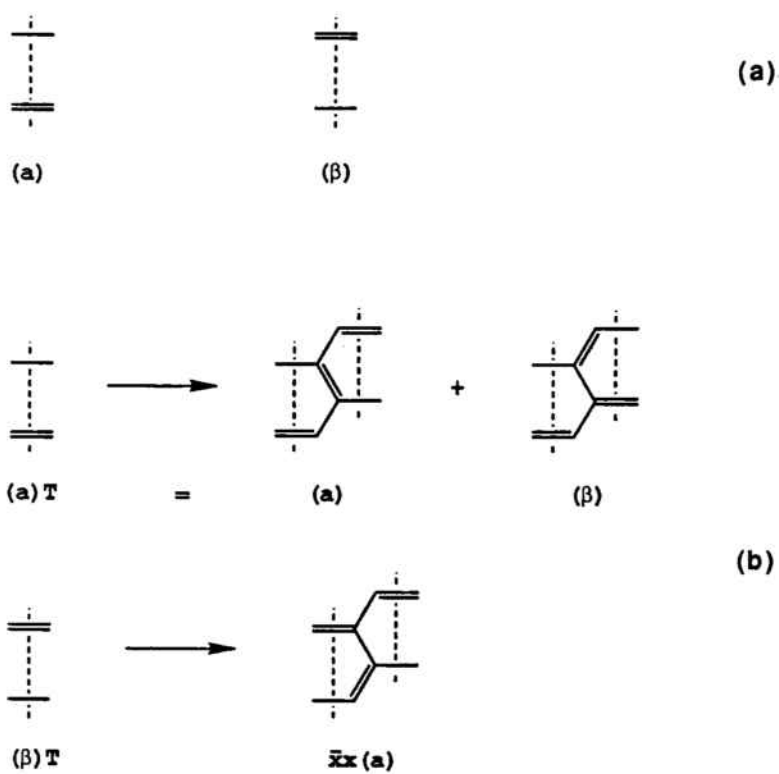$$\begin{pmatrix} 1 & 1 \\ \bar{x}_j x_j & 0 \end{pmatrix}$$

164

Figure 5: Transfer matrix elements defined between two consecutive rings j and $j+1$.

165

<u>Hamiltonian matrix element.</u>

The Herndon-Simpson Hamiltonian, $\mathcal{H}$, allows interaction between pairs of Kekulé structures differing only in a *local* region. Following the expression in (3.11), it is observed that the first type of matrix element is that over a conjugated six-circuit operator $\hat{\rho}_j = \hat{p}_{j-1}(s_j^+ + s_j^-)\hat{p}_{j+1}$ acting at the region of ring j. To analyse this matrix element, one "propagates" along the strip as it was done for the overlap $< \Psi|\Psi >$, the only difference in propagation occurs when crossing ring j. Due to the projectors $\hat{p}_{j-1}$ and $\hat{p}_{j+1}$, for a nonzero result, the double step from ring $j-1$ to ring $j+1$ must start and end in an α state. This double step can be represented by a *connection matrix*, $C_{j-1\to j+1}$, with all elements set to zero except the α, α^{th} element. Therefore, a weight $x_j + \bar{x}_j$ is given to the ring j. And the $C_{j-1\to j+1}$ connection matrix is:

$$\begin{pmatrix} x_j + \bar{x}_j & 0 \\ 0 & 0 \end{pmatrix}$$

By translational symmetry, $C_{j-1\to j+1} = C_{1\to 2}$, and the variational parameters are independent of the ring j. Then,

$$< \Psi|\hat{\rho}_j|\Psi >= tr(C_{1\to 2}T^{L-2}). \tag{3.20}$$

The second type of matrix element is that over a conjugated ten-circuit operator $\hat{\rho}_{jj+1} = \hat{p}_{j-1}(s_j^+ s_{j+1}^- + s_j^- s_{j+1}^+)\hat{p}_{j+2}$ acting at the region of rings $j, j+1$. A similar argument like the one done for $\hat{\rho}_j$, applies here. A *connection matrix* over a triple step from $j-1$ to $j+2$, $C_{j-1\to j+2}$, is defined:

$$\begin{pmatrix} x_j\bar{x}_{j+1} + \bar{x}_j x_{j+1} & 0 \\ 0 & 0 \end{pmatrix}$$

By translational symmetry, $C_{j-1\to j+2} = C_{1\to 3}$, and,

$$< \Psi|\bar{\rho}_{jj+1}|\Psi >= tr(C_{1\to 3}T^{L-3}). \tag{3.21}$$

Then,

$$< \Psi|\mathcal{H}|\Psi >= L\{R_1 tr(C_{1\to 2}T^{L-2}) + R_2 tr(C_{1\to 3}T^{L-3})\}. \tag{3.22}$$

In the limit of long strips $L \longrightarrow \infty$, the maximum eigenvalue Λ of T dominates and the overlap and hamiltonian matrix element reduce to:

$$< \Psi | \Psi > \sim \Lambda^L$$

$$< \Psi | H | \Psi > \sim L(\Lambda, l | \{ R_1 \Lambda C_{1 \to 2} + R_2 C_{1 \to 3} \} | \Lambda, r) \Lambda^{L-3} \qquad (3.23)$$

as in preceding chapters. Diagonalizing the T matrix, where $\bar{x} = x$, a maximum and minimum eigenvalues are obtained,

$$\Lambda \equiv \frac{1}{2} + (\frac{1}{4} + x^2)^{1/2}$$
$$\nu \equiv \frac{1}{2} - (\frac{1}{4} + x^2)^{1/2} \qquad (3.24)$$

and their corresponding biorthonormalized left- and right- eigenvectors are:

$$(\lambda, l | = \frac{1}{2\lambda - 1} (\lambda, 1) \qquad (3.25)$$

and

$$| \lambda, r) = \begin{pmatrix} 1 \\ \lambda - 1 \end{pmatrix} \qquad (3.26)$$

where λ stands for Λ or ν. The ground state energy reduces to,

$$E_0 \equiv \frac{< \Psi | \mathcal{H} | \Psi >}{< \Psi | \Psi >}$$
$$= 2L(\Lambda, l | \alpha)(\alpha | \Lambda, r) \{ R_1 x \Lambda + R_2 x^2 \} \Lambda^{-3}$$
$$= \frac{2xL}{\Lambda^2(2\Lambda - 1)} \{ R_1 \Lambda + R_2 x \} \qquad (3.27)$$

where x may be varied to obtain an optimal energy per ring. It is worthwhile to note that a very simple expression has been obtained for the ground state energy.

3.3.4 Excited States

The expressions defined in the general case for the excited states computation are now particularized to the polyphenanthrene case. Then:

$$\nu \equiv \frac{\Lambda e^{ik}}{\Lambda - \nu e^{ik}} \qquad (3.28)$$

$$T_{\lambda\mu}(\bar{x}) = T_{\lambda\mu}(x) =$$

$$(\lambda, l|\begin{pmatrix} 1 & 1 \\ xx' & 0 \end{pmatrix}|\mu, r)\Lambda^{-1} =$$

$$\frac{\lambda\mu - \Lambda^2}{\Lambda(2\lambda - 1)} \tag{3.29}$$

$$D_{\lambda\mu}^{2,0} = \{(\lambda, l|C_{1\to 2}|\mu, r) - (\frac{\lambda}{\Lambda})^2(\Lambda, l|C_{1\to 2}|\Lambda, r)(\lambda, l|\lambda, r)\}\Lambda^{-2}$$

$$= 2x\{\frac{\lambda}{2\lambda - 1} - \frac{\Lambda}{2\Lambda - 1}(\frac{\lambda}{\Lambda})^2\delta_{\lambda\mu}\}\Lambda^{-2} \tag{3.30}$$

$$D_{\lambda\mu}^{3,0} = 2x^2\{\frac{\lambda}{2\lambda - 1} - (\frac{\lambda}{\Lambda})^3\frac{\Lambda}{2\Lambda - 1}\delta_{\lambda\mu}\}\Lambda^{-2} \tag{3.31}$$

$$D_{\lambda\mu}^{2,k}(x) = \{D_{\lambda\mu}^{2k}\}^*$$

$$= e^{ik}\{\frac{\lambda}{2\lambda - 1}[2x + (x + x')e^{ik}] -$$

$$2x\frac{\Lambda}{2\Lambda - 1}(\lambda, l|T(x)|\mu, r)(\mu + \lambda e^{-ik})\Lambda^{-2}\}\Lambda^{-2} \tag{3.32}$$

$$D_{\lambda\mu}^{3,k}(x) = e^{ik}\{\frac{\lambda}{2\lambda - 1}[2x^2 + x(x' + x)e^{ik} + x(x + x')e^{2ik}]$$

$$-2x^2\frac{\Lambda}{2\Lambda - 1}(\lambda, l|T(x)|\mu, r)(\mu^2 + \lambda\mu e^{ik} + \lambda^2 e^{2ik})\Lambda^{-3}\}\Lambda^{-3} \tag{3.33}$$

$$D_{\Lambda\Lambda}^{2,k}(\bar{x}, x) = \frac{2\Lambda}{2\Lambda - 1}\sqrt{\frac{\Lambda}{\Lambda - 1}}\{-(2\Lambda + 1) + (2\Lambda - 3)cosk\}\Lambda^{-2} \tag{3.34}$$

$$D_{\Lambda\Lambda}^{3,k}(\bar{x}, x) = \frac{2\Lambda}{2\Lambda - 1}\{-\Lambda(4\Lambda - 1) + [6\Lambda(\Lambda - 1) + \frac{\Lambda^3}{\Lambda - 1}]cosk$$

$$-[2\Lambda^2 - 3\Lambda + 2]cos2k\}\Lambda \tag{3.35}$$

<u>Excitations</u>

The single excitations obtained by replacing x for x' in the nth unit cell are, following the general treatment:

$$| \Psi_n > = \sum_K x'^{\delta(\sigma_n(K),\beta)} \prod_j^{\neq n} x^{\delta(\sigma_j(k),\beta)} | K) \qquad (3.36)$$

where x' is chosen to satisfy the Brillouin condition and is determined by,

$$(\Lambda, l | T(x) | \Lambda, r) = 0 \qquad (3.37)$$

where the matrix $T(x)$ differs from T in (3.18) in that $x_j = x$ is replaced by x'. Solving this equation with $(\Lambda, l|$ and $|\Lambda, r)$ given by (3.25), the value of x' is obtained:

$$x' = \frac{-\Lambda^2}{x}. \qquad (3.38)$$

If the value of x is the one that optimizes the ground state energy, this choice of x' guaranties that single excitations don't mix with the ground state.

As the model characterizes by one relevant variational parameter, x, only one *symmetry-adapted excited state* is defined:

$$| k \; x > \equiv | k > = \frac{1}{\sqrt{L\Lambda^L}} \sum_{n=1}^{L} e^{ikn} | \Psi_n(x) > . \qquad (3.39)$$

The overlap matrices between pairs of the localized single excitations may be developed in a similar way to the ground state. But, given the ground state development and the satisfaction of the Brillouin condition, we may follow the general formulae (2.19) and (2.24) for the overlap and Hamiltonian matrix elements between pairs of **symmetry-adapted single excitations**.

Particularizing them to this case:

$$< k \; | \; k' > = \delta(k,k')\{T_{\Lambda\Lambda}(\bar{x},x) + T_{\Lambda\nu}(x)T_{\nu\Lambda}(x)(\nu_k + \nu_{-k})\} \qquad (3.40)$$

And,

$$< k|(\mathcal{H} - E_0|k' > = \delta(k,k')\{R_2 D_{\Lambda\Lambda}^{3,k}(\bar{x},x) + R_1 D_{\Lambda\Lambda}^{2,0}(\bar{x},x)$$
$$+ [R_1 D_{\Lambda\nu}^{2,0} + R_2 D_{\Lambda\nu}^{3,0}]\nu_0 [T_{\nu\Lambda}(\bar{x},x) + T_{\nu\nu}(x)(\nu_k + \nu_{-k})T_{\nu\Lambda}(x)]$$
$$+ [R_1 D_{\nu\Lambda}^{2,0} + R_2 D_{\nu\Lambda}^{3,0}]\nu_0 [T_{\Lambda\nu}(\bar{x},x) + T_{\Lambda\nu}(x)(\nu_k + \nu_{-k})T_{\nu\nu}(x)]$$

169

$$+R_1[D_{\Lambda\nu}^{2,-k}(x)\nu_k e^{i2k} + D_{\Lambda\nu}^{2,k}(x)\nu_{-k}e^{-i2k}]T_{\nu\Lambda}(x)$$
$$+R_2[D_{\Lambda\nu}^{3,-k}(x)\nu_k e^{i3k} + D_{\Lambda\nu}^{3,k}(x)\nu_{-k}e^{-i3k}]T_{\nu\Lambda}(x)$$
$$+R_1[D_{\nu\Lambda}^{2,k}(x)\nu_k e^{-ik} + D_{\nu\Lambda}^{2,-k}(x)\nu_{-k}e^{ik}]T_{\Lambda\nu}(x)$$
$$+R_2[D_{\nu\Lambda}^{3,k}(x)\nu_k e^{-ik} + D_{\nu\Lambda}^{3,-k}(x)\nu_{-k}e^{ik}]T_{\Lambda\nu}(x)$$
$$+R_1 D_{\nu\nu}^{2,0}[\nu_k^2 e^{i2k} + \nu_{-k}^2 e^{-2ik}]T_{\Lambda\nu}(x)T_{\nu\Lambda}(x)$$
$$+R_2 D_{\nu\nu}^{3,0}[\nu_k^2 e^{i2k} + \nu_{-k}^2 e^{-2ik}]T_{\Lambda\nu}(x)T_{\nu\Lambda}(x)\} \qquad (3.41)$$

3.4 RESULTS

The ground state wavefunction and energy per monomer unit of the infinite strip is obtained by varying x to optimize the energy E_0 in (3.27). Then, considering single excitations where the variational parameter has been replaced by (3.38) in a single monomer unit, and, using equations (3.40) and (3.41), the overlap and energy-difference matrix elements are computed to give the desired excitation energies,

$$\varepsilon(k) = \frac{< k \mid (\mathcal{H} - E_0 \mid k >}{< k \mid k >} \qquad (3.42)$$

where the wavevector k ranges over the first Brillouin zone. Excitation energies in terms of k are obtained.

The results depend on the parameters R_1 and R_2 that appear in the Herndon-Simpson hamiltonian. The computations have been done for three parameterizations:

(1) parameterization used by Randić [Randic 76], [Randic 77].

(2) parameterization for which the ansatz here used corresponds to the exact ground state [Klein3 89].

(3) parameterization used by Herndon [Herndon 73], [Herndon1 74], [Herndon2 74].

The parameterizations of Herndon and Randić were obtained by empirical fitting and parametrization (2) is intermediate between those two. In Table 2 numerical results are presented at different values of the wavevector k, $k\epsilon[0,\pi]$, the representation of these values is done in Fig. 6. Excitation energies in the other half of the Brillouin zone are related by symmetry, and $\epsilon(k) = \epsilon(-k)$.

170

The minimum excitation energy occurs at $k \simeq \pm 0.77\pi$ in any of the three parameterizations and it is of the order $\sim 1.5eV$.

	Randic	"Exact"	Herndon
R_1	0.869 eV	$-$	0.841 eV
R_2	0.246 eV	$R_1/8^{1/2}$	0.336 eV
E_0/R_1L	0.6854	$1/2^{1/2}$	0.7214
x	0.694	$1/2^{1/2}$	0.715
$\epsilon(0)/R_1$	2.636	2.668	2.691
$\epsilon(\pi/10)/R_1$	2.768	2.808	2.836
$\epsilon(\pi/5)/R_1$	3.076	3.136	3.177
$\epsilon(3\pi/10)/R_1$	3.340	3.422	3.478
$\epsilon(2\pi/5)/R_1$	3.327	3.426	3.492
$\epsilon(\pi/2)/R_1$	2.944	3.047	3.115
$\epsilon(3\pi/5)/R_1$	2.321	2.419	2.483
$\epsilon(7\pi/10)/R_1$	1.785	1.882	1.945
$\epsilon(4\pi/5)/R_1$	1.647	1.764	1.839
$\epsilon(9\pi/10)/R_1$	1.880	2.035	2.135
$\epsilon(\pi)/R_1$	2.055	2.231	2.345

Table 2: Results computed with the three different parametrizations.

From an experimental point of view, at $k = 0$ the energy-gap obtained can be compared to a dipole-allowed transition in the visible region. Our result is $2.3eV$. For polyphene chains of lengths $L = 1, 2, 3, 4, 5$, the observed transitions [Clar 64] are, respectively 4.70, 4.01, 3.61, 3.45, 3.30 eV so that in the limit of very long chains they might extrapolate fairly reasonably to a region around our calculated energy-gap.
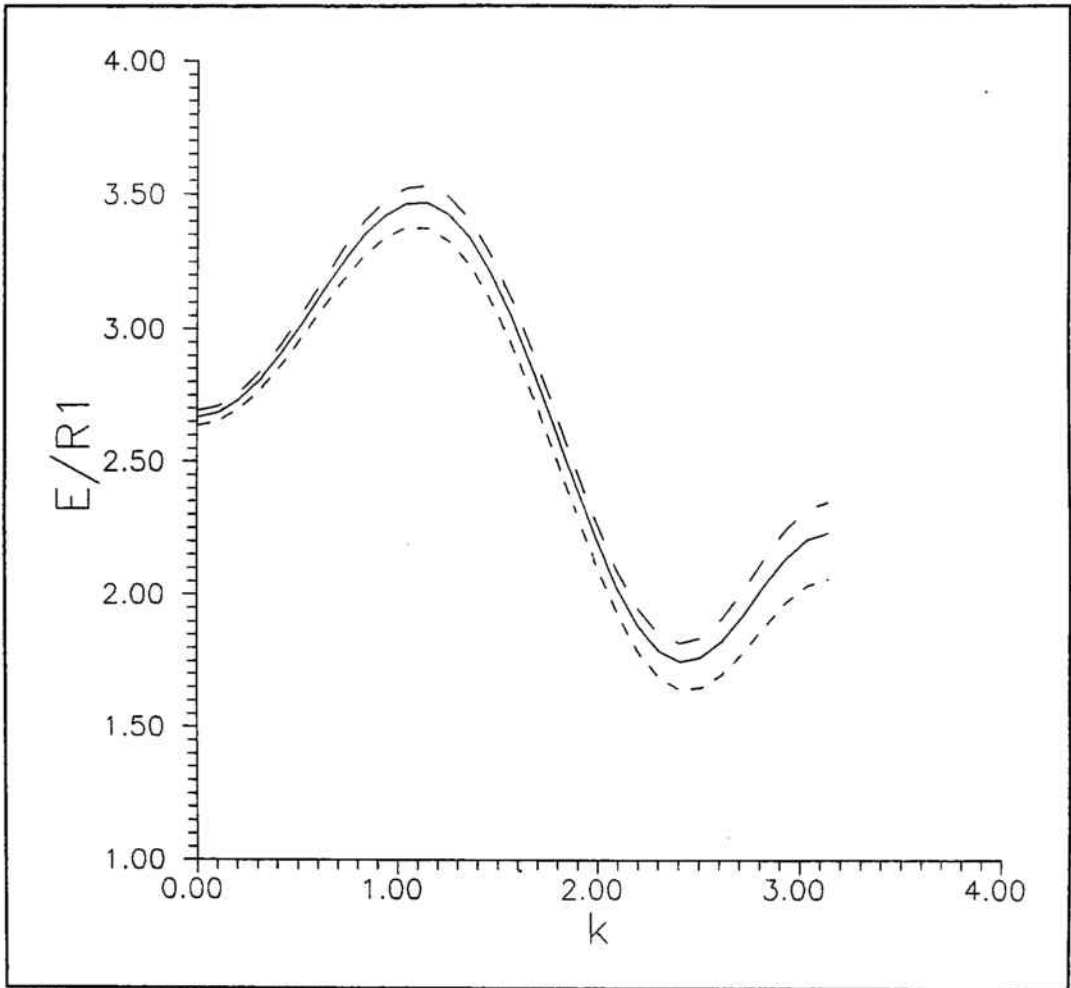
Figure 6: Representation of the energy gap of the excitations in the k space, $E \equiv \epsilon(k)$, for the different parameterizations of R_i. (- -) Randic's, (—) "Exact", (- -) Herndon's.

CONCLUSIONS

We have presented, within a localized scheme, a study of the ground state nature of a family of polymers -polyacenacene, poly(benz[m,n]anthracene) (PBA), polyperylene, polyphenanthrene- and of square-lattice strips described by a Heisenberg hamiltonian.

Following the general treatment of the variational principle, attention has been focused on alternative localized-site cluster-expanded wavefunctions, i.e. RVB-type ansätze and a Néel-based ansatz.

We have shown that simple expressions of the physical magnitudes we were interested in, were easily obtained by using the transfer matrix technique, as energy and correlation functions in the square lattice systems.

From our results, we conclude that the **RVB** wavefunctions considered, which are of "short range" type, don't give, as expected, the best upper bound to the ground state energy of these systems. But they may be relevant for studying such phenomena as the *Peierls instability* and elementary excitations as hole excitations [Anderson2 87] or excitonic excitations.

From **RVB** results we have obtained that:

- Polyacenacene shows a *totally-antisymmetric* distortion.
- PBA shows also a *totally-antisymmetric* distortion.
- Polyperylene is ustable to a *totally-symmetric* distortion.
- Polyphenanthrene is not subjected to a Peierls instability.

The **Néel-state-based ansatz** chosen gives a fairly good upper bound to the ground state energy for all the systems considered.

We have made an attempt to extrapolate the results obtained with this ansatz for the square-lattice strips, to infinite-width strips and obtained a value in J units $E_\infty \simeq -0.662(7)$ for the ground state energy per site of the two dimensional square lattice, comparable to other computations [Sachdev 89] $E_\infty \simeq -0.663(4)$ with an equivalent ansatz.

We have shown that with such a simple "modified Néel" wavefunction, the corresponding energy is fastly lowered in comparison to the energy of the Néel state and computations are very simple. Values of the correlation function defined for square lattice strips, confirmed that this Néel-based ansatz has still nonzero AFLRO.

The Néel-state-based ansatz predicts for the polymers studied, the same distor-

tions as the RVB description, except for the case of polyacenacene where this ansatz, is unable to show whether the distortion is going to take place or not.

Within the band theory picture, Hückel model has been studied for all the polymer systems.

Results obtained for every π-network system are the following:

- Polyacenacene is not predicted a favored distortion and when better approximations are considered, contradicting results are obtained.

- PBA shows a *totally antisymmetric* distortion.

- Polyperylene shows a *totally symmetric* distortion

- Polyphenanthrene is not subject to a Peierls distortion.

From band theory and localized descriptions results it can be concluded that predictions of the two opposite limits seem to lead to similar consequences under similar structural circumstances, i.e. both approaches predict the same instability behaviour for the polymers when band theory is able to give a clear answer. Nevertheless, band theory results depend on the level of approximation, as it is observed in the study of polyacenacene, where this picture at different levels of approximation gives rise to different results. While, the localized approach has proven to give non-contradicting predictions even if better descriptions were considered.

Therefore, it is concluded that the localized view gives a good description of these systems and that it is not necessary at all, to neglect electron correlation to predict a Peierls-like transition, as has been suggested in the past by the fact that including correlation 'a posteriori', as a perturbation, leads to the lowering of the distortion [Dixit 84].

Also, a novel many-body approach for extended system excitations based on a localized view that includes electron correlation has been presented.

It has been shown that this treatment is computationally feasible specially for quasi-one dimensional systems where the transfer matrix technique proves to be a powerful tool of work also for excitations. It's important to note that the results are developed in terms of quantities which remain finite as the strip-length goes to infinity.

Neutral spin-0 excitations that characterize for having a localized correlated nature are obtained and, at the same time, they can be given a bosonic quasi-particle

175

interpretation like phonons or Frenkel-excitons excitations.

We have applied the method to a polyphene chain described by a Herndon-Simpson model and comparison with experimental results has been quite satisfactory.

Finally, this treatment is not only restricted to the model hamiltonian and the ground state ansatz presented but, can be applied to any system with effective short range interactions described by a localized-site cluster expanded ground state wavefunction and it also provides a methodology for seeking other interesting excitations.

Work on hole excitations is in progress, though it is beyond the scope of this disertation.

References

[Anderson 52] P.W. Anderson, Phys. Rev. **86** (1952) 694

[Anderson1 87] P.W. Anderson, Science, **235** (1987) 1196

[Anderson2 87] P.W. Anderson, G. Baskaran, Z. Zou, T. Hsu, Phys. Rev. Lett., **58** (1987) 2790

[Anderson 88] P.W. Anderson *Cargese Lectures* (May 1988)

[Bardeen 57] J. Bardeen, L.N. Cooper, J.R. Schrieffer, Phys. Rev. **106** (1957) 162. *ibid* **108** (1957) 1175

[Barnes 88] T. Barnes, E.S. Swanson, Phys. Rev. Lett. B, **37** (1988) 9405

[Baskaran 87] G. Baskaran, Z. Zou, P.W. Anderson, Solid State Comm., **63** (1987) 973

[Becker 88] K.W. Becker, P. Fulde, Proceedings on *Physics on Low-Dimensional Systems* Gräftavallen, (1988)

[Bednorz 86] J.G. Bednorz, K.A. Müller, Z. Phys. B, **64** (1986) 189

[Bednorz 88] J.G. Bednorz and K.A. Müller, Rev. Mod. Phys., **60** (1988) 585

[Bonca 89] J. Bonca, P. Prelovsek, I. Sega, Phys. Rev B, **39** (1989) 7074

[Boudreaux 85] D.S. Boudreaux, R.R. Chance, R.L. Elsenbaumer, J.E. Frommer, J.L. Brédas, R. Silbey, Phys. Rev. B, **31** (1985) 652

[Bozovic 85] I. Bozović, Phys. Rev. B **32** (1985) 8136

[Bredas 82] L. Brédas, R.R. Chance, R.H. Baughman, R. Silbey, J. Chem. Phys., **76** (1982) 3673

[Burdette 84] J.K. Burdette, Progr. Solid Chem. **15** (1984) 173

[Campbell 87] D.K. Campbell, D. Baeriswyl, S. Mazumbdar, Synth. Met., **17** (1987) 197

[Chien 84] J.C.W. Chien, *Polyacetylene* Academic Press, N.Y. (1984).

177

[Clar 64]   E. Clar, *Polycyclic Hidrocarbons*, Vol.1, Ac. Press, N.Y. (1964)

[Cooper 56]   L.N. Cooper, Phys. Rev. **104** (1956) 1189

[Coulson 52] C.A. Coulson, *Valence*, Clarendon, Oxford, (1952)

[Dagotto 88] E. Dagotto, J.R. Schrieffer, A. Moreo, T. Barnes (preprint NSF-ITP-88-176)

[Dasgupta 81] C. Dasgupta, P. Pfeuty, J. Phys. C., **14** (1981) 717

[Dixit 84]   S.N. Dixit, S. Mazumdar, Phys. Rev. B, **29** (1984) 1824

[Doucot 89]   B. Doucot, F. Nori (preprint 1989)

[Duke 82]   C.B. Duke, H.W. Gibson, *Encyclopedia of Chemical Technology* Wiley, N.Y. **18** (1982) 755

[Durcasse 82] L.R. Durcasse et al., J. Chem. Phys., **76** (1982) 4094

[Dzyaloshin. 88] I.E. Dzyaloshinskii, A.M. Polyakov, P.B. Wiegman, Phys. Rev. Lett. A, **137** (1988) 112

[Epstein 74] S.T. Epstein,
              The Variation Method in Quantum Chemistry, Academis Press, N.Y., (1974), Chap. III

[Fan 88]   Y. Fan, M. Ma, Phys. Rev. B, 37 (1988) 1820

[Figueirido 89] F. Figueirido, A. Karlhede, S. Kivelson, S. Sondhi, M. Rocek, D.S. Rokshar (preprint 1989)

[Garcia-Bach 88] M.A. García-Bach, D.J. Klein, R. Valentí, Int. Journal Mod. Phys.B, 1 (1988) 1035

[Garcia-Bach1 89] M.A. García-Bach, R. Valentí, D.J. Klein,
              J. Mol. Struct (Theochem), 185 (1989) 287

[Garcia-Bach2 89] M.A. García-Bach, A. Peñaranda. *Private communication*

[Garcia-Bach3 89] M.A. García-Bach, R. Valentí, D.J. Klein, *to be published*

[Ginzburg 50] V.L. Ginzburg, L.D. Landau, Zh. Eksp. Teor. Fiz., **20** (1950) 1064

178

[Graovac 77]   A. Graovac, I. Gutman, R. Randić, N. Trinajstić, Colloid and Polym. Sci. **255** (1977) 480

[Gros 87]   C. Gros, R. Joynt, T.M. Rice, Phys. Rev. B, **36** (1987) 381

[Haldane 88]   F.D.M. Haldane, Phys. Rev. Lett., **60** (1988) 635

[Hasegawa 89]   Y. Hasegawa, D. Poilblanc (preprint 1989)

[Hayes 85]   W. Hayes, Contemp. Phys. **26** (1985) 421

[Heeger 81]   A.J. Heeger, Comments in Solid State Physics **10** (1981) 53

[Herndon 73]   W.C. Herndon, J. Am. Chem. Soc., **95** (1973) 1404

[Herndon1 74]   W.C. Herndon, Thermochim. Acta, **8** (1974) 225

[Herndon2 74]   W.C. Herndon, M.L. Ellzey, J. Am. Chem. Soc., **96** (1974) 6631

[Hirsch 85]   J.E. Hirsch, Phys. Rev. B, **31** (1985) 4403

[Horsch 88]   P. Horsch, W. von der Linden, Physica C, **153** (1988) 1285. P. Horsch, W. von der Linden, Z. Phys. B, **72** (1988) 181

[Hubbard 63]   J. Hubbard, Proc. Roy. Soc. A, **276** (1963) 238

[Hudson 82]   B.S. Hudson, B. Kohler, K. Schulten, *Excited States* Ac. Press, N.Y. 1982

[Hulthen 38]   L. Hulthén, Arkiv. Math. Astron. Fysik, **26a** (1938) 11

[Huse 88]   D.A. Huse, Phys. Rev. B, **37** (1988) 2380

[Inui 86]   M. Inui, S. Doniach, P.J. Hirschfeld, A.E. Ruckenstein, Phys. Rev. B, **37** (1986) 2320

[Josephson 62]   B.D. Josephson, Phys. Lett., **1** (1962) 251.

[Kane 89]   C.L. Kane, P.A. Lee, N. Read, Phys. Rev. B, **39** (1989) 6880

[Kertesz 83]   M. Kertesz, R. Hoffmann, Solid State Commun., **47** (1983) 97

[Kivelson 83]   S. Kivelson, O.L. Chapman, Phys. Rev. B, **28** (1983) 7236

[Kivelson 87] S. Kivelson, D. Rokhsar, J. Sethna, Phys. Rev. B, 35 (1987) 8865

[Kivelson 89] S. Kivelson, Phys. Rev. B, **39** (1989) 259

[Klein 74] D.J. Klein, W.A. Seitz, Phys. Rev. B, **10** (1974) 3217

[Klein1 76] D.J. Klein, J. Chem. Phys, **64** (1976) 4868

[Klein2 76] D.J. Klein, M.A. García-Bach, Molec. Phys., **31** (1976) 797

[Klein1 79] D.J. Klein, Phys. Rev. B, **19** (1979) 870

[Klein2 79] D.J. Klein, M.A. García-Bach, Phys. Rev. B, **19** (1979) 877

[Klein 83] D.J. Klein, W.A. Seitz, M.A. García-Bach, J.M.N. Picone, D.C. Foyt, Int. Jour. Quant. Chem., **17** (1983) 555

[Klein1 86] D.J. Klein, G.E. Hite and T.G. Schmalz, J. Comput. Chem., **7** (1986) 443

[Klein2 86] D.J. Klein, T.G. Schmalz, W.A. Seitz, G.E. Hite, Int. Jour. Quant. Chem.: Quant. Chem. Symp. **19** (1986) 707

[Klein3 86] D.J. Klein, S.A. Alexander, W.A. Seitz, T.G. Schmaltz, G.E. Hite, Theor. Chim. Acta **69** (1986) 393

[Klein1 89] D.J. Klein, M.A. García-Bach, W.A. Seitz, J. Mol. Struct (Theochem), 185 (1989) 275

[Klein2 89] D.J. Klein, N. Trinajstić, to be published in Pure & Appl. Chem.

[Klein3 89] D.J. Klein, T.G. Schmalz, Int. Journal Quant. Chem., **35** (1989)

[Klein4 89] D.J. Klein, *Private communication*

[Kopp 88] T. Kopp, F.J. Seco, S. Schiller, P. Wölfle, Phys. Rev. B, **38** (1988) 11835

[Kotliar 88] G. Kotliar, Phys. Rev. B, **37** (1988) 3664

[Kuroda 87] S. Kuroda, H. Shirakawa, Synth. Met., **17** (1987) 423

[Liang 88] S. Liang, B. Doucot, P.W. Anderson, Phys. Rev. Lett., **61** (1988) 365

[Lieb 62]   E.H. Lieb, D.C. Mattis, J. Math. Phys. **3** (1962) 749

[Lieb 68]   E.H. Lieb, F.Y. Wu, Phys. Rev. Lett. **20** (1968) 1445

[London 35]   F. London and H. London, Proc. Roy. Soc. A (London) **149** (1935) 72

[McWeeny 69]   R. McWeeny, B.T. Sutcliffe, *Methods of Molecular Quantum Mechanics*, Ac. Press. Inc. (London) LTD (1969)

[Malrieu 82]   J.P. Malrieu, D. Maynau, J. Am. Chem. Soc. **104** (1982) 3021

[Mattis 88]   D.C. Mattis, C.Y. Pan, Phys. Rev. Lett., **61** (1988) 463

[Mott 49]   N.F. Mott, Proc. Phys. Soc. A **62** (1949) 416

[Murakami 86] M. Murakami, S. Yoshimura, Mol. Cryst. Liq. Cryst. (1986)

[Ohmine 78]   I. Ohmine, M. Karplus, K. Schulten, J. Chem. Phys., **68** (1978) 2298

[Oitmaa 78]   J. Oitmaa, D.D. Betts, Can. J. Phys., **56** (1978) 897

[Oles 87]   A.M. Olés, J. Zaanen, P. Fulde, Physica **148B** (1987) 260

[Orenstein 84] J. Orenstein, Z. Vardeny, G.L. Baker, G. Eagle, S. Etemad, Phys. Rev. B, **30** (1984) 786

[Ovchinnokov 77] A.A. Ovchinnokov, I.A. Misurkin, Russ. Chem. Rev. **46** (1977) 967

[Paldus 79]   Paldus *et al.*, Int. J. Quant. Chem., **15** (1979) 463

[Pauling 58]   L. Pauling, *The Nature of Chemical Bond*, Cornell Univ. Press, Ithaca, NY, (1958), 12th edn.

[Peierls 55]   R.E. Peierls, *Quantum Theory of Solids* Ed. Clarendon, Oxford Univ. Press, London, Chap.5

[Pohl 67]   H.A. Pohl, J. Polym. Sci. **C17** (1967) 13

[Poilblanc 89] D. Poilblanc, Phys. Rev. B, **39** (1989) 140

[Poshusta 89] R.D. Poshusta, T.G. Schmalz, D.J. Klein, Mol. Phys., **66** (1989) 317

[Pullman 62]   B. Pullman, *The Modern Theory of Molecular Structure*, Dover, NY, (1962)

[Ramsak 89]   A.Ramsak, P. Prelovsek (preprint 1989)

[Randic 76]   M. Randić, Chem. Phys. Lett., **38** (1976) 68

[Randic 77]   M. Randić, J. Am. Chem. Soc., **99** (1977) 444

[Reger 88]   J.D. Reger, A.P. Young, Phys. Rev. B, **37** (1988) 5978

[Rembaum 70]   A. Rembaum, J. Polym. Sci. **C29** (1970) 157

[Rice 79]   M.J. Rice, Phys. Lett. A, **71** (1979) 152

[Rokshar 88]   D.S. Rokshar, S.A. Kivelson, Phys. Rev. Lett., **61** (1988) 2376

[Ruckenstein 87] A.E. Ruckenstein, P.J. Hirschfeld, J. Appel, Phys. Rev. B, **36** (1987) 857

[Rumer 32]   G. Rümer, Nachr. Wiss. Göttingen (1932) 337

[Sachdev 89]   S. Sachdev, Phys. Rev. B, **39** (1989) 12232

[Salem 66]   L. Salem, *The Molecular Orbital Theory of Conjugated Systems* Ed. Benjamin, N.Y (1966)

[Schmitt-R 88] S. Schmitt-Rink, C.M. Varma, A.E. Ruckenstein, Phys. Rev. Lett., **60** (1988) 2793

[Shastry 88]   B.S. Shastry, Phys. Rev. Lett., **60** (1988) 639

[Soos 83]   Z.G. Soos *et al.*, Chem. Phys. Lett., **101** (1983) 34

[Sorella 88]   S. Sorella, E. Tosatti, S. Baroni, R. Car, M. Parrinello, Int. J. Mod. Phys. B **1** (1988) 457

[Su 80]   W.P. Su, J.R. Schrieffer, A.J. Heeger, Phys. Rev. B, **22** (1980) 2099

[Suzuki 67]   H. Suzuki, *Electronic Absorption Spectra and Geometry of Organic Molecules* Ac. Press, N.Y. (1967)

[Tanaka 84]   K. Tanaka, K. Ueda, T. Koike, T. Yamabe, Solid St. Commun. **51** (1984) 943

[Tavan 79]   P. Tavan, K. Schulten, J. Chem. Phys. **70** (1979) 5407

[Thomann 83] H. Thomann et al., Phys. Rev. Lett., **50** (1983) 533

[Valenti 87] R.Valentí, *Master Thesis* (1987) unpublished.

[Weinberger 84] B.R. Weinberger et al., Phys. Rev. Lett., **53** (1984)

[Wheland 56] G.W. Wheland, *The Theory of Resonance*, Wiley, NY, (1956), sixth edn.

[Wiegman 88] P.B. Wiegman, Phys. Rev. Lett., **60** (1988) 821

[Wu 87]   M.K. Wu, J.R. Ashburn, C.J. Torng, P.H. Hor, R.L. Meng, L. Gao, Z.J. Huang, Y.Q. Wang, C.W. Chu, Phys. Rev. Lett., **58** (1987) 908

[Yamabe 82]   T. Yamabe, K. Tanaka, K. Ohzeki, S. Yata, Solid State Commun., **44** (1982) 823

[Yannoni 83] C.S. Yannoni, T.C. Clarke, Phys. Rev. Lett., **51** (1983) 1191

[Zaanen 88]   J. Zaanen, A.M. Oles, Phys. Rev. B, **37** (1988) 9423

[Zivkovic 89] T.P. Živković, B.L. Sandleback, T.G. Schmalz, D.J. Klein, submitted to Phys. Rev.B